

Optical properties of a thin film of coated, truncated, spheres

Leif Amund Lie

May 31, 2010

Preface

This work has been a master's degree thesis at the Norwegian University of Science and Technology. The thesis work was initiated in fall 2008 and finished at spring 2010. The supervisor has been Ingve Simonsen, who has given inspired and thorough guidance. Also, Dick Bedeaux and Rémi Lazzari deserve to be thanked for occasional inputs.

Abstract

This thesis describes an approach to calculate the optical properties of a surface consisting of small, truncated spherical particles, covered with a coating layer. The treatment follows Bedeaux and Vlieger's approach for describing the optical properties of granular and rough interfaces using the notion of integrated electromagnetic excess field and surface susceptibilities, as described in the book '*Optical Properties of Surfaces*' (Imperial College Press, London, 2001), where truncated islands have been considered, but without a coating layer. Equations describing the optical properties has been derived, and have been checked analytically for consistency with the theory of Bedeaux and Vlieger. Also, a routine to solve the equations numerically has been implemented in Ingve Simonsen and Rémi Lazzari's software package GranFilm, where the theory from Bedeaux and Vlieger's original work has been implemented. The numerical results have been tested, with varying results.

Contents

List of Figures	ix
List of Tables	xi
1 Introduction	1
2 General theory	5
2.1 Optical properties of a flat surface	5
2.2 Solving Maxwell's equations for a non-flat surface	6
2.3 Excess quantities and constitutive relations	8
2.4 Fresnel coefficients for a granular film	10
3 Coated island geometry	13
3.1 Computation of the island polarisabilities	13
3.1.1 Coordinate systems	13
3.1.2 Brief derivation of the system of equations for the potential	15
3.2 Interaction between islands	20
4 Numerical implementation	23
5 Results	25
6 Analytical and numerical evaluation	27
6.1 Analytical validation	27
6.1.1 Vanishing coating thickness	27
6.1.2 A coating of island material	28
6.1.3 A coating of ambient material	28
6.2 Evaluation of the numerical results	28
6.2.1 Consistency with original GranFilm code	28
6.2.2 Fulfilment of boundary conditions	31
6.3 Convergence	35
6.3.1 Convergence of multipole expansion coefficients	35
6.3.2 Convergence of the dipole term	39
6.3.3 Convergence of differential reflectivity	39
6.3.4 Convergence of the field continuity	42
7 Conclusion	43
A Validation of the potential form	45
B Detailed derivation of the system of equations	47
B.1 Properties of the spherical harmonics	47
B.2 Potentials with reflected and transmitted amplitudes eliminated	48

Contents

B.3	Continuity on the outer coating surface	49
B.3.1	Continuity of the potential at the outer shell	49
B.3.2	Continuity of the normal derivative of the potential times the permittivity at the outer shell	54
B.4	Continuity on the inner coating surface	56
B.4.1	Continuity of the potential at the inner shell	56
B.4.2	Continuity of the normal derivative of the potential times the permittivity at the inner shell	58
B.5	Summary of the linear system of equations	61
C	Parameters for default test case	63
	Bibliography	65

List of Figures

1.1	a) Example of a granular film of silver islands on a magnesium oxide substrate and b) differential reflectivity of the surface calculated using the GranFilm software, compared to experimental values.	1
2.1	A flat interface between two half-infinite media with a beam of light reflected and transmitted.	5
2.2	An example of a granular surface, with a typical coordinate system. The exact dielectric properties of the clusters are not specified.	7
3.1	Coordinate system of the coated sphere geometry, with multipole expansion centre in the centre of the sphere.	14
5.1	a) real and b) imaginary parts of the relative dielectric functions of Ag and SiO.	25
5.2	Differential reflectivity for the default case of 8 nm Ag hemispheres on a MgO substrate, coated with a layer of SiO with varying thickness and with $M = 16$	26
6.1	Comparison between modified and original code, for the case of Ag hemispheres on a MgO substrate, with coating thickness set to zero in the modified code, and with $M = 16$. a) shows the two differential reflectivity spectra, while b) shows the difference between them.	29
6.2	Comparison between modified and original code, for Ag spheres with a truncation ratio 0.3 on a MgO substrate, and with $M = 16$. a) shows the differential reflectivity spectra when the modified code uses a coating thickness of exactly zero, while in b) a SiO coating 0.0001 nm thick has been added to the spheres.	30
6.3	Differential reflectivity for a surface of 11 nm radius Ag hemispheres on a MgO substrate, calculated using the original GranFilm code, compared with the equivalent case from the modified code where Ag spheres are covered with a coating of Ag of varying thickness, but so that the total radius of inner sphere and coating remains 11 nm. M is set to 16.	31
6.4	Differential reflectivity of a surface of a MgO substrate covered with 8 nm radius Ag hemispheres surrounded by vacuum, calculated using the original Granfilm code, compared with the equivalent case from the modified code with a MgO substrate covered with Ag hemispheres with a vacuum coating of varying thickness. M is set to 16.	32
6.5	The discontinuity of the potential over the island-coating boundary for the default parameters where 8 nm radius Ag hemispheres with 3 nm SiO coating covers a MgO substrate, and with $M = 16$, a) in the θ - ϕ -plane and b) on the sphere.	33
6.6	The discontinuity of the normal displacement field over the island-coating boundary for the default parameters where 8 nm radius Ag hemispheres with 3 nm SiO coating covers a MgO substrate, and with $M = 16$, a) in the θ - ϕ -plane and b) on the sphere.	34
6.7	The discontinuity of the potential over the coating-ambient boundary for the default parameters where 8 nm radius Ag hemispheres with 3 nm SiO coating covers a MgO substrate, and with $M = 16$, a) in the θ - ϕ -plane and b) on the sphere.	34

LIST OF FIGURES

6.8	The discontinuity of the normal displacement field over the coating-ambient boundary for the default parameters where 8 nm radius Ag hemispheres with 3 nm SiO coating covers a MgO substrate, and with $M = 16$, a) in the θ - ϕ -plane and b) on the sphere.	35
6.9	$A_{\ell m}/(E_0 R_c^{-\ell-2})$ for the case of a MgO substrate covered with 8 nm radius Ag hemispheres with a 3 nm thick SiO coating, for multipole orders ℓ up to $M = 40$, and for a) $m = 0$ and b) $m = 1$	36
6.10	$B_{\ell m}/(E_0 R_c^{\ell-1})$ for the case of a MgO substrate covered with 8 nm radius Ag hemispheres with a 3 nm thick SiO coating, for multipole orders ℓ up to $M = 40$, and for a) $m = 0$ and b) $m = 1$	36
6.11	$\mathcal{A}_{\ell m}/(E_0 R_c^{-\ell-2})$ for the case of a MgO substrate covered with 8 nm radius Ag hemispheres with a 3 nm thick SiO coating, for multipole orders ℓ up to $M = 40$, and for a) $m = 0$ and b) $m = 1$	37
6.12	$\mathcal{B}_{\ell m}/(E_0 R_c^{\ell-1})$ for the case of a MgO substrate covered with 8 nm radius Ag hemispheres with a 3 nm thick SiO coating, for multipole orders ℓ up to $M = 40$, and for a) $m = 0$ and b) $m = 1$	37
6.13	B_{400} and B_{401} from figure 6.10, plotted together with the differential reflectivity, where the latter has been scaled up so that it is visible in the graph.	38
6.14	a) $A_{\ell 0}/(E_0 R_c^{-\ell-2})$ and b) $B_{\ell 0}/(E_0 R_c^{\ell-1})$ for a MgO substrate covered with 8 nm radius Ag hemispheres, calculated using the unmodified GranFilm code, for multipole orders ℓ up to $M = 40$	38
6.15	Rate of change with increasing M for a) A_{10} and b) A_{11} , measured as the difference between the coefficients for two consecutive M 's. The surface consists of a MgO substrate covered with 8 nm radius Ag hemispheres with a 3 nm thick SiO coating.	39
6.16	Differential reflectivity for a substrate of MgO covered with 8 nm radius Ag hemispheres with a 3 nm thick SiO coating, for different M , for a) the full energy range, and b) zoomed on the peak movement.	40
6.17	Change in differential reflectivity for the thin film from figure 6.16, when M is varied as $M = 2, 4, 6, \dots, 40$, measured as the L_2 -norm between two consecutive curves, normalized by the number of energy points.	40
6.18	a) The energy of the peak in the differential reflectivity of the surface from figure 6.16, and b) the change in this peak position measured as the difference between peak energy for two consecutive curves, for $M = 2, 4, 6, \dots, 40$	41
6.19	a) The energy of the dip in the differential reflectivity of the surface from figure 6.16, and b) the change in this dip position measured as the difference between dip energy for two consecutive curves, for $M = 2, 4, 6, \dots, 40$	41
6.20	Mean value across the two spherical interfaces of the absolute value of the error in the boundary conditions, as a function of the multipole expansion cut-off M . The surface consist of the standard case of a MgO substrate covered with 8 nm radius Ag hemispheres with 3 nm thick SiO.	42

List of Tables

6.1 Indication of typical error for different variations of the default case. All cases has a MgO substrate, and have been calculated for both $t_r = 0$ and $t_r = 0.3$. Two of the cases have 8 nm Ag islands with 3 nm SiO coating, two has 8 nm Au islands with 3 nm SiO coating, and two cases are calculated using the unmodified code, with 8 nm Ag islands. All calculations are done with $M = 16$.	35
C.1 The most relevant parameters for the default setting introduced in section 6.2	63

1 Introduction

Optical techniques have been used widely as a means to characterise surfaces. The reasons for this range from the relative cheapness of the required equipment, it's relative simplicity and the ability it has not to disturb the surface and the formation of the surface.

A special type of surface that may be studied using visible light is the so-called granular thin film. Such a surface consist of a substrate covered with some type of deposit distributed into clusters. It may arise when a thin film is grown in the so-called Volmer-Weber growth mode, where the deposit wets the substrate poorly. An example of such a film is shown in figure 1.1 a), where a magnesium oxide substrate is covered with silver drops. In industry applications, when such thin films are grown, optical techniques may have large advantages as a method for growth monitoring [10].

Also, these surfaces may have certain characteristic optical properties, making visible light monitoring especially ideal. Studies into this matter has been performed by several to be credited later, and especially the supervisor of this thesis, Ingve Simonsen. Together with Rémi Lazzari he made the software package GranFilm [6] which calculates the optical properties of such a granular surface, by modelling the clusters as spherical or spheroidal islands. Figure 1.1 b) shows a sample of the results their software may achieve. Here, experimental measurements [7, 9] of the thin film in figure 1.1 a) are compared to the numerical results calculated using GranFilm. The scale of measurement is differential reflectivity, which is a measure of reflection properties that will be defined more precisely later.

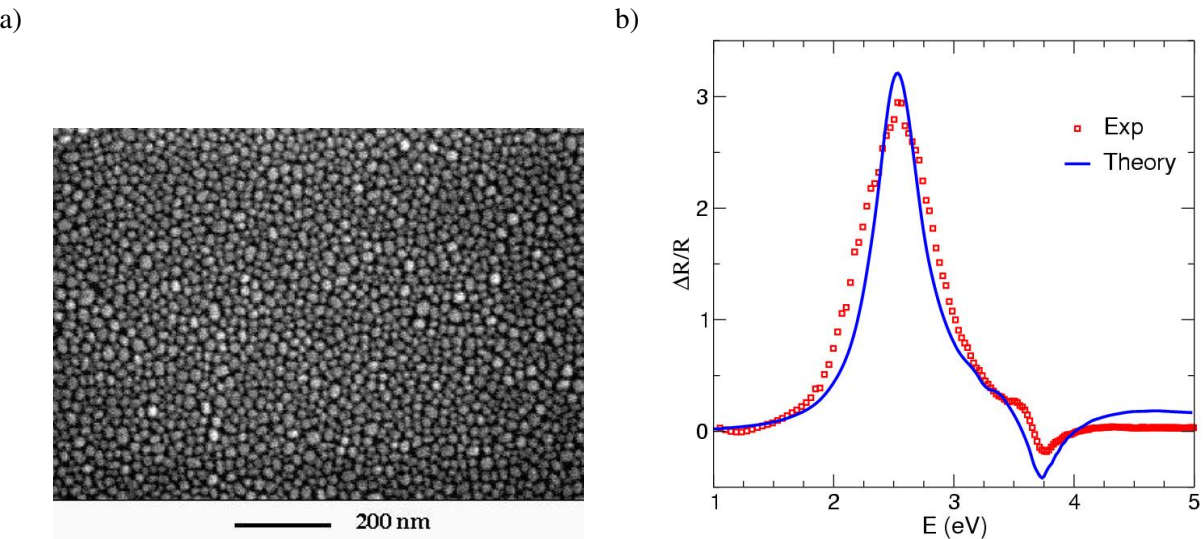


Figure 1.1: a) Example of a granular film of silver islands on a magnesium oxide substrate and b) differential reflectivity of the surface calculated using the GranFilm software, compared to experimental values.

A natural extension of this work, it seems, is the possibility of adding a coating layer onto the islands. In addition to the fundamental aspect of describing surface properties, the need for such an extension may arise in various applications. One thinkable scenario is a biological sensor, where an island film is exposed

1 Introduction

to a substance containing molecules that is attracted to the islands. If so, optical measurement of the surface may help determine the thickness of the coating layer, and thus the concentration of the molecules.

Before diving into the theory of such coated island films, a brief overview of the field of granular thin film growth is appropriate, starting with the theory of metallic cluster deposits on a substrate. For relatively low coverages, before the clusters begin to overlap, the film will be discontinuous. Then, for metallic clusters on a non-conducting substrate, eventual charge movements will be confined to within the clusters. That is not to say the clusters should be considered as isolated, since they still may interact through electromagnetic coupling with the surrounding clusters and with the substrate.

When visible light is used as a surface probe for such films, certain charge oscillation modes may be excited. These plasmon absorption modes are usually called Mie resonances, and they strongly affect the Fresnel coefficients. Also, the frequencies at which these oscillation modes occur are highly sensitive to the shape and size of the clusters.

Such a sensitivity makes light a promising candidate for probing this type of surface layer. But in order to extract information about film thickness and cluster morphology from measured reflection spectra, a theory for optical properties of metallic clusters is needed. The pioneering work in this field was done by Maxwell Garnett [8] at the turn of the nineteenth century. His approach was to describe the optical properties of metallic clusters using an effective medium theory, where only the relative fraction of each component is taken into account. This theory has had some success, but in order to extract information about the cluster polarisabilities that governs the experimentally interesting far-field behaviour, a more sophisticated approach is needed.

In addition to the interaction between clusters, a successful theory must account for the interaction between the clusters and the substrate. This polarisation was modelled to dipolar order in the theory developed by Yamaguchi, Yoshida and Kinbara [14, 15]. However, this model did not allow for a quantitative description of the size and shape of the deposited clusters. This led Bedeaux and Vlieger [2] to develop their theory for describing the optical properties of a granular thin films. In short, the approach was to introduce a set of auxiliary fields named excess fields that allowed macroscopic optical properties to be described without requiring knowledge of the field's exact behaviour close to the interface. This formalism may also describe the optical properties of rough surfaces, but this will not be considered in the following.

The optical properties of the surface is described by the Fresnel coefficients, which are essentially related to the polarisabilities of the clusters. In calculating these polarisabilities, it is assumed that the wavelength of the light is large compared to the size of the clusters. Then, the quasi-static limit is reached, where retardation effects may be neglected [2, p. 173] and the system is described by electrostatics.

A model treating the clusters as truncated spheres have been developed by Wind et al. [12, 13]. There, the Laplace equation is solved for a single spherical island using a multipole expansion technique [2, p. 78], where the potential is expanded in a complete set of functions satisfying the Laplace equation. Such a complete set is known for both spherical and spheroidal clusters, but the latter will not be treated in the following. Interaction with the substrate is also conveniently handled by adding expansion terms originating from within the substrate, describing the effect of excited image multipoles. Lastly, the polarisability of a single island is modified due to the interaction with the surrounding islands, taking into account interaction up to dipolar or quadropolar order.

This model has been successful in many circumstances [1, 5, 11], and with a few modifications [10] it has been implemented in the GranFilm software package [6] by Lazzari and Simonsen. And this is where the subject of this thesis enters the stage, namely that of allowing for a coating layer to be added to the islands. It turns out that the theory of Bedeaux and Vlieger may be used unmodified up to the point where the coated island polarisabilities are calculated. Also, task of finding these polarisabilities may be approached

in a very similar manner as that of the uncoated case. To be concrete this means that although the equations involved turn out to be somewhat more complex, they do share a common structure with their uncoated equivalents. Also, a lot of calculated quantities and numerical integrals needed are identical to the ones already implemented in the GranFilm software. Therefore an expansion of the old software to support island coating seems quite natural.

2 General theory

In the following, the general theory for calculating optical properties of granular films, as developed by Bedeaux and Vlieger [2], will be presented. It should be noted that this theory also applies to so-called rough surfaces, but this will not be treated explicitly. First there will be a short recapitulation of some basic electromagnetic theory for clean interfaces, before extending this to the theory for granular films.

2.1 Optical properties of a flat surface

A surface may be seen as a discontinuity between two media with different dielectric and magnetic properties. In this section a simple case of such a surface will be briefly studied, namely a flat surface. Such a surface is shown in figure 2.1, where the upper media has dielectric and magnetic constants ϵ_1 and μ_1 , while the lower has ϵ_2 and μ_2 . These constants are often called permittivity and permeability, respectively, as will be done in the following. When an electromagnetic wave is incident on a flat surface, the field is

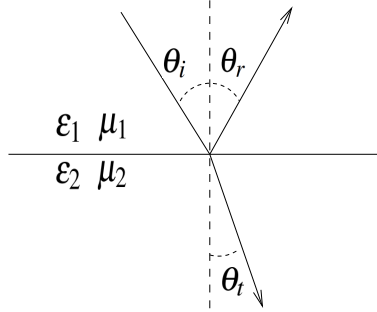


Figure 2.1: A flat interface between two half-infinite media with a beam of light reflected and transmitted.

split into a reflected and a transmitted part, and the relation between the incident, reflected and transmitted fields is what will be called the optical properties of the surface. In finding these relations, the starting point is Maxwell's equations, giving a general description of electromagnetic waves [3, 326],

$$\nabla \cdot \mathbf{D} = \rho_f, \quad \nabla \times \mathbf{E} = -\frac{\partial \mathbf{B}}{\partial t}, \quad (2.1a)$$

$$\nabla \cdot \mathbf{B} = 0, \quad \nabla \times \mathbf{H} = \mathbf{J}_f + \frac{\partial \mathbf{D}}{\partial t}. \quad (2.1b)$$

Here \mathbf{E} and \mathbf{B} are the electric field and magnetic induction, respectively, and \mathbf{D} and \mathbf{H} the electric displacement field and the magnetic field. The displacement field and the magnetic field are related to the material response to the fields. For linear media, where polarisation and magnetisation increase linearly with the incident field, they are given by

$$\mathbf{H} = \frac{1}{\mu} \mathbf{B}, \quad \mathbf{D} = \epsilon \mathbf{E}, \quad (2.2)$$

with permittivity ϵ and permeability μ , respectively, as introduced in figure 2.1. (2.1) also contains the terms ρ_f and \mathbf{J}_f , which are the free charge and the free current, respectively. That they are free means that they are not originating from any polarisation of the media.

2 General theory

Now, a set of boundary conditions for the fields may be derived from (2.1). This derivation will not be done explicitly, but the end result is [3, p. 384]

$$D_1^\perp = D_2^\perp, \quad \mathbf{E}_1^\parallel = \mathbf{E}_2^\parallel, \quad (2.3a)$$

$$B_1^\perp = B_2^\perp, \quad \mathbf{H}_1^\parallel = \mathbf{H}_2^\parallel, \quad (2.3b)$$

where subscripts 1 and 2 refers to the fields directly above and directly below the boundary, respectively, as seen in figure 2.1, and where \perp and \parallel denotes the normal and tangential component, respectively.

Using the boundary conditions in (2.3), coefficients describing the reflection and transmission may be found. The ones often used are the reflectance R and the transmittance T , defined as the reflected and transmitted power, respectively, divided by the incoming power. They are often defined in terms of the reflection and transmission coefficients, r and t , respectively, which are the reflected and transmitted electric field amplitude, divided by the incident amplitude. Instead of giving a thorough presentation of all these mentioned quantities, as may be found in any standard optics textbook [4, 113], the result for the reflectance and transmittance is given directly as

$$R = r^2, \quad T = \frac{n_2 \cos \theta_t}{n_1 \cos \theta_i} t^2, \quad (2.4)$$

where n_1 and n_2 are the refractive indices for the upper and lower medium. θ_i and θ_t are the angles of incidence and transmission, as indicated in figure 2.1, which together with the angle of reflection θ_r is given by Snell's law,

$$n_1 \cos \theta_i = n_2 \cos \theta_t, \quad \theta_r = \theta_i. \quad (2.5)$$

Snell's law is found when the boundary conditions in (2.3) are applied to a plane wave at the surface. Some further algebra also gives the values of the Fresnel coefficients r and t . These expressions for these coefficients depend on the polarisation of the incident light. For p- and s-polarisation, with electric field parallel and perpendicular to the plane of incidence, respectively, the flat surface Fresnel coefficients are [4, p. 114]

$$r_p = \frac{n_2 \cos \theta_i - n_1 \cos \theta_t}{n_1 \cos \theta_t + n_2 \cos \theta_i}, \quad t_p = \frac{2n_1 \cos \theta_i}{n_1 \cos \theta_t + n_2 \cos \theta_i} \quad (2.6a)$$

$$r_s = \frac{n_1 \cos \theta_i - n_2 \cos \theta_t}{n_1 \cos \theta_t + n_2 \cos \theta_i}, \quad t_s = \frac{2n_1 \cos \theta_i}{n_1 \cos \theta_t + n_2 \cos \theta_i} \quad (2.6b)$$

Thus, the optical properties of the plane surface of figure 2.1 are given by (2.4) – (2.6).

2.2 Solving Maxwell's equations for a non-flat surface

In the previous section, optical properties were found by studying the behaviour of plane waves incident on a flat surface. Otherwise, if the surface is somehow non-flat, more work is required. An example of such a surface is the granular surface shown in figure 2.2, which will be treated more specific later. Then, the field around a spherical cluster needs to be calculated.

As a first step, the assumption will be made that the system may be treated as quasi-static. In this limit the size of the clusters is small compared to the incident wavelength, so that retardation effects become

unimportant. This means that the propagation of the fields is considered to be instantaneous, so that the time variation of the fields is neglected. Then, the system may be described by electrostatics, where all time derivatives in Maxwell's equations in (2.1) have vanished. If in addition it is assumed that there is no free charge or current present, (2.1) reduce to

$$\nabla \cdot \mathbf{D} = 0, \quad \nabla \times \mathbf{E} = 0, \quad (2.7a)$$

$$\nabla \cdot \mathbf{B} = 0, \quad \nabla \times \mathbf{H} = 0. \quad (2.7b)$$

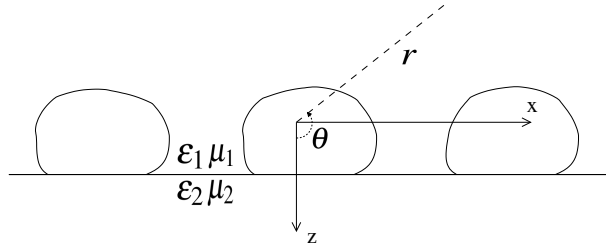


Figure 2.2: An example of a granular surface, with a typical coordinate system. The exact dielectric properties of the clusters are not specified.

In electrostatics, the electric field may be expressed in terms of a scalar potential [3, p. 417],

$$\mathbf{E} = -\nabla \psi, \quad (2.8)$$

where ψ is required to be finite. If then the electric field in (2.8) is related to \mathbf{D} through (2.2) and inserted into Maxwell's equation for the gradient of \mathbf{D} , as given in (2.7b), the result is the Laplace equation,

$$\nabla^2 \psi = 0. \quad (2.9)$$

Then, with the two assumptions made, that of the quasi-static limit and that there is no free charge or current, the task of finding the behaviour of the field in (2.1) has simplified significantly. Now the behaviour of the field may be found by solving the scalar Laplace equation. But still, the Laplace equation does not give a complete description of the field, since the laplacian operator ∇^2 allows the Laplace equation to have infinitely many solution. The correct solution of (2.9) must therefore be chosen as the one which also satisfies (2.7). Alternatively, the potential must satisfy a set of boundary conditions derived from (2.7), which will be given in (2.13).

Now, a possible approach to finding the potential is to express it in a complete basis of functions that all satisfy the Laplace equation. One such basis, which will be useful later when dealing with spherical clusters, is a multipole expansion with spherical harmonics. Then the potential is expressed as the sum of potentials from multipoles of all orders, but where hopefully the first terms in the expansion are most important. In spherical coordinates, a typical multipole expansion is given as [2, p. 78]

$$\psi(\vec{r}) = \sum_{\ell m} A_{\ell m} r^{-\ell-1} Y_{\ell}^m(\theta, \phi) + \sum_{\ell m} B_{\ell m} r^{\ell} Y_{\ell}^m(\theta, \phi), \quad (2.10)$$

where $\ell = 0, 1, 2, \dots$ and $m = 0, \pm 1, \pm 2, \dots, \pm \ell$, with spherical coordinates (r, θ, ϕ) , as introduced in figure 2.2. $A_{\ell m}$ and $B_{\ell m}$ are multipole expansion coefficients, and the spherical harmonics are given by

$$Y_{\ell}^m(\theta, \phi) = \left[\frac{2\ell+1}{4\pi} \frac{(\ell-m)!}{(\ell+m)!} \right]^{1/2} P_{\ell}^m(\cos \theta) (-1)^m e^{im\phi}, \quad (2.11)$$

using associated Legendre functions,

$$\begin{aligned} P_\ell^m(x) &= \frac{1}{2^\ell \ell!} (1-x^2)^{m/2} \left(\frac{d}{dx} \right)^{\ell+m} (x^2 - 1)^\ell, \quad m \geq 0, \\ P_\ell^m(x) &= (-1)^m \frac{(\ell+m)!}{(\ell-m)!} P_\ell^{-m}(x), \quad m < 0. \end{aligned} \quad (2.12)$$

In this expansion, the multipoles are all placed at the same point. However, although this is a complete description of the potential, it may be difficult to find the expansion coefficients. Therefore, in some situations it may be wise to add other terms originating in other points, as will be done in chapter 3.

With the potential written in multipole expansion form, the task consist of determining the unknown expansion coefficients. This may be done by imposing certain boundary conditions on the potentials. The first, as previously stated, is that the potential has to be finite everywhere,

$$|\psi(\mathbf{r})| < \infty, \quad \text{for all } \mathbf{r}. \quad (2.13a)$$

Second, the boundary conditions in (2.3) may be expressed in terms of the potential [3, p. 87], which gives

$$\varepsilon_1 \frac{\partial \psi_1}{\partial \hat{n}} = \varepsilon_2 \frac{\partial \psi_2}{\partial \hat{n}}, \quad \psi_1 = \psi_2, \quad (2.13b)$$

where $\partial/\partial \hat{n}$ refers to the normal derivative, the derivative in the direction perpendicular to the surface. Thus, what is to be solved is (2.9), with the boundary conditions in (2.13) imposed. This will be used later when the potential around the clusters is sought in section 3.1.

2.3 Excess quantities and constitutive relations

The description of optical properties derived in section 2.1 demands that there is a sharp boundary between the two media. For granular films, this demand is certainly not met. Also, brute-force calculations of the entire surface using Maxwell's equations as suggested in section 2.2 quickly become very complex. This led Bedeaux and Vlieger [2] to develop their approach where the optical properties may be calculated without an exact knowledge of the behaviour of the electromagnetic fields near the surface.

The starting point for this formalism is the definition of the so-called *excess quantities*. These are given as the difference between the real field and the bulk field extrapolated to the surface. For the case of E it is defined as

$$\mathbf{E}_{\text{ex}}(\mathbf{r}) = \mathbf{E}(\mathbf{r}) - \mathbf{E}^-(\mathbf{r})\theta(-z) - \mathbf{E}^+(\mathbf{r})\theta(z), \quad (2.14)$$

where $\theta(z)$ is the Heaviside step function, $E(r)$ is the actual electrical field and E^\pm are the extrapolated bulk fields in the region above (+) and below (-) the plane $z=0$, which is the defined interface plane (see figure 3.1). The frequency dependence of the fields is implicitly included in the notation. Similar definitions may be used for the other electromagnetic fields.

Now, since the excess fields will only be significant close to the surface, they may be though of as perturbations to the simple case of a flat interface. Then, instead of tediously using the boundary conditions given in (2.7) for the field at a microscopic level close to the surface, new boundary conditions may be made that incorporate the total effect of the non-sharp boundary. This is done by inserting the fields of the

form given in (2.14) into the full Maxwell equations (2.1). For a full derivation, see Vlieger and Bedeaux's *Optical Properties of Surfaces* [2, p.21]. The result reads

$$[\mathbf{E}_\parallel^+(\mathbf{r}) - \mathbf{E}_\parallel^-(\mathbf{r})]|_{z=0} = i\omega\hat{z} \times \mathbf{M}_\parallel^s(\mathbf{r}_\parallel) - \nabla_\parallel \mathbf{P}_z^s(\mathbf{r}_\parallel), \quad (2.15a)$$

$$[\mathbf{D}_z^+(\mathbf{r}) - \mathbf{D}_z^-(\mathbf{r})]|_{z=0} = -\nabla_\parallel \mathbf{P}_\parallel^s(\mathbf{r}_\parallel), \quad (2.15b)$$

$$[\mathbf{H}_\parallel^+(\mathbf{r}) - \mathbf{H}_\parallel^-(\mathbf{r})]|_{z=0} = i\omega\hat{z} \times \mathbf{P}_\parallel^s(\mathbf{r}_\parallel) - \nabla_\parallel \mathbf{M}_z^s(\mathbf{r}_\parallel), \quad (2.15c)$$

$$[\mathbf{B}_z^+(\mathbf{r}) - \mathbf{B}_z^-(\mathbf{r})]|_{z=0} = -\nabla_\parallel \mathbf{M}_\parallel^s(\mathbf{r}_\parallel), \quad (2.15d)$$

where ∇_\parallel is the nabla operator parallel to the surface, subscripts \parallel denote the projection of a vector into the xy -plane, the subscript z denotes the z -component, and \hat{z} is the unit vector normal to the surface $z = 0$ and pointing upwards. The quantities \mathbf{E} and \mathbf{D} are still the electric field and the electric displacement, respectively, while \mathbf{H} and \mathbf{B} are the magnetic field and the magnetic induction. The quantities with superscript s are the so-called excess polarization and magnetization densities, defined as

$$\mathbf{P}^s(\mathbf{r}_\parallel) = (\mathbf{D}_\parallel^s(\mathbf{r}_\parallel), \epsilon_0 \mathbf{E}_z^s(\mathbf{r}_\parallel)), \quad (2.16a)$$

$$\mathbf{M}^s(\mathbf{r}_\parallel) = (\mathbf{B}_\parallel^s(\mathbf{r}_\parallel), \mu_0 \mathbf{H}_z^s(\mathbf{r}_\parallel)), \quad (2.16b)$$

where ϵ_0 and μ_0 are the vacuum permittivity and permeability, respectively, and the quantities on the right hand side are the excess fields integrated along the z -axis,

$$\mathbf{D}_\parallel^s(\mathbf{r}) = \int_{-\infty}^{\infty} dz \mathbf{D}_{ex,\parallel}(\mathbf{r}), \quad \mathbf{E}_\parallel^s(\mathbf{r}) = \int_{-\infty}^{\infty} dz \mathbf{E}_{ex,\parallel}(\mathbf{r}), \quad (2.17a)$$

$$\mathbf{B}_\parallel^s(\mathbf{r}) = \int_{-\infty}^{\infty} dz \mathbf{B}_{ex,\parallel}(\mathbf{r}), \quad \mathbf{H}_\parallel^s(\mathbf{r}) = \int_{-\infty}^{\infty} dz \mathbf{H}_{ex,\parallel}(\mathbf{r}). \quad (2.17b)$$

The interfacial polarization and magnetisation densities in (2.16) may be linked to the extrapolated bulk field at the surface by a set of constitutive relations characteristic for the interface. If the perturbed surface layer is small compared to the optical wavelength, a local relation may be postulated, since the excess fields are only relevant close to the surface [6]. In the following, for convenience, only non-magnetic systems will be treated, which leads to $\mathbf{M} = 0$ and a great simplification of (2.15). For a complete study of magnetic systems, see Bedeaux and Vlieger's book [2]. The simplest possible relation is then given by [2, p. 30]

$$\mathbf{P}^s(\mathbf{r}_\parallel) = \xi_e^s(\omega) [\mathbf{E}_{\parallel,\Sigma}(\mathbf{r}_\parallel), \mathbf{D}_{z,\Sigma}(\mathbf{r}_\parallel)], \quad (2.18)$$

where subscript Σ denotes the arithmetic mean of the bulk field on both sides of the surface. For a homogeneous, isotropic, symmetric interface, ξ is a diagonal tensor, given by [2, p. 30]

$$\xi_e^s(\omega) = \begin{pmatrix} \gamma & 0 & 0 \\ 0 & \gamma & 0 \\ 0 & 0 & \beta \end{pmatrix}. \quad (2.19)$$

Here, γ and β are called the first order surface susceptibilities. Physically they describe the ability of the surface to polarize in parallel and perpendicular direction, respectively, in response to the incident field.

So far spatial variations in the excess quantities have been ignored, which have led to local relations between the bulk extrapolated field and the total integrated surface polarization. Considering these spatial variations would lead to a non-local dependence described by second order coefficients. However, the magnitude of these terms will be of an order d/λ smaller, where d is the thickness of the perturbed layer and λ is the optical wavelength [6]. For systems where the particle size is small compared to the wavelength of the incident light, these terms may be ignored. This is especially so when dealing with metallic clusters,

2 General theory

where the higher order constitutive coefficients prove less important [6] in describing the response of the clusters. A treatment of the correction using higher order coefficients may be found in Bedeaux and Vlieger's book [2] and is also implemented in the GranFilm software package [6], but in the following the treatment will be limited to the first order constitutive coefficients γ and β .

2.4 Fresnel coefficients for a granular film

The derivation of expressions for the Fresnel coefficients in terms of surface susceptibilities can be quite tedious, and may be found in Bedeaux and Vlieger's book [2, p. 45]. The derivation follows the same method as used for a flat interface in section 2.1, but with the effect of the granular film accounted for by using the boundary conditions (2.15). Also, the definitions of the surface susceptibilities in (2.18) is used. Due to this approach, the angles of incidence, reflection and transmission are still found using the standard Snell's law in (2.5), unmodified by the perturbed layer, so that only the reflection and transmission amplitudes are sensitive to the perturbation.

For s-polarization, the result reads [6]

$$r_s(\omega) = \frac{n_2 \cos \theta_i - n_1 \cos \theta_t + i \frac{\omega}{c} \gamma}{n_2 \cos \theta_i + n_1 \cos \theta_t - i \frac{\omega}{c} \gamma}, \quad (2.20a)$$

$$t_s(\omega) = \frac{2n_2 \cos \theta_i}{n_2 \cos \theta_i + n_1 \cos \theta_t - i \frac{\omega}{c} \gamma}, \quad (2.20b)$$

where θ_i , θ_r and θ_t are the angles of incidence, reflection and transmission, and n_1 and n_2 are the refraction indices of the media. For p-polarization, the result is

$$r_p(\omega) = \frac{\kappa_-(\omega) - i \frac{\omega}{c} \gamma \cos \theta_i \cos \theta_t + i \frac{\omega}{c} n_2 n_1 \epsilon_2 \beta \sin^2 \theta_i}{\kappa_+(\omega) - i \frac{\omega}{c} \gamma \cos \theta_i \cos \theta_t - i \frac{\omega}{c} n_2 n_1 \epsilon_2 \beta \sin^2 \theta_i}, \quad (2.20c)$$

$$t_p(\omega) = \frac{2n_2 \cos \theta_i \left[1 + \frac{\omega^2}{4c^2} \epsilon_2 \gamma \beta \sin^2 \theta_i \right]}{\kappa_+(\omega) - i \frac{\omega}{c} \gamma \cos \theta_i \cos \theta_t - i \frac{\omega}{c} n_2 n_1 \epsilon_2 \beta \sin^2 \theta_i}, \quad (2.20d)$$

with κ_{\pm} defined by

$$\kappa_{\pm}(\omega) = [n_1 \cos \theta_i \pm n_2 \cos \theta_t] \left[1 - \frac{\omega^2}{4c^2} \epsilon_2 \gamma \sin^2 \theta_i \right]. \quad (2.20e)$$

In s-polarization the Fresnel quantities are independent of the surface normal constitutive coefficient β . This is because s-polarized light has no component in the direction normal to the surface, making it impossible to excite modes in this direction. For the case of p-polarization, on the other hand, the Fresnel coefficients have a β -dependence, indicating p-polarized light's ability to excite modes both parallel and perpendicular to the surface.

Also, if the constitutive coefficients γ and β are set to zero, the Fresnel coefficients in (2.20) reduce to those for the flat surface in section 2.1. Setting the constitutive coefficients to zero means that the granular film disturbance is reduced to zero. The retrieval of the coefficients for the flat surface then shows that the two approaches are consistent in the limit where the film vanishes.

In obtaining the constitutive coefficients needed for the Fresnel coefficients, the imposed restriction will be used that the clusters are small compared to the wavelength of the incident light. Then the scattering from the surface layer will typically be negligible, so that the angular distribution of light will not be far from that of a flat surface. Then, the surface polarization density $P^s(\mathbf{r}_\parallel)$ will mainly be related to the density of islands and to the polarisability, giving [2, p. 99]

$$\gamma = \rho \alpha_\parallel, \quad \beta = \frac{\rho \alpha_\perp}{\epsilon_1^2}. \quad (2.21)$$

Thus, the task left is to find the polarisability of the clusters. As argued by Bedeaux and Vlieger [2], this may be done by solving for the potential of a cluster expressed by a multipole expansion, as discussed in section 2.2. Then, the dipole terms $A_{\ell m}$ with $\ell = 1$ will give the most significant contribution in the far-field limit. After a lengthy derivation by Bedeaux and Vlieger [2, p. 98], the end result reads

$$\alpha_\perp = 2\pi\epsilon_1 A_{10}/(\sqrt{\frac{\pi}{3}} E_0 \cos \theta_0), \quad (2.22a)$$

$$\alpha_\parallel = -4\pi\epsilon_1 A_{11}/(\sqrt{\frac{2\pi}{3}} E_0 \sin \theta_0 \exp(-i\phi_0)). \quad (2.22b)$$

To proceed from this point, the dipole terms A_{10} and A_{11} must be calculated for a specific cluster geometry, which will be done in chapter 3.

3 Coated island geometry

The preceding theory has in a sense been general in that the geometry of the surface clusters has not been specified. And in principle, any shape may be treated using discrete dipole approximations, although possibly with a high computational cost. However, if the geometry is limited to that of identical truncated spheres, Bedeaux and Vlieger [2] showed that the numerics may be significantly simplified. The following treatment will follow the work of Bedeaux and Vlieger closely, but with the extension of a coating layer applied to the spheres. Also, the notation to a large extent follows that in Bedeaux and Vlieger's book [2], more specifically that in a paper by Simonsen and Lazzari [10].

In section 3.1 a scheme is developed for finding the polarisability of an isolated, coated sphere. Then, in section 3.2, the calculated polarisabilities for the isolated cluster are modified due to the interaction with the surrounding clusters, which becomes important if the islands are not far apart.

3.1 Computation of the island polarisabilities

According to (2.22), the polarisability of an island may be found by calculating the unknown coefficients in the multipole expansion of the potential. The expansion centre will be placed inside the island, above the substrate, and at a freely chosen position on the vertical z -axis pointing through the island centre. The possibility of freely varying the expansion centre along the z -axis was introduced in a paper by Simonsen and Lazzari [10], and this is the formalism used in the GranFilm code [6]. However, this freedom of choice only gives a considerable advantage when dealing with spheres with a centre below the substrate surface [10]. So, since the following work will be restricted to the case where the sphere centre lies above the substrate, the multipoles will be placed in the centre of the sphere.

For a correct description of the island response, the interaction with the substrate must be included. This will be done by use of the classical method of images [3, p. 121], in this case by letting the potentials include terms originating from within the substrate. These image multipoles will be placed at the image position, which is directly opposite of the sphere centre, with respect to the substrate interface.

3.1.1 Coordinate systems

The coordinate systems used are shown in figure 3.1, with the multipole expansion centre lying in the centre of the sphere. Here, (r, θ, ϕ) are the coordinates in the coordinate system centered in the sphere centre, while $(r_\mu, \theta_\mu, \phi_\mu)$ and $(r_{\bar{\mu}}, \theta_{\bar{\mu}}, \phi_{\bar{\mu}})$ are for the systems centered in the multipole expansion position and the image position, respectively. Note that since the multipole expansion point is set to be in the centre of the sphere, $(r_\mu, \theta_\mu, \phi_\mu)$ equals (r, θ, ϕ) .

In the following the relation between these different coordinate systems is presented [10]. It should first of all be noted that several of the presented expressions give a certain quantity in relation to the radius of the inner sphere, R , but that in a completely similar manner all the quantities should also be defined in relation to the radius of the sphere including it's coating, R_c . These expressions will not be written explicitly in the following definitions, since they may be acquired intuitively by adding a subscript c to the quantities R, χ, η, μ and $\bar{\mu}$, which will also be defined in the following.

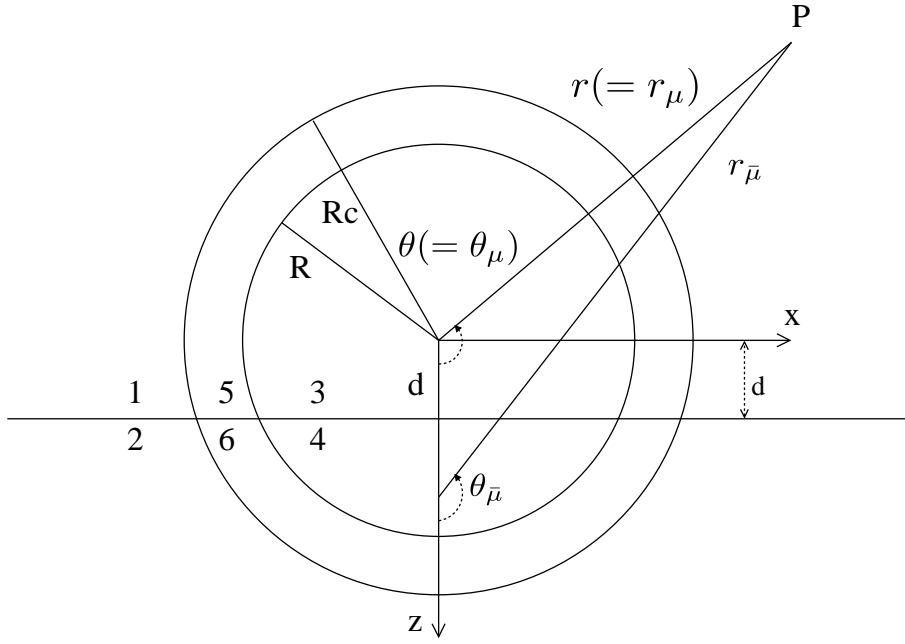


Figure 3.1: Coordinate system of the coated sphere geometry, with multipole expansion centre in the centre of the sphere.

The quantity η is a generalisation of the position of the multipole expansion centre and that of its image, so that the subscript $\eta = \mu$ denotes a quantity in relation to the multipole expansion centre, while $\eta = \bar{\mu}$ indicates a quantity in relation to the location of the image multipoles. The values of μ and $\bar{\mu}$ are given by

$$\mu = \frac{z_\mu}{R}, \quad (3.1a)$$

$$\bar{\mu} = \frac{z_{\bar{\mu}}}{R}, \quad (3.1b)$$

where R is the radius of the sphere and z_η is the position of the multipole/image expansion centre along the z -axis. Thus, with a multipole expansion centre lying in the centre of the sphere, the above gives simply $\mu = 0$ and $\bar{\mu} = 2d/R$, where d is the distance from the sphere centre to the substrate interface. Using this definition together with the cosine law results in the definition of

$$\chi[\eta](x, r) = \left(\frac{r}{R}\right)^2 - 2\eta(t_r) \frac{r}{R} x + \eta^2(t_r), \quad x = \cos \theta, \quad (3.2)$$

where $\chi[\eta](x, r)$ is to be interpreted according to the relation

$$r_\eta = R \sqrt{\chi[\eta](x, r)}, \quad (3.3)$$

where r_μ is the distance to a point from the multipole expansion centre, and $r_{\bar{\mu}}$ is the distance from the image position. The angle between the z -axis and the line from a multipole expansion centre to a given point is given by

$$\cos \theta_\eta = \frac{\frac{r}{R}x - \eta(t_r)}{\sqrt{\chi[\eta](x, r)}}. \quad (3.4)$$

Finally, since the multipole expansion centres is only allowed to move along the z -axis, the azimuthal angle is independent of the choice of η , giving

$$\phi_\eta = \phi \quad (3.5)$$

3.1.2 Brief derivation of the system of equations for the potential

As seen in figure 3.1, the physical system is divided into six separate regions. These regions are given different multipole expansions, which will be linked by imposing the boundary conditions given in (2.13b). Note that even though the three even-numbered regions all lie in the substrate and thus has the same dielectric properties, they are given three different permittivities. This is simply for mathematical convenience, and their permittivities will be set equal in the end.

In general, all potentials in the odd-numbered regions above the substrate should contain terms of both positive and negative powers of r_μ , and positive and negative powers of $r_{\bar{\mu}}$. These are the potentials from the multipoles in the island and in the image, respectively. Similarly, all potentials in the even-numbered regions should contain terms of both positive and negative terms of r_μ , describing the transmitted field from the multipoles above the substrate. However, when applying the multipole expansion of the potential, the conditions in (2.13) may be applied in order to reduce the number of unknown coefficients.

First, the three odd-numbered regions above the substrate is considered. In the interior region 3, the terms in the multipole expansion containing negative powers of r_μ will lead to a potential that is not finite in the origin, and thus fails to meet the requirement in (2.13a). Therefore these terms must be discarded in region 3. Similarly, in the exterior region 1 the terms containing positive powers of r_μ would fail the same requirement, so that these terms must also be discarded. Inside the coating, in region 5, none of these arguments may be used, so all terms there must be considered.

Next, the even-numbered regions in the substrate are considered. In region 2 the terms containing positive powers of r_μ may be discarded using the same argument as above the substrate. In region 4, however, this argument may not be applied. The reason for this is that r_μ will never be zero in this region when the sphere centre lies above the substrate. However, due to the continuity requirements in (2.13) for the boundary between regions 3 and 4, the terms in region 4 with negative powers of r_μ must also be discarded. The full derivation will not be given, but it may be performed in the same manner as in appendix A, where the continuity of the potential at the substrate interface between regions 5 and 6 is verified. Lastly, for the same reason as above the substrate, all terms has to be considered in region 6.

3 Coated island geometry

Then, in analogy with the definitions of Bedeaux and Vlieger [2, p. 228], the potentials in the six different regions are given as

$$\psi_1(\mathbf{r}) = \psi_{inc}(\mathbf{r}) + \sum'_{\ell m} A_{\ell m} r_\mu^{-\ell-1} Y_\ell^m(\theta_\mu, \phi_\mu) + \sum'_{\ell m} A_{\ell m}^r r_{\bar{\mu}}^{-\ell-1} Y_\ell^m(\theta_{\bar{\mu}}, \phi_{\bar{\mu}}), \quad (3.6a)$$

$$\psi_2(\mathbf{r}) = \psi_{inc}^t(\mathbf{r}) + \sum'_{\ell m} A_{\ell m}^t r_\mu^{-\ell-1} Y_\ell^m(\theta_\mu, \phi_\mu), \quad (3.6b)$$

$$\psi_3(\mathbf{r}) = \psi_0 + \sum'_{\ell m} B_{\ell m} r_\mu^\ell Y_\ell^m(\theta_\mu, \phi_\mu) + \sum'_{\ell m} B_{\ell m}^r r_{\bar{\mu}}^\ell Y_\ell^m(\theta_{\bar{\mu}}, \phi_{\bar{\mu}}), \quad (3.6c)$$

$$\psi_4(\mathbf{r}) = \psi_0 + \sum'_{\ell m} B_{\ell m}^t r_\mu^\ell Y_\ell^m(\theta_\mu, \phi_\mu), \quad (3.6d)$$

$$\begin{aligned} \psi_5(\mathbf{r}) = & \psi_c + \sum'_{\ell m} \mathcal{A}_{\ell m} r_\mu^{-\ell-1} Y_\ell^m(\theta_\mu, \phi_\mu) + \sum'_{\ell m} \mathcal{B}_{\ell m} r_\mu^\ell Y_\ell^m(\theta_\mu, \phi_\mu), \\ & + \sum'_{\ell m} \mathcal{A}_{\ell m}^r r_{\bar{\mu}}^{-\ell-1} Y_\ell^m(\theta_{\bar{\mu}}, \phi_{\bar{\mu}}) + \sum'_{\ell m} \mathcal{B}_{\ell m}^r r_{\bar{\mu}}^\ell Y_\ell^m(\theta_{\bar{\mu}}, \phi_{\bar{\mu}}), \end{aligned} \quad (3.6e)$$

$$\psi_6(\mathbf{r}) = \psi_c + \sum'_{\ell m} \mathcal{A}_{\ell m}^t r_\mu^{-\ell-1} Y_\ell^m(\theta_\mu, \phi_\mu) + \sum'_{\ell m} \mathcal{B}_{\ell m}^t r_\mu^\ell Y_\ell^m(\theta_\mu, \phi_\mu), \quad (3.6f)$$

with $\ell = 1, 2, 3, \dots$ and $m = 0, \pm 1, \pm 2, \dots, \pm \ell$, with coordinates as shown in figure 3.1, and the apostrophes above the sums are just reminders that the $\ell = 0$ terms have been extracted. The $\ell = 0$ terms in the sums with positive powers of the radius are constant and have been named ψ_0 inside the sphere and ψ_c in the coating layer. In the ambient, the constant potential term is set to zero, since the reference point for the potential may be chosen freely. The $\ell = 0$ terms in the sums with negative powers of the radius, on the other hand, is zero due to the assumption that there is no free charge present. $\psi_{\text{inc}}^t(\mathbf{r})$ and $\psi_{\text{inc}}^t(\mathbf{r})$ are the potential terms originating from the incident field, and are given by

$$\psi_{\text{inc}}(\mathbf{r}) = -rE_0\sqrt{\frac{2\pi}{3}} \left[\cos\theta_0 Y_1^0(\theta, \phi)\sqrt{2} + \sin\theta_0 \{e^{i\phi_0}Y_1^{-1}(\theta, \phi) - e^{-i\phi_0}Y_1^1(\theta, \phi)\} \right], \quad (3.7a)$$

$$\begin{aligned} \psi_{\text{inc}}^t(\mathbf{r}) = E_0 & \left[d\{(\varepsilon_1/\varepsilon_2) - 1\} \cos\theta_0 \right. \\ & \left. - r\sqrt{\frac{2\pi}{3}} [(\varepsilon_1/\varepsilon_2) \cos\theta_0 Y_1^0(\theta, \phi)\sqrt{2} + \sin\theta_0 \{e^{i\phi_0}Y_1^{-1}(\theta, \phi) - e^{-i\phi_0}Y_1^1(\theta, \phi)\}] \right] \end{aligned} \quad (3.7b)$$

These expressions are nothing more than $-\mathbf{r} \cdot \mathbf{E}_0$ written in terms of spherical harmonics, as defined in (2.11).

The reflected and transmitted amplitudes are handled using the classical image charge technique [3, p. 121], giving

$$A_{\ell m}^r = (-1)^{\ell+m} \frac{\varepsilon_1 - \varepsilon_2}{\varepsilon_1 + \varepsilon_2} A_{\ell m}, \quad A_{\ell m}^t = \frac{2\varepsilon_1}{\varepsilon_1 + \varepsilon_2} A_{\ell m}, \quad (3.8a)$$

$$B_{\ell m}^r = (-1)^{\ell+m} \frac{\varepsilon_3 - \varepsilon_4}{\varepsilon_3 + \varepsilon_4} B_{\ell m}, \quad B_{\ell m}^t = \frac{2\varepsilon_3}{\varepsilon_3 + \varepsilon_4} B_{\ell m}, \quad (3.8b)$$

$$\mathcal{A}_{\ell m}^r = (-1)^{\ell+m} \frac{\varepsilon_5 - \varepsilon_6}{\varepsilon_5 + \varepsilon_6} \mathcal{A}_{\ell m}, \quad \mathcal{A}_{\ell m}^t = \frac{2\varepsilon_5}{\varepsilon_5 + \varepsilon_6} \mathcal{A}_{\ell m}, \quad (3.8c)$$

$$\mathcal{B}_{\ell m}^r = (-1)^{\ell+m} \frac{\varepsilon_5 - \varepsilon_6}{\varepsilon_5 + \varepsilon_6} \mathcal{B}_{\ell m}, \quad \mathcal{B}_{\ell m}^t = \frac{2\varepsilon_5}{\varepsilon_5 + \varepsilon_6} \mathcal{B}_{\ell m}. \quad (3.8d)$$

These relations may be indirectly verified by demonstrating that they lead to the fulfilment of the boundary conditions in (2.13) across the substrate boundary. In appendix A this is as mentioned demonstrated for the continuity of the potential between the coating regions 5 and 6, and it may easily be shown that it holds for both boundary conditions at all the required interfaces, namely between region 1 and 2, 3 and 4 and 5 and 6.

Still there remains four unknown coefficients for every multipole order, and these are handled by considering the continuity of the potential and the normal derivative times the permittivity on the two spherical surfaces. In order to take full advantage of the orthogonality of the spherical harmonics, a weak formulation of the boundary conditions is used, where the continuity relations are multiplied by a complex conjugated spherical harmonic and integrated across the spherical interface, i.e. they are projected upon the spherical

3 Coated island geometry

harmonics, giving [2, p. 229]

$$\begin{aligned} & \int_{-1}^{t_{rc}} d(\cos \theta) \int_0^{2\pi} d\phi \ (\psi_1 - \psi_5)|_{r=R_c} [Y_{\ell'}^{m'}(\theta, \phi)]^* \\ & + \int_{t_{rc}}^1 d(\cos \theta) \int_0^{2\pi} d\phi \ (\psi_2 - \psi_6)|_{r=R_c} [Y_{\ell'}^{m'}(\theta, \phi)]^* = 0, \end{aligned} \quad (3.9a)$$

$$\begin{aligned} & \int_{-1}^{t_r} d(\cos \theta) \int_0^{2\pi} d\phi \ (\psi_5 - \psi_3)|_{r=R} [Y_{\ell'}^{m'}(\theta, \phi)]^* \\ & + \int_{t_r}^1 d(\cos \theta) \int_0^{2\pi} d\phi \ (\psi_6 - \psi_4)|_{r=R} [Y_{\ell'}^{m'}(\theta, \phi)]^* = 0, \end{aligned} \quad (3.9b)$$

$$\begin{aligned} & \int_{-1}^{t_{rc}} d(\cos \theta) \int_0^{2\pi} d\phi \left[\frac{\partial}{\partial r} (\varepsilon_1 \psi_1 - \varepsilon_5 \psi_5) \right] \Big|_{r=R_c} [Y_{\ell'}^{m'}(\theta, \phi)]^* \\ & + \int_{t_{rc}}^1 d(\cos \theta) \int_0^{2\pi} d\phi \left[\frac{\partial}{\partial r} (\varepsilon_2 \psi_2 - \varepsilon_6 \psi_6) \right] \Big|_{r=R_c} [Y_{\ell'}^{m'}(\theta, \phi)]^* = 0, \end{aligned} \quad (3.9c)$$

$$\begin{aligned} & \int_{-1}^{t_r} d(\cos \theta) \int_0^{2\pi} d\phi \left[\frac{\partial}{\partial r} (\varepsilon_5 \psi_5 - \varepsilon_3 \psi_3) \right] \Big|_{r=R} [Y_{\ell'}^{m'}(\theta, \phi)]^* \\ & + \int_{t_r}^1 d(\cos \theta) \int_0^{2\pi} d\phi \left[\frac{\partial}{\partial r} (\varepsilon_6 \psi_6 - \varepsilon_4 \psi_4) \right] \Big|_{r=R} [Y_{\ell'}^{m'}(\theta, \phi)]^* = 0, \end{aligned} \quad (3.9d)$$

where $\ell' = 0, 1, \dots$ and $m' = 0, \pm 1, \dots, \pm \ell'$, and with the following definitions for the truncation parameters

$$t \equiv \frac{z}{R}, \quad t_c \equiv \frac{z}{R_c}, \quad (3.10a)$$

$$t_r \equiv \frac{d}{R}, \quad t_{rc} \equiv \frac{d}{R_c}. \quad (3.10b)$$

Thus, when the potentials (3.6) are inserted, the result will be four infinite sets of linear equations for the multipole expansion coefficients. In practice, this set is solved numerically by truncating the multipole expansion for a certain $\ell = M$. Investigations performed in by Simonsen and Lazzari [10] showed that $M = 16$ in many cases was sufficient for the uncoated system, but in general the M -dependence should be investigated thoroughly, which is to be done in section 6.2.

Before stating the resulting finite set of linear equations, some simplification may be done by noting that the equations for different m 's do not couple for $|m| > 1$. This means that all the right hand side terms of the equations, to be stated in (3.12), are zero for $|m| > 1$, so that all systems of equations with higher m 's are homogeneous and thus gives the unique and trivial solution that the corresponding expansion coefficients are zero. Therefore only $|m| \leq 1$ has to be considered.

In addition it is easily shown that the $m = -1$ equation is superfluous. Following Bedeaux and Vlieger [2, p. 232], this is done by noting that the integrals defined in (3.15) are invariant to a change of sign of m , while the right hand side, H_l^m and J_l^m , both gains a phase factor $-\exp(-i\phi_0)$. Thus the solution of the $m = -1$ system gives the exact same information as the $m = 1$ system, with solutions only differing by a phase factor $-\exp(-i2\phi_0)$. A full derivation of the system of equations is given in appendix B, and the

result reads

$$\sum_{\ell_1=1}^M R_c^{-\ell_1-2} A_{\ell_1 m} C_{\ell\ell_1}^m(t_{rc}) - \sum_{\ell_1=1}^M R_c^{-\ell_1-2} \mathcal{A}_{\ell_1 m} \mathcal{C}_{\ell\ell_1}^m(t_{rc}) + \sum_{\ell_1=1}^M R_c^{\ell_1-1} \mathcal{B}_{\ell_1 m} \mathcal{D}_{\ell\ell_1}^m(t_{rc}) = H_\ell^m(t_{rc}), \quad (3.11a)$$

$$\sum_{\ell_1=1}^M R^{\ell_1-1} B_{\ell_1 m} D_{\ell\ell_1}^m(t_r) + \sum_{\ell_1=1}^M R^{-\ell_1-2} \mathcal{A}_{\ell_1 m} \mathcal{C}_{\ell\ell_1}^m(t_r) - \sum_{\ell_1=1}^M R^{\ell_1-1} \mathcal{B}_{\ell_1 m} \mathcal{D}_{\ell\ell_1}^m(t_r) = 0, \quad (3.11b)$$

$$\sum_{\ell_1=1}^M R_c^{-\ell_1-2} A_{\ell_1 m} F_{\ell\ell_1}^m(t_{rc}) - \sum_{\ell_1=1}^M R_c^{-\ell_1-2} \mathcal{A}_{\ell_1 m} \mathcal{F}_{\ell\ell_1}^m(t_{rc}) + \sum_{\ell_1=1}^M R_c^{\ell_1-1} \mathcal{B}_{\ell_1 m} \mathcal{G}_{\ell\ell_1}^m(t_{rc}) = J_\ell^m(t_{rc}), \quad (3.11c)$$

$$\sum_{\ell_1=1}^M R^{\ell_1-1} B_{\ell_1 m} G_{\ell\ell_1}^m(t_r) + \sum_{\ell_1=1}^M R^{-\ell_1-2} \mathcal{A}_{\ell_1 m} \mathcal{F}_{\ell\ell_1}^m(t_r) - \sum_{\ell_1=1}^M R^{\ell_1-1} \mathcal{B}_{\ell_1 m} \mathcal{G}_{\ell\ell_1}^m(t_r) = 0, \quad (3.11d)$$

where $\ell = 1, 2, 3, \dots, M$ and $m = 0, 1$, and where left hand side, which originates from the incident field, is given by

$$H_\ell^m(t_r) = \sqrt{\frac{4\pi}{3}} E_0 \cos \theta_0 \delta_{m0} \left\{ \frac{\varepsilon_1}{\varepsilon_2} \delta_{\ell 1} + \left(\frac{\varepsilon_1 - \varepsilon_2}{\varepsilon_2} \right) \left[\sqrt{3} t_r \zeta_{\ell 0}^0 Q_{\ell 0}^0(t_r) - \zeta_{\ell 1}^0 Q_{\ell 1}^0(t_r) \right] \right\} \\ + \sqrt{\frac{2\pi}{3}} E_0 \sin \theta_0 \delta_{\ell 1} \left\{ e^{i\phi_0} \delta_{m-1} - e^{-i\phi_0} \delta_{m1} \right\}, \quad (3.12a)$$

$$J_\ell^m(t_r) = \sqrt{\frac{4\pi}{3}} E_0 \cos \theta_0 \varepsilon_1 \delta_{\ell 1} \delta_{m0} \\ + \sqrt{\frac{2\pi}{3}} E_0 \sin \theta_0 \left\{ \varepsilon_2 \delta_{\ell 1} [e^{i\phi_0} \delta_{m-1} - e^{-i\phi_0} \delta_{m1}] \right. \\ \left. + (\varepsilon_1 - \varepsilon_2) [e^{i\phi_0} \zeta_{\ell 1}^{-1} Q_{\ell 1}^{-1}(t_r) \delta_{m-1} - e^{-i\phi_0} \zeta_{\ell 1}^1 Q_{\ell 1}^1(t_r) \delta_{m1}] \right\}, \quad (3.12b)$$

where the prefactors from the spherical harmonics has been denoted by

$$\zeta_{\ell\ell_1}^m \equiv \frac{1}{2} \left[\frac{(2\ell+1)(2\ell_1+1)(\ell-m)!(\ell_1-m)!}{(\ell+m)!(\ell_1+m)!} \right]^{\frac{1}{2}}. \quad (3.13)$$

In the system of equations, (B.33), certain other quantities have been introduced,

$$C_{\ell\ell_1}^m(\varepsilon_1, \varepsilon_2, t_r) \equiv \zeta_{\ell\ell_1}^m \left[K_{\ell\ell_1}^m[\mu](t_r) + \left(\frac{\varepsilon_1 - \varepsilon_2}{\varepsilon_1 + \varepsilon_2} \right) (-1)^{\ell_1+m} K_{\ell\ell_1}^m[\bar{\mu}](t_r) \right. \\ \left. + \left(\frac{2\varepsilon_1}{\varepsilon_1 + \varepsilon_2} \right) \{ K_{\ell\ell_1}^m[\mu](t_r=1) - K_{\ell\ell_1}^m[\bar{\mu}](t_r) \} \right], \quad (3.14a)$$

$$D_{\ell\ell_1}^m(\varepsilon_3, \varepsilon_4, t_r) \equiv -\zeta_{\ell\ell_1}^m \left[M_{\ell\ell_1}^m[\mu](t_r) + \left(\frac{\varepsilon_3 - \varepsilon_4}{\varepsilon_3 + \varepsilon_4} \right) (-1)^{\ell_1+m} M_{\ell\ell_1}^m[\bar{\mu}](t_r) \right. \\ \left. + \left(\frac{2\varepsilon_3}{\varepsilon_3 + \varepsilon_4} \right) \{ M_{\ell\ell_1}^m[\mu](t_r=1) - M_{\ell\ell_1}^m[\bar{\mu}](t_r) \} \right], \quad (3.14b)$$

$$F_{\ell\ell_1}^m(\varepsilon_1, \varepsilon_2, t_r) \equiv \zeta_{\ell\ell_1}^m \left[\left(\frac{2\varepsilon_1}{\varepsilon_1 + \varepsilon_2} \right) L_{\ell\ell_1}^m[\mu](t_r=1) \right. \\ \left. + \varepsilon_1 \left(\frac{\varepsilon_1 - \varepsilon_2}{\varepsilon_1 + \varepsilon_2} \right) \{ L_{\ell\ell_1}^m[\mu](t_r) + (-1)^{\ell_1+m} L_{\ell\ell_1}^m[\bar{\mu}](t_r) \} \right], \quad (3.14c)$$

$$G_{\ell\ell_1}^m(\varepsilon_3, \varepsilon_4, t_r) \equiv -\zeta_{\ell\ell_1}^m \left[\left(\frac{2\varepsilon_3}{\varepsilon_3 + \varepsilon_4} \right) N_{\ell\ell_1}^m[\mu](t_r=1) \right. \\ \left. + \varepsilon_3 \left(\frac{\varepsilon_3 - \varepsilon_4}{\varepsilon_3 + \varepsilon_4} \right) \{ N_{\ell\ell_1}^m[\mu](t_r) + (-1)^{\ell_1+m} N_{\ell\ell_1}^m[\bar{\mu}](t_r) \} \right], \quad (3.14d)$$

3 Coated island geometry

and with integrals over the product of different associated Legendre functions denoted by

$$Q_{\ell\ell_1}^m(t_r) \equiv \int_{-1}^{t_r} P_\ell^m(x) P_{\ell_1}^m(x) dx, \quad (3.15a)$$

$$K_{\ell\ell_1}^m[\eta](t_r) \equiv \int_{-1}^{t_r} P_\ell^m(x) P_{\ell_1}^m(\cos\theta_\eta|_{r=R}) \times (\chi[\eta](x, R))^{-(\ell_1+1)/2} dx, \quad (3.15b)$$

$$L_{\ell\ell_1}^m[\eta](t_r) \equiv \int_{-1}^{t_r} \left[P_\ell^m(x) \partial_r \left\{ P_{\ell_1}^m(\cos\theta_\eta) \times (\chi[\eta](x, r))^{-(\ell_1+1)/2} \right\} \right]_{r=R} dx, \quad (3.15c)$$

$$M_{\ell\ell_1}^m[\eta](t_r) \equiv \int_{-1}^{t_r} P_\ell^m(x) P_{\ell_1}^m(\cos\theta_\eta|_{r=R}) \times (\chi[\eta](x, R))^{\ell_1/2} dx, \quad (3.15d)$$

$$N_{\ell\ell_1}^m[\eta](t_r) \equiv \int_{-1}^{t_r} \left[P_\ell^m(x) \partial_r \left\{ P_{\ell_1}^m(\cos\theta_\eta) \times (\chi[\eta](x, r))^{\ell_1/2} \right\} \right]_{r=R} dx. \quad (3.15e)$$

using the definition $x = \cos\theta$, and with the following shorthand forms:

$$C_{\ell\ell_1}^m(t_r) = C_{\ell\ell_1}^m(\varepsilon_1, \varepsilon_2, t_r), \quad \mathcal{C}_{\ell\ell_1}^m(t_r) = C_{\ell\ell_1}^m(\varepsilon_5, \varepsilon_6, t_r), \quad (3.16a)$$

$$D_{\ell\ell_1}^m(t_r) = D_{\ell\ell_1}^m(\varepsilon_3, \varepsilon_4, t_r), \quad \mathcal{D}_{\ell\ell_1}^m(t_r) = D_{\ell\ell_1}^m(\varepsilon_5, \varepsilon_6, t_r), \quad (3.16b)$$

$$F_{\ell\ell_1}^m(t_r) = F_{\ell\ell_1}^m(\varepsilon_1, \varepsilon_2, t_r), \quad \mathcal{F}_{\ell\ell_1}^m(t_r) = F_{\ell\ell_1}^m(\varepsilon_5, \varepsilon_6, t_r), \quad (3.16c)$$

$$G_{\ell\ell_1}^m(t_r) = G_{\ell\ell_1}^m(\varepsilon_3, \varepsilon_4, t_r), \quad \mathcal{G}_{\ell\ell_1}^m(t_r) = G_{\ell\ell_1}^m(\varepsilon_5, \varepsilon_6, t_r). \quad (3.16d)$$

3.2 Interaction between islands

The preceding result gave the polarisability of a single coated island without regard for the interaction with the surrounding islands, and in the low coverage limit this may be satisfying. However, for higher coverages, a correction is needed. If the restriction is imposed that the separation between the islands is much smaller than the wavelength of the incident light, so that all the islands are considered to be excited by the same incident field, a correction may be acquired. In the simplest approximation, the dipole approximation, all the particles are influenced by excited dipoles in the surrounding islands and in their images. For a regular array of spheres with sphere centres lying above the substrate, the polarisabilities are modified according to [2, p. 181][6]

$$\alpha_\perp^I = \frac{\alpha_\perp}{1 - 2\alpha_\perp I_\perp^{20}}, \quad \alpha_\parallel^I = \frac{\alpha_\parallel}{1 - \alpha_\parallel I_\parallel^{20}} \quad (3.17)$$

where α_\perp and α_\parallel are the polarisabilities of the single island considered so far. I_\perp^{20} and I_\parallel^{20} are the interaction functions, defined as [6]

$$I_\perp^{20} = \frac{1}{\sqrt{20\pi L^3 \varepsilon_2}} \left[S_{20} - \left(\frac{\varepsilon_2 - \varepsilon_1}{\varepsilon_2 + \varepsilon_1} \right) S_{20}^r \right], \quad (3.18a)$$

$$I_\parallel^{20} = \frac{1}{\sqrt{20\pi L^3 \varepsilon_2}} \left[S_{20} + \left(\frac{\varepsilon_2 - \varepsilon_1}{\varepsilon_2 + \varepsilon_1} \right) S_{20}^r \right], \quad (3.18b)$$

where ε_1 and ε_2 are the permittivities of the ambient and the substrate, respectively, and S_{20} and S_{20}^r are the direct and image lattice sums, given by [6]

$$S_{20} = \sum_{i \neq 0} \left(\frac{L}{r} \right)^3 Y_2^0(\theta, \phi)|_{r=R_i}, \quad (3.19a)$$

$$S_{20}^r = \sum_{i \neq 0} \left(\frac{L}{r} \right)^3 Y_2^0(\theta, \phi) |_{r=R_i^r}, \quad (3.19b)$$

with L as the lattice constant, and the first sum is over all the multipole expansion centres, and the second over all the image locations. Note that the sums exclude the $i = 0$ term, since this corresponds to the interaction with the island's own image, which is already taken into account.

The validity of this approximation has been tested by Ingve Simonsen and Rémi Lazzari [6] for the case of uncoated islands. There, they showed that the difference between the dipole and the more precise quadrupole approximation was small up to a coverage of about 40 percent, a coverage higher than what is experimentally interesting [6]. This test has as of now not been performed for a coated system, but there seems no reason that the results would be critically different for the coated system, and the dipole approximation will be used in the following.

4 Numerical implementation

The presented expansion of Bedeaux and Vlieger's work [2] has been implemented into Lazzari and Simonsen's software package GranFilm [6] under the supervision of Ingve Simonsen himself. The implementation has been rather tentative in that robustness has not been given priority and that various hacks have been used, and the possible parameter space has been greatly reduced. This means that the large range of possible methods and cases supported in the original GranFilm code are not available for the coated island geometry. Eventual improvements on this point would come at a later stage, after numerical, and perhaps experimental, validation have been seen.

Partly because of this hacker's approach and the resulting unfinishedness of the modifications, a full presentation of the code is not included in this thesis. Another reason is that the vastness of the original code makes such a documentation a considerable task. Anyway, using the original GranFilm documentation [6], the necessary modifications should be relatively intuitive. The main task is to expand the system of linear equations that GranFilm computes. The original code calculated two sets of expansion coefficients, while the modified needs to calculate four sets, namely $A_{\ell m}$, $B_{\ell m}$, $\mathcal{A}_{\ell m}$ and $\mathcal{B}_{\ell m}$. Luckily, the various integrals and defined quantities are strikingly equal to those of the unmodified system, so that the expansion of the equation set up is mostly straightforward.

After the system of equations has been solved and the expansion coefficients found, the constitutive coefficients and the Fresnel coefficients are found in the exact same way as in the unmodified code. However, in various points in the code the different quantities are normalized by quantities depending on the radius of the islands. In these cases it is important to make sure that the appropriate radius, either R or R_c , is used. But unfortunately it is not always easy to chose which radius is appropriate. Sometimes the various quantities involving the radius is interdependent in a way so that unexpected errors may appear. This danger arises partially because the current architecture of the GranFilm code is not directly tailored to make room for such coated sphere support, so that some of the tricks used in the original code may make the modification troublesome.

A representative example of such an error is the definition of the island density as the coverage percent divided by the area covered by a single island. If the area covered by a single island is calculated using the total radius R_c , an increase in coating thickness would lead to a lower island density. This, of course, does not fit the experimental situation where the coating is applied to a surface with a fixed number of islands. Other issues concerning the choice of radius arise in the calculation of boundary condition errors, where various quantities are normalized by different powers of different radii.

Since these types of error have proven to be fatal in the early process of the implementation, great care has been taken in seeing that the appropriate radii has been chosen. But still, the issue seems worth mentioning, since the numerical testing in section 6.2 will reveal some disquieting results, and programming error can of course not be excluded as a possible source of these results.

5 Results

At this point, some results will be given to ease the curiosity of the reader. However, bear in mind that these results are not to be taken for final due to a number of issues to be discussed further in section 6.2.

For this first test drive of the modified code, a system will be used that is similar to one studied by Simonsen and Lazzari [6], shown in figure 1.1. Basically, the system consists of silver islands of radius 8 nm deposited on a substrate of magnesium oxide and coated with a layer of silicon oxide, surrounded by an ambient of vacuum. The permittivity for silver and silicon oxide is given in figure 5.1, showing the typical relation between the imaginary and real parts of metals and semiconductors. The coverage of the silver islands is set to 30% of the substrate area. The incoming light falls at an angle of $\theta_0 = 45^\circ$, and with p-polarization, since this leads to charge excitation in direction both parallel and normal to the substrate, as argued from (2.20c). The truncation ratio t_r will be set to zero. These parameters, together with the full set of parameters given in appendix C, will in the following treatment be used as a standard test case, if not otherwise specified.

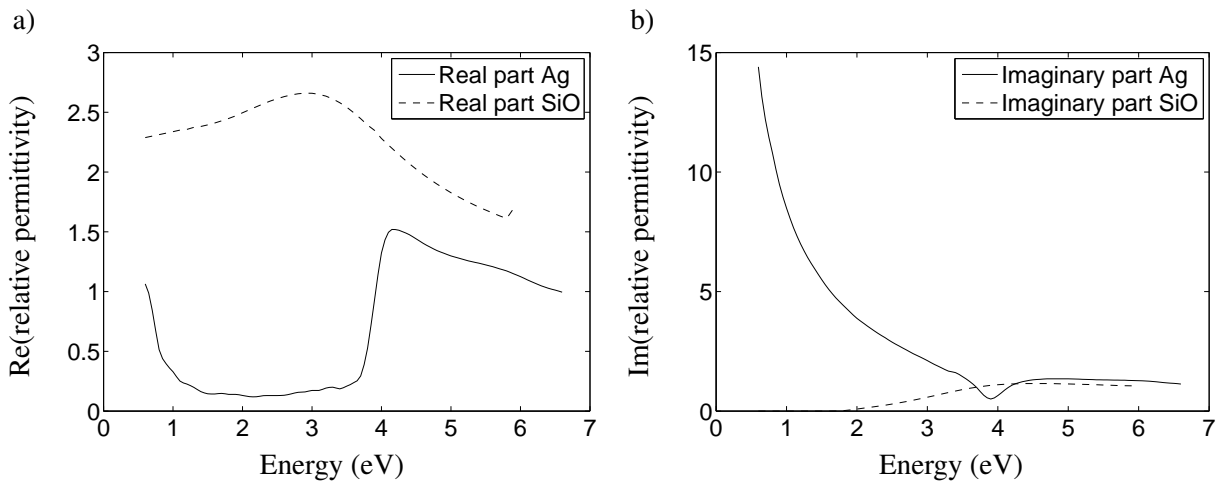


Figure 5.1: a) real and b) imaginary parts of the relative dielectric functions of Ag and SiO.

GranFilm offers a variety of types of output, but in this thesis the standard form will be the differential reflectivity, given as

$$\frac{\Delta R}{R} = \frac{R - R_0}{R}, \quad (5.1)$$

where R is the reflection coefficient, and R_0 is the reflection coefficient of the substrate without the coated islands. With the presented default case, but with varying coating thickness, the differential reflectivity of the surface is given in figure 5.2. In the figure, a peak and a dip is highly visible, originating from excited charge vibration in perpendicular and normal direction, respectively. As discussed in the introduction, if the goal is to find an unknown coating thickness from a measured differential reflectivity spectrum, the movement of this peak and dip with respect to the coating thickness is of prime interest. A peak or dip position highly sensitive to the coating thickness could give relatively accurate results for the coating thickness, to the extent that the presented model is correct. The behaviour shown in figure 5.2 does indeed seem satisfying, at least the movement of the peak position. However, a meaningful evaluation of these

5 Results

results require some concept of the intended case and experimental set up, which is not fully developed at this early stage.

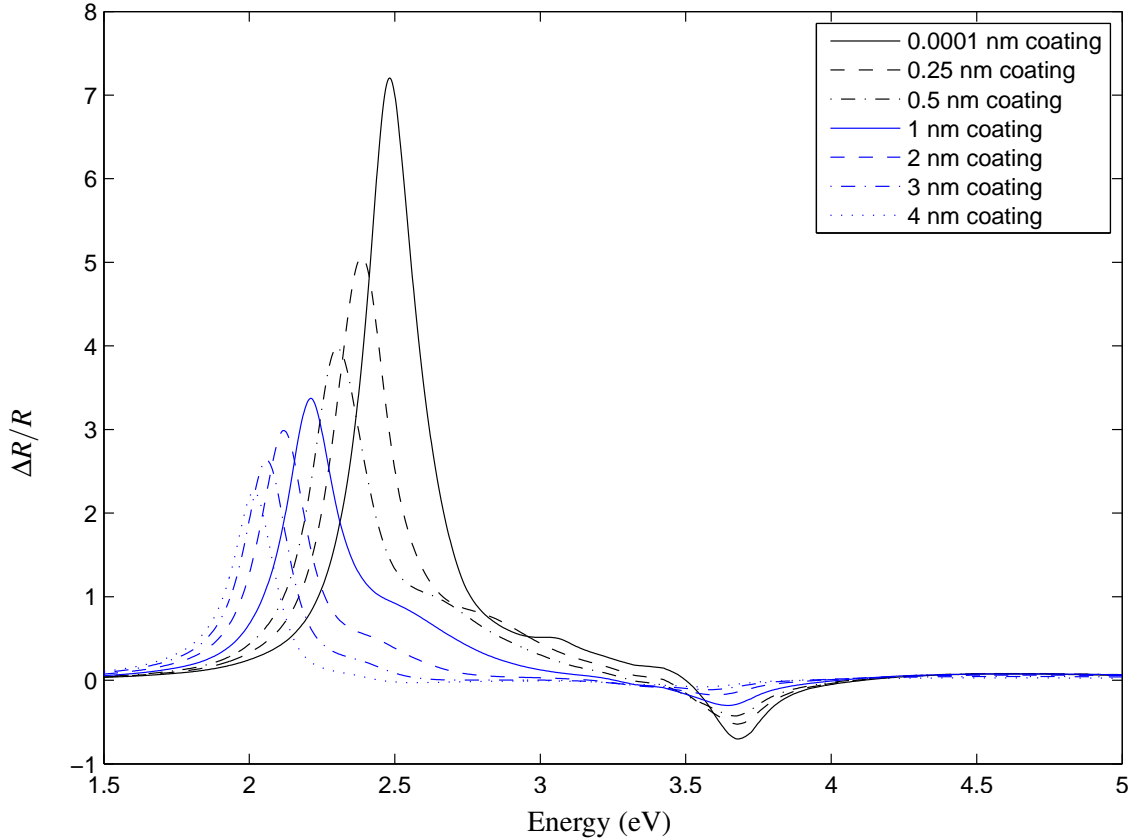


Figure 5.2: Differential reflectivity for the default case of 8 nm Ag hemispheres on a MgO substrate, coated with a layer of SiO with varying thickness and with $M = 16$

From the figure it is also evident that even a thin layer of silicon oxide greatly reduces the size of the differential reflectivity peak and dip. In an experimental setup this would lead to a lower signal-to-noise ratio. To what degree this would be a problem, depends on the specific experimental setup.

The behaviour of the differential reflectivity shown in figure 5.2, namely that the peak moves towards lower energies, seems from the model to be fairly general for this type of system, i.e. metal islands coated with a semiconductor. It has been tested for several types of materials and truncation parameters, but it does not seem necessary to include any more plots showing the exact details, since the results as mentioned should be considered as work in progress.

6 Analytical and numerical evaluation

In the following the results obtained so far will be evaluated and tested. First, in section 6.1 the system of equations in (B.33) is checked for consistency with the system of equations derived by Bedeaux and Vlieger for uncoated spheres. Next, the numerical results will be evaluated in various ways.

6.1 Analytical validation

The coated system studied in this thesis may be seen as a general case, with the uncoated spheres studied Bedeaux and Vlieger [2] as a special case where the coating has in some way vanished. It would therefore be expected that in certain limits where the coating vanishes the derived system of equations, (B.33), should reduce to that derived by Bedeaux and Vlieger [2]. Even if this is not a complete verification of the derived equations, it does provide an opportunity to discover inconsistencies and may at least give an indication that it might be correct. For reference, the set of equations for the uncoated system, taken from Bedeaux and Vlieger's book [2, 233], reads

$$\sum_{\ell_1=1}^M R^{-\ell_1-2} A_{\ell_1 m} C_{\ell\ell_1}^m(t_r) + \sum_{\ell_1=1}^M R^{\ell_1-1} B_{\ell_1 m} D_{\ell\ell_1}^m(t_r) = H_\ell^m(t_r), \quad (6.1a)$$

$$\sum_{\ell_1=1}^M R^{-\ell_1-2} A_{\ell_1 m} F_{\ell\ell_1}^m(t_r) + \sum_{\ell_1=1}^M R^{\ell_1-1} B_{\ell_1 m} G_{\ell\ell_1}^m(t_r) = J_\ell^m(t_r), \quad (6.1b)$$

6.1.1 Vanishing coating thickness

The first test is when the coating thickness becomes zero, i.e. the limit where $R_c \rightarrow R$, or equivalently, where $t_{rc} \rightarrow t_r$. Then (3.11a) and (3.11b) may be added, giving

$$\begin{aligned} & \sum_{\ell_1=1}^M R_c^{-\ell_1-2} A_{\ell_1 m} C_{\ell\ell_1}^m(t_{rc}) + \sum_{\ell_1=1}^M R^{\ell_1-1} B_{\ell_1 m} D_{\ell\ell_1}^m(t_r) \\ & + \sum_{\ell_1=1}^M \mathcal{A}_{\ell_1 m} \left[R^{-\ell_1-2} \mathcal{C}_{\ell\ell_1}^m(t_r) - R_c^{-\ell_1-2} \mathcal{C}_{\ell\ell_1}^m(t_{rc}) \right] + \sum_{\ell_1=1}^M \mathcal{B}_{\ell_1 m} \left[R_c^{\ell_1-1} \mathcal{D}_{\ell\ell_1}^m(t_{rc}) - R^{\ell_1-1} \mathcal{D}_{\ell\ell_1}^m(t_r) \right] \\ & = H_\ell^m(t_{rc}). \end{aligned} \quad (6.2)$$

By studying the expressions in square brackets, it is clear that they vanish in the limit of zero coating thickness, so that what is left is exactly (6.1a). (6.1b) may be obtained in the exact same manner by adding equations (3.11c) and (3.11d). So, although not conclusive, this consistency is a good sign.

6.1.2 A coating of island material

The second test is a system where the islands has a coating of finite thickness, but where the coating is made of the same material as the island. Specifically, this means that the island and coating are given the same dielectric function, i.e. $\epsilon_5 = \epsilon_3$ and $\epsilon_6 = \epsilon_4$. In this case, $\mathcal{D}_{\ell\ell_1}^m(t_r) = D_{\ell\ell_1}^m(t_r)$ and $\mathcal{G}_{\ell\ell_1}^m(t_r) = G_{\ell\ell_1}^m(t_r)$. Equations (3.11b) and (3.11d) then reduce to

$$\sum_{\ell_1=1}^M R^{\ell_1-1} (B_{\ell_1 m} - \mathcal{B}_{\ell_1 m}) D_{\ell\ell_1}^m(t_r) + \sum_{\ell_1=1}^M R^{-\ell_1-2} \mathcal{A}_{\ell_1 m} \mathcal{C}_{\ell\ell_1}^m(t_r) = 0, \quad (6.3a)$$

$$\sum_{\ell_1=1}^M R^{\ell_1-1} (B_{\ell_1 m} - \mathcal{B}_{\ell_1 m}) G_{\ell\ell_1}^m(t_r) + \sum_{\ell_1=1}^M R^{-\ell_1-2} \mathcal{A}_{\ell_1 m} \mathcal{F}_{\ell\ell_1}^m(t_r) = 0, \quad (6.3b)$$

which is a square, homogeneous system of linear equations. Such a system has the trivial and unique solution zero, which means that $\mathcal{A}_{\ell_1 m} = 0$ and $\mathcal{B}_{\ell_1 m} = B_{\ell_1 m}$ for ℓ_1 and m in the relevant range. After inserting these solutions into equations (3.11a) and (3.11c), the system of equation in 6.1 is retrieved, as hoped.

6.1.3 A coating of ambient material

It would also be expected that in the limit where the islands are coated with the ambient material, the equations should reduce to (6.1) in a similar manner as in the case of a coating made of island material. However, it turns out not to be that simple. A coating made of ambient material implies $\epsilon_5 = \epsilon_1$ and $\epsilon_6 = \epsilon_2$, and moreover that $\mathcal{C}_{\ell\ell_1}^m(t_{rc}) = C_{\ell\ell_1}^m(t_{rc})$ and $\mathcal{F}_{\ell\ell_1}^m(t_{rc}) = F_{\ell\ell_1}^m(t_{rc})$. If then equations (3.11a) and (3.11c) were to be added in an analogous way to what was done in section 6.1.2, the resulting system of equations would not be homogeneous, and the argument previously used may not be used for setting the coefficients to zero. Therefore, this approach here seems futile. This is of course not to say that the system of equations in (B.33) necessarily fails in this limit. There might be other ways to prove consistency in this limit, but the issue will not be stressed further here.

6.2 Evaluation of the numerical results

As emphasized earlier, the numerical results given by the coating-modified GranFilm code should be tested throughly in various ways. In the following the code will first be tested for it's consistency with the original GranFilm code. This is an easy way to uncover some types of errors in the implementation. But the real test is whether the boundary conditions are fulfilled, which will be investigated in the following section.

6.2.1 Consistency with original GranFilm code

As a simple way to check the validity of the modified GranFilm code, certain limit cases have been studied where the old and new code should give the same result. Eventual discrepancies could indicate errors in the implementation, or error in the analytical work overlooked in the analytical validation. However, it should be kept in mind that a consistency between the old and new code for a set of limiting cases does not fully imply that the code as a whole is correctly implemented. Implementation errors may still be presented, but rendered insignificant in the limit cases so that they pass by the consistency tests.

In the following tests, several disquieting results will be found, which adds to the uneasiness that something is wrong at some point in the code. The discrepancies uncovered in this section may to a certain degree be explained by the convergence issues uncovered in section 6.3.

6.2.1.1 Coating thickness approaching zero

When running the modified GranFilm code with coating thickness set to zero, the problem should reduce to that of a surface covered with uncoated spheres, as shown analytically in section 6.1.1. Then, the problem is also solvable using the unmodified code, thus providing a simple test of how the modified code functions in this certain limit. And as hoped, this test does indeed give as near as perfect results, as figure 6.1 shows. Figure 6.1a) displays both differential reflectivity spectra, and they are as good as indistinguishable. Figure 6.1b) shows the difference between the two spectra.

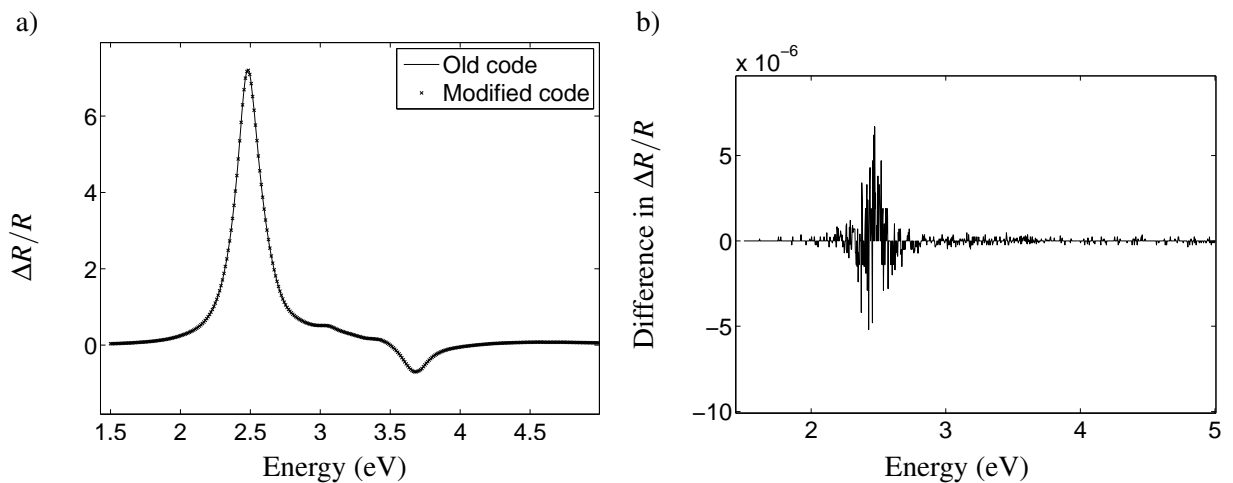


Figure 6.1: Comparison between modified and original code, for the case of Ag hemispheres on a MgO substrate, with coating thickness set to zero in the modified code, and with $M = 16$. a) shows the two differential reflectivity spectra, while b) shows the difference between them.

While figure 6.1 showed good consistency, the same can not be said if the truncation ratio is increased somewhat from zero. Figure 6.2 a) shows large discrepancies between the result of the original and modified code. However, this inconsistency is eliminated when the modified code is allowed a very thin coating layer, in figure 6.2 b) only 0.0001 nm thick.

The exact reason for the bad result for zero coating thickness may not at the present be explained fully. The determinant of the matrix being solved in the code does not at any point reach near to zero. However, the condition numbers tends to reach high levels. For the case of zero coating thickness the condition numbers reaches up to almost 20 000. When the 0.0001 nm thick SiO coating was applied, however, the condition numbers reduced to no more than 3000. This suggests that the problem lies in the numerical handling of the system of equations, and may serve as a reminder that limit cases should be approached carefully in numerical treatments.

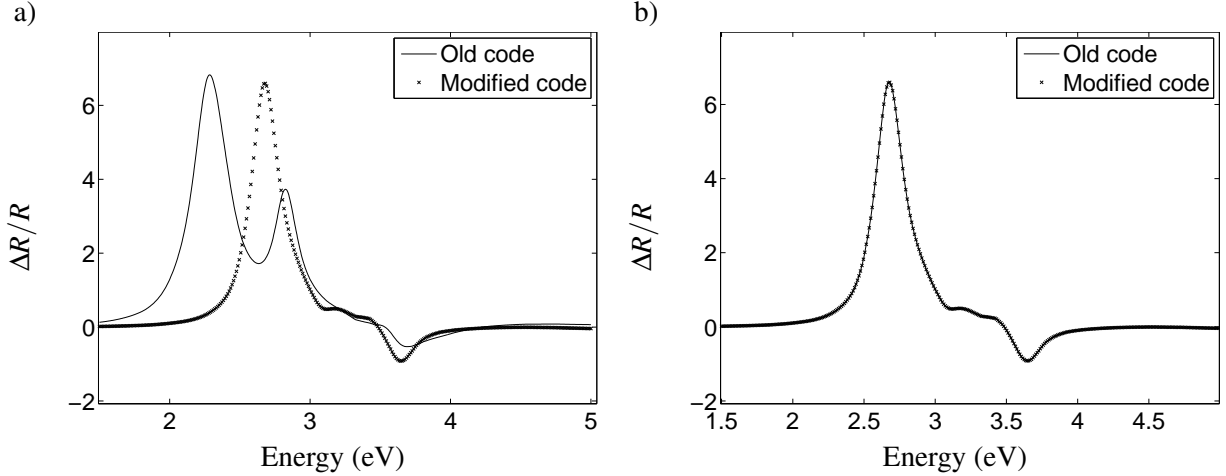


Figure 6.2: Comparison between modified and original code, for Ag spheres with a truncation ratio 0.3 on a MgO substrate, and with $M = 16$. a) shows the differential reflectivity spectra when the modified code uses a coating thickness of exactly zero, while in b) a SiO coating 0.0001 nm thick has been added to the spheres.

6.2.1.2 Coating permittivity equal to the particle permittivity

The second test is to coat the islands with a layer made of the same material as the island itself, i.e. letting $\epsilon_3 \rightarrow \epsilon_5$. This is the same as was done analytically in section 6.1.2, and should thus ideally lead to the same numerical results as that from the unmodified code with an island radius equal to the total island radius in the modified code. Unfortunately, this does not seem to hold, as seen in figure 6.3. The figure shows differential reflection curves for the unmodified code with 11 nm Ag hemispheres on MgO, together with curves for the equivalent case from the modified code with varying coating thickness. The inner island radius for the modified code has been varied according to the formula $R = 11\text{nm} - t$, where t is the coating thickness, so that the total island radius stays constant.

This unexpected behaviour is a serious indication that something is wrong at some point, either in the analytical part or in the implementation. It should also be noted that if the coating permittivity is set almost but not exactly equal to the permittivity of silver, in analogy to the zero-coating limit of section 6.2.1.1, the results are no better.

6.2.1.3 Coating permittivity approaching ambient permittivity

Another testable limit case is when the islands are coated with a layer made of the same material as the ambient, i.e. $\epsilon_3 = \epsilon_5$. As argued in the analytical validation of section 6.1.3, this coating layer should have no impact on the results. But alas, also here the modified code fails. Figure 6.4 shows differential reflection curves for a surface of 8 nm Ag hemispheres on a MgO substrate calculated with the original code, together with curves from the equivalent case of the modified code, with a vacuum coating layer of varying size. Neither this discrepancy can be accounted for, but noting that the consecutive curves seem to drop but otherwise keep their shape, it might stem from a normalisation error in the implementation.

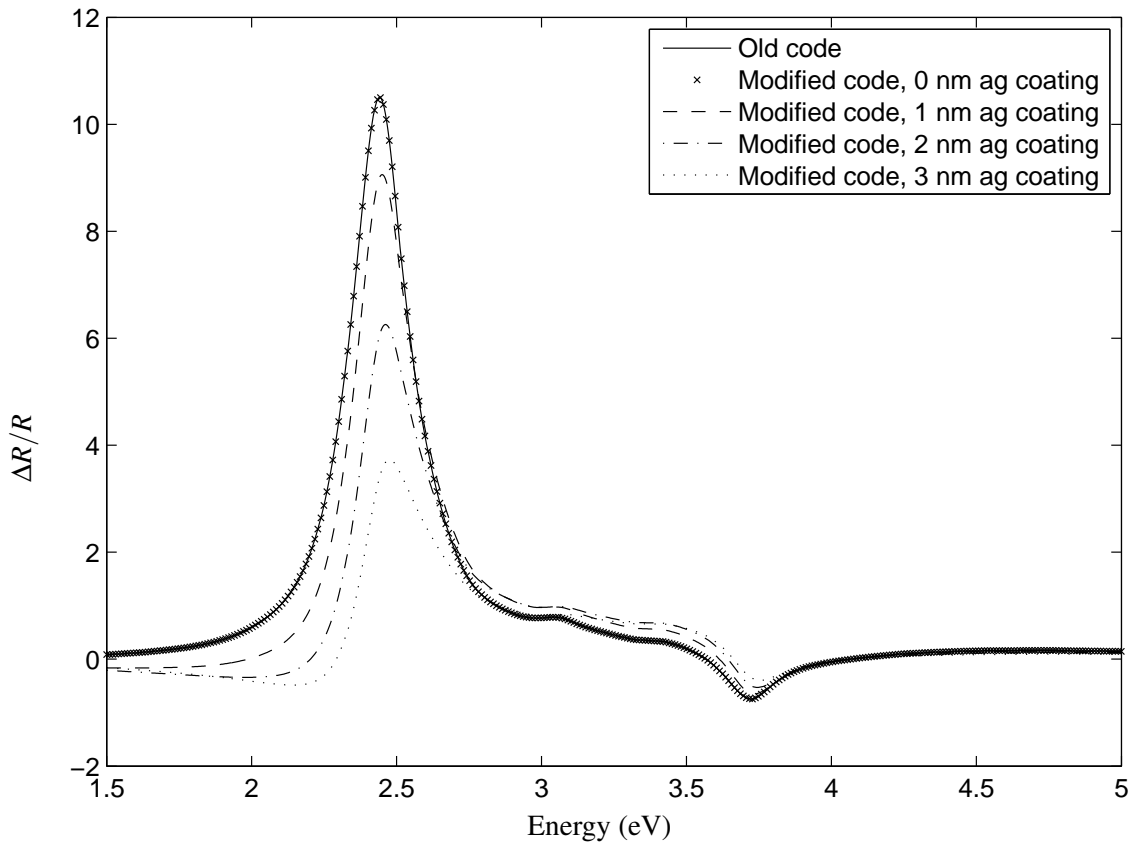


Figure 6.3: Differential reflectivity for a surface of 11 nm radius Ag hemispheres on a MgO substrate, calculated using the original GranFilm code, compared with the equivalent case from the modified code where Ag spheres are covered with a coating of Ag of varying thickness, but so that the total radius of inner sphere and coating remains 11 nm. M is set to 16.

6.2.2 Fulfilment of boundary conditions

The real numerical test of the calculated results are the fulfilment of the required boundary conditions in (2.13). By construction, the multipole expansion of the potentials satisfies the Laplace equation, so that if the boundary conditions are satisfied, the correct and unique solution has been found. The boundary conditions on the substrate boundary were automatically satisfied due to the amplitude relations in (3.8), so what is left is the continuity across the island-coating interface and the coating-ambient interface.

6.2.2.1 Calculation of the boundary condition error

Boundary condition errors are calculated directly in a slightly modified routine within the GranFilm code, and the results are plotted in Matlab. When GranFilm calculates the potential in the various regions, the constant potential terms ψ_0 and ψ_c are needed. They may be found using equations (B.15) and (B.26). The

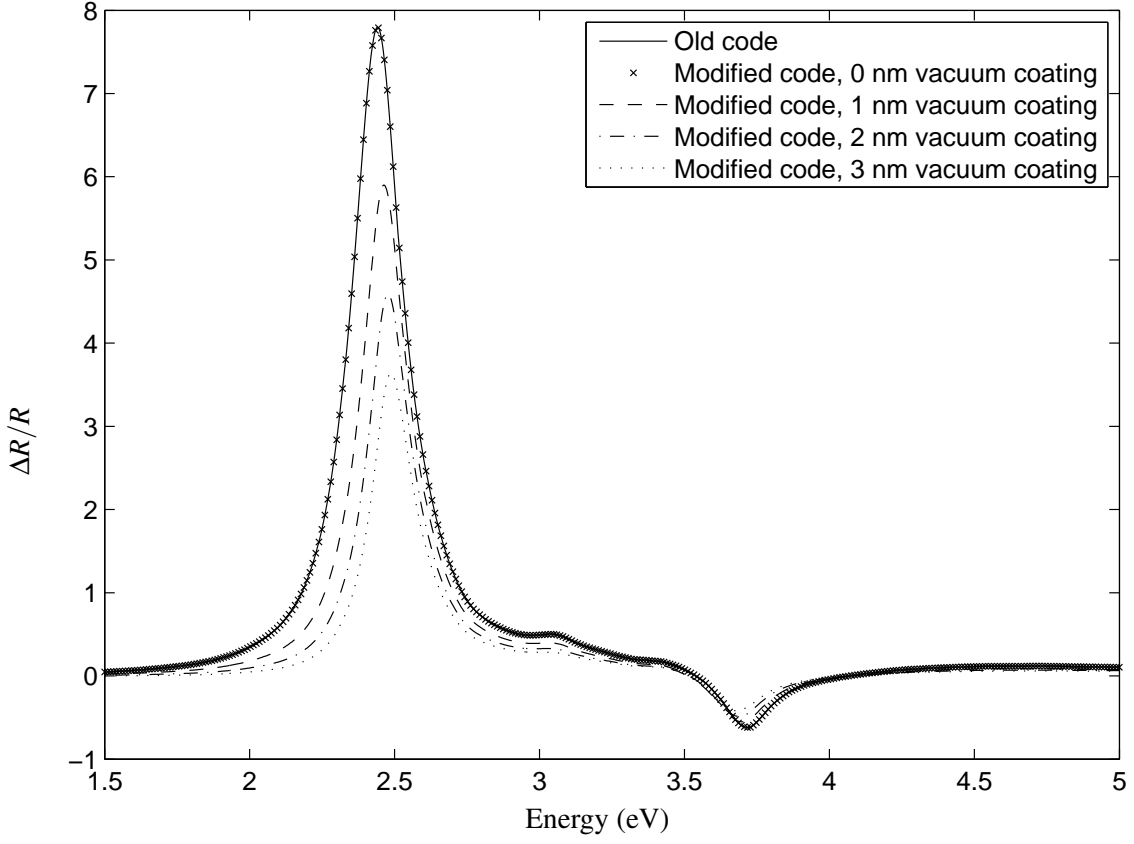


Figure 6.4: Differential reflectivity of a surface of a MgO substrate covered with 8 nm radius Ag hemispheres surrounded by vacuum, calculated using the original Granfilm code, compared with the equivalent case from the modified code with a MgO substrate covered with Ag hemispheres with a vacuum coating of varying thickness. M is set to 16.

previously discarded $\ell' = 0$ term in (B.15) then gives ψ_c as

$$\begin{aligned} \psi_c/(E_0 R_c) &= \cos \theta_0 \left(\frac{\varepsilon_1 - \varepsilon_2}{\varepsilon_2} \right) \frac{1}{\sqrt{3}} \zeta_{01}^0 Q_{01}^0(t_{rc}) + t_{rc} \cos \theta_0 \left(\frac{\varepsilon_1 - \varepsilon_2}{\varepsilon_2} \right) (1 - \zeta_{00}^0 Q_{00}^0(t_{rc})) \\ &+ \frac{1}{\sqrt{4\pi}} \left\{ \sum_{\ell=0}^M \left[\frac{R_c^{-\ell-2} A_{\ell 0}}{E_0} \right] C_{0\ell}^0(t_{rc}) - \sum_{\ell=0}^M \left[\frac{R_c^{-\ell-2} \mathcal{A}_{\ell 0}}{E_0} \right] \mathcal{C}_{0\ell}^0(t_{rc}) + \sum_{\ell=0}^M \left[\frac{R_c^{\ell-1} \mathcal{B}_{\ell 0}}{E_0} \right] \mathcal{D}_{0\ell}^0(t_{rc}) \right\}, \end{aligned} \quad (6.4)$$

where ψ_c has been non-dimensionalized with the radius of the coating layer and the amplitude of the incident electric field. The square brackets show the non-dimensionalized multipole expansion coefficients as they are calculated in the software. Then, when ψ_c has been calculated, ψ_0 may be found from (B.26), giving

$$\begin{aligned} \psi_0/(E_0 R) &= \psi_c/(E_0 R) \\ &+ \frac{1}{\sqrt{4\pi}} \left\{ \sum_{\ell=0}^M \left[\frac{R^{\ell-1} B_{\ell m}}{E_0} \right] D_{0\ell}^0(t_r) + \sum_{\ell=0}^M \left[\frac{R^{-\ell-2} \mathcal{A}_{\ell 0}}{E_0} \right] \mathcal{C}_{0\ell}^0(t_r) - \sum_{\ell=0}^M \left[\frac{R^{\ell-2} \mathcal{B}_{\ell 0}}{E_0} \right] \mathcal{D}_{0\ell}^0(t_r) \right\}. \end{aligned} \quad (6.5)$$

In all the continuity error calculations in this thesis, the fields are normalized by the maximum of the incident field over the whole boundary. This choice will give dimensionless numbers that ideally should be considerably smaller than one. Another natural choice would be to divide by the mean of the potential at

both sides of the interface, since such a normalisation would give a better indication as to how large the error is compared to the potential at that point. However, this normalisation may lead to divisions by zero, which would leave the plots useless in certain areas.

6.2.2.2 Boundary condition error results

For the default test case, a MgO substrate with 8 nm radius Ag spheres with a 3 nm coating layer, the boundary condition errors over the two spherical surfaces is plotted in figure 6.5 – 6.8. The error is calculated simply as the difference between the outer and inner potential or normal derivative times the permittivity across the spherical surfaces, and normalised by the maximum of the incident. The error is calculated at a specific energy, and for these plots the value is chosen to be 3.571 eV, which lies within the dip of the differential reflectivity spectrum. The a) plots show the error in the θ - ϕ -plane, while in the b) plots the error has been plotted on the sphere surface. For all of these plots, $t_r = 0$, so that the first half of the θ -range and the lower half of the sphere lies in the substrate.

The plots show that the continuity is worst at the inner interface. There, the potential continuity has an error varying around 0.2, while the normal derivative times permittivity error mostly varies between +0.5 and -0.5. On the outer interface the results are much better, with potential errors mostly within 0.005 away from zero, and with normal derivative times permittivity error within 0.05 away from zero. The results are summarized in table 6.1. Note that the errors except from that of the potential at the inner interface vary around zero, which will be investigated further in the discussion about convergence of the continuity errors in section 6.3.4.

Note also that the continuity is always worst close to the substrate. This is to be expected, since these sharp corners are triple points between tree media, and thus hard to handle using multipole expansions [6]. Also, errors tend to be higher at the sphere top and bottom. These extremities are not considered in table 6.1, which only indicates a typical range of the errors.

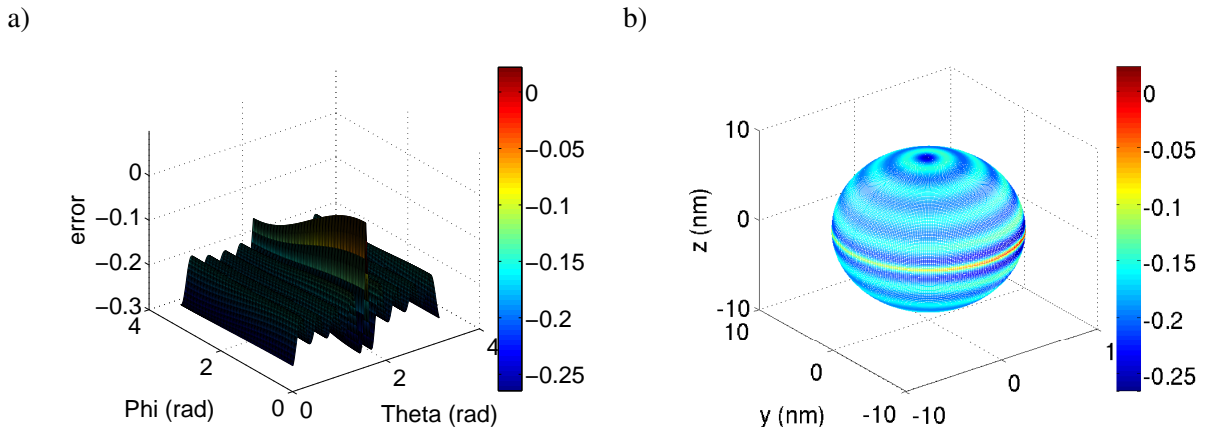


Figure 6.5: The discontinuity of the potential over the island-coating boundary for the default parameters where 8 nm radius Ag hemispheres with 3 nm SiO coating covers a MgO substrate, and with $M = 16$, a) in the θ - ϕ -plane and b) on the sphere.

When the truncation ratio is increased from 0 to 0.3, the continuities at the inner boundary becomes worse for the potential and better for the normal derivative times permittivity. Instead of showing the plots, the

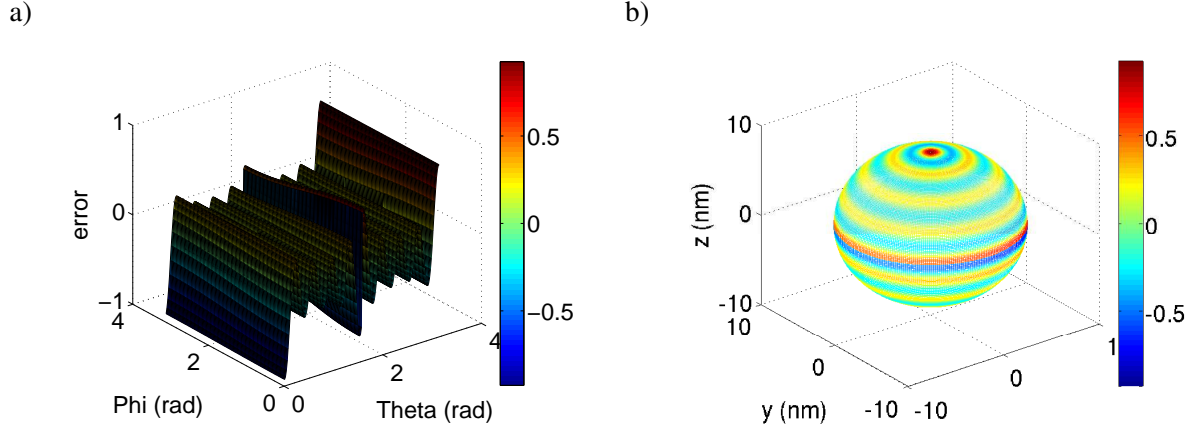


Figure 6.6: The discontinuity of the normal displacement field over the island-coating boundary for the default parameters where 8 nm radius Ag hemispheres with 3 nm SiO coating covers a MgO substrate, and with $M = 16$, a) in the θ - ϕ -plane and b) on the sphere.

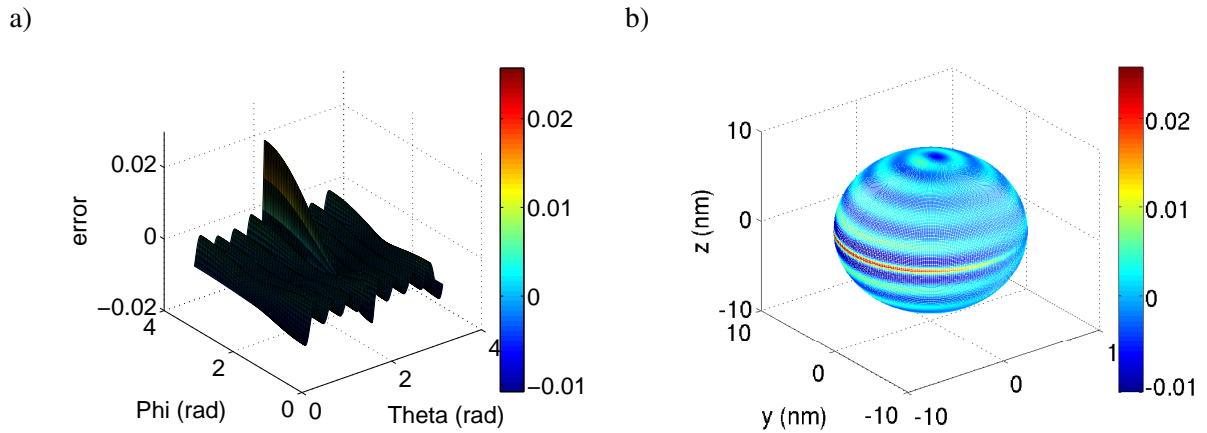


Figure 6.7: The discontinuity of the potential over the coating-ambient boundary for the default parameters where 8 nm radius Ag hemispheres with 3 nm SiO coating covers a MgO substrate, and with $M = 16$, a) in the θ - ϕ -plane and b) on the sphere.

approximate mean and the typical deviation are given in table 6.1, together with data from the case with zero truncation. A different case is also shown, with islands of gold rather than silver. From the table, it is clear that gold islands give far better continuity results on the inner boundary and therefore might have been a more forgiving test case. Table 6.1 also includes data from the unmodified GranFilm code, for a thin film of 8 nm radius Ag spheres on a MgO substrate. The boundary condition error across the one spherical boundary of this system shows a very similar behaviour to those of figures 6.5 – 6.8, with oscillations along the θ -axis. Also, the typical magnitude of the error for the original code is comparable to the that achieved with the modified code. However, the error is in general smaller in the original code results, and the high mean error at the inner boundary for the modified code, as seen in table 6.1, is not found in the original code result.

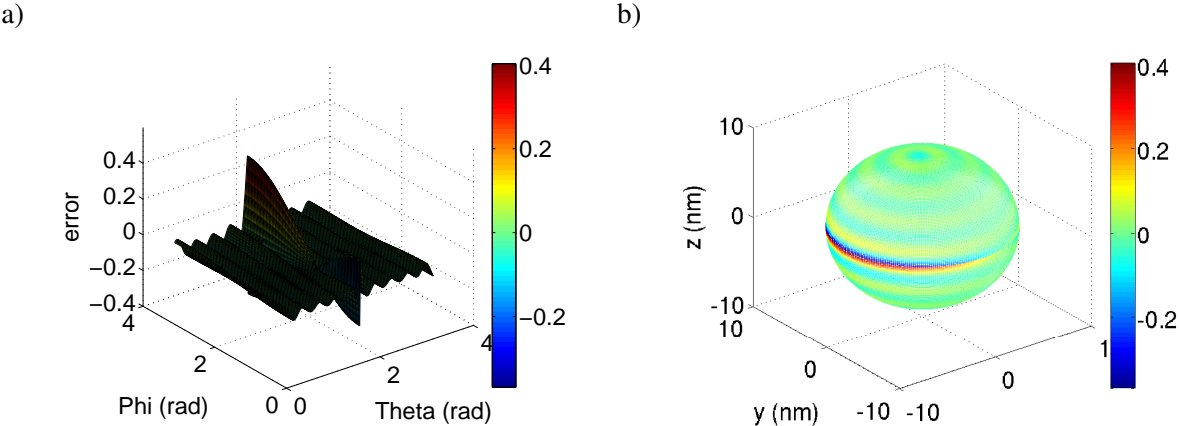


Figure 6.8: The discontinuity of the normal displacement field over the coating-ambient boundary for the default parameters where 8 nm radius Ag hemispheres with 3 nm SiO coating covers a MgO substrate, and with $M = 16$, a) in the θ - ϕ -plane and b) on the sphere.

Case \ error in	ψ inner	$\frac{\partial \psi}{\partial r} \epsilon$ inner	ψ outer	$\frac{\partial \psi}{\partial r} \epsilon$ outer
Ag-island, SiO coating, $t_r = 0$	0.2 ± 0.05	0 ± 0.5	0 ± 0.005	0 ± 0.05
Ag-island, SiO coating, $t_r = 0.3$	0.37 ± 0.03	0 ± 0.15	0 ± 0.005	0 ± 0.03
Au-island, SiO coating, $t_r = 0$	0.022 ± 0.001	0 ± 0.02	0 ± 0.005	0 ± 0.05
Au-island, SiO coating, $t_r = 0.3$	0.048 ± 0.001	0 ± 0.01	0 ± 0.01	0 ± 0.05
Ag-island, No coating, $t_r = 0$	0 ± 0.01	0 ± 0.1	N/A	N/A
Ag-island, No coating, $t_r = 0.3$	0 ± 0.015	0 ± 0.1	N/A	N/A

Table 6.1: Indication of typical error for different variations of the default case. All cases has a MgO substrate, and have been calculated for both $t_r = 0$ and $t_r = 0.3$. Two of the cases have 8 nm Ag islands with 3 nm SiO coating, two has 8 nm Au islands with 3 nm SiO coating, and two cases are calculated using the unmodified code, with 8 nm Ag islands. All calculations are done with $M = 16$.

6.3 Convergence

One of the approximations in the herein described approach that should be justified, is the truncation of the multipole expansion at a certain $\ell = M$. This is what gives the linear system of equations a finite size so that it may be solved numerically. In the current section, convergence of various quantities with respect to increasing M will be investigated, searching for an indication as to in what situations convergence is achievable, and at what M it would be reasonable to truncate the expansions. The case studied will be the standard case of a MgO substrate with 8 nm radius Ag hemispheres with a 3 nm thick coating layer of SiO.

6.3.1 Convergence of multipole expansion coefficients

Truncation of the multiple expansions at $\ell = M$ rests on the assumption that the expansion has converged reasonably at that M . This assumption is critical and must be tested thoroughly. In figures 6.9 – 6.12 the multipole expansion coefficients have been plotted for all ℓ up to M and for all energies in the energy range, for both $m = 0$ and $m = 1$. The coefficients are non-dimensionalized as earlier introduced in (6.4), so that the quantities plotted are $A_{\ell m}/(E_0 R_c^{-\ell-2})$, $B_{\ell m}/(E_0 R_c^{\ell-1})$, $\mathcal{A}_{\ell m}/(E_0 R_c^{-\ell-2})$ and $\mathcal{B}_{\ell m}/(E_0 R_c^{\ell-1})$. With this

normalisation, the quantities should preferably be of an order smaller than one, and they should be expected to approach zero when ℓ is increased towards M if M is set sufficiently high.

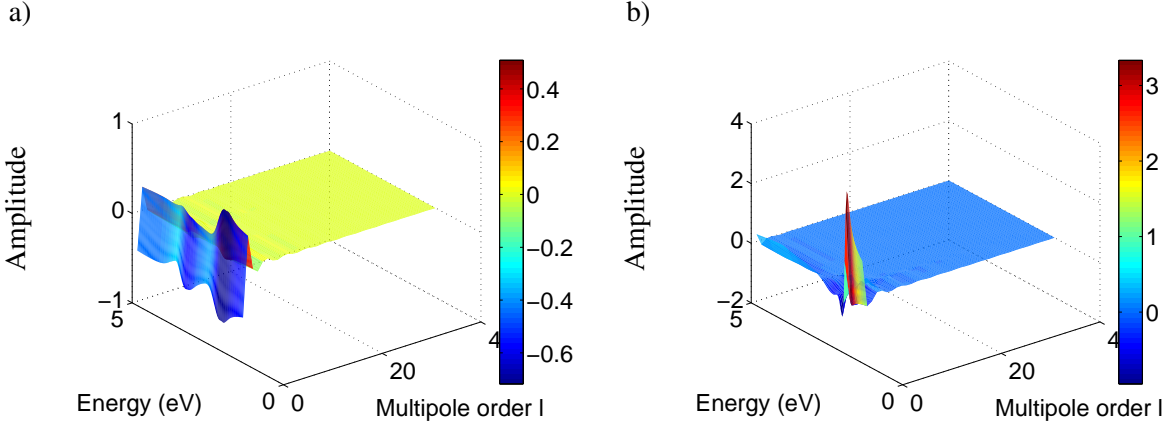


Figure 6.9: $A_{\ell m}/(E_0 R_c^{-\ell-2})$ for the case of a MgO substrate covered with 8 nm radius Ag hemispheres with a 3 nm thick SiO coating, for multipole orders ℓ up to $M = 40$, and for a) $m = 0$ and b) $m = 1$.

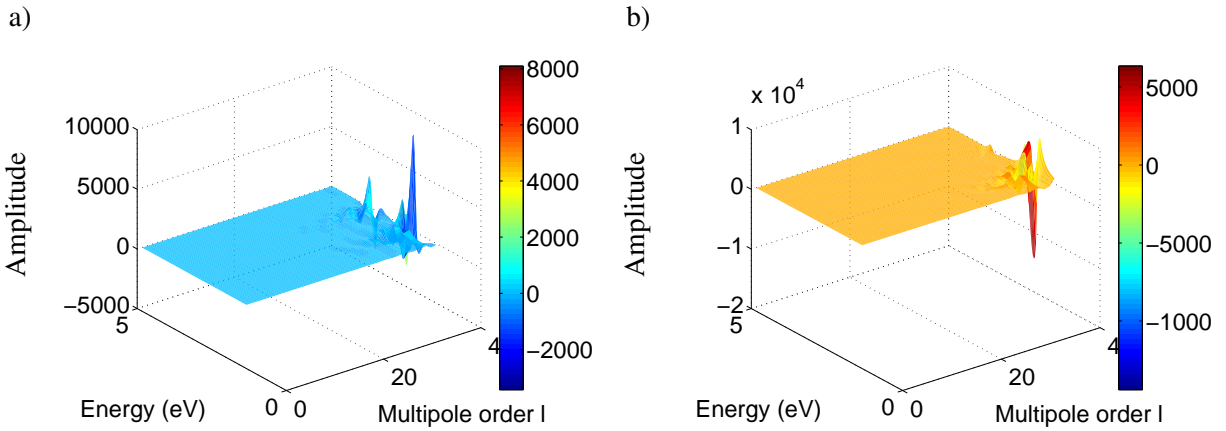


Figure 6.10: $B_{\ell m}/(E_0 R_c^{\ell-1})$ for the case of a MgO substrate covered with 8 nm radius Ag hemispheres with a 3 nm thick SiO coating, for multipole orders ℓ up to $M = 40$, and for a) $m = 0$ and b) $m = 1$.

As seen from figures 6.9, 6.11 and 6.12, this convergence requirement holds fairly well for $A_{\ell m}$, $\mathcal{A}_{\ell m}$ and $\mathcal{B}_{\ell m}$, with oscillations diminishing towards zero for increasing ℓ . For $B_{\ell m}$, however, it is evident from figure 6.10 that there is no such convergence with increasing ℓ for certain energies. Unfortunately, these troublesome energies seem to be right in the interesting energy area where the peak and dip are located, as seen clearly when the highest order B -terms, $B_{40,m}$, are plotted together with the differential reflectivity in figure 6.13. Note that the differential reflectivity curve has been scaled up so that it may be compared with the much larger B -terms.

The divergence of $B_{\ell m}$ means that the potential in regions 3 and 4, inside the inner island, at certain energies has not converge even when ℓ reaches $M = 40$. This might of course be a major problem, and may be a step in explaining the issues of consistency with the unmodified code and the fulfilment of the boundary

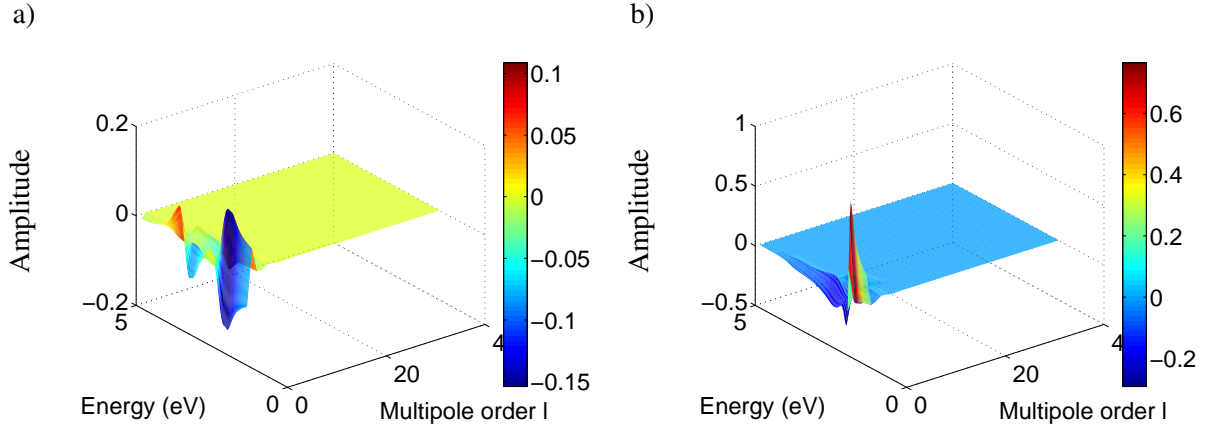


Figure 6.11: $\mathcal{A}_{\ell m}/(E_0 R_c^{\ell-2})$ for the case of a MgO substrate covered with 8 nm radius Ag hemispheres with a 3 nm thick SiO coating, for multipole orders ℓ up to $M = 40$, and for a) $m = 0$ and b) $m = 1$.

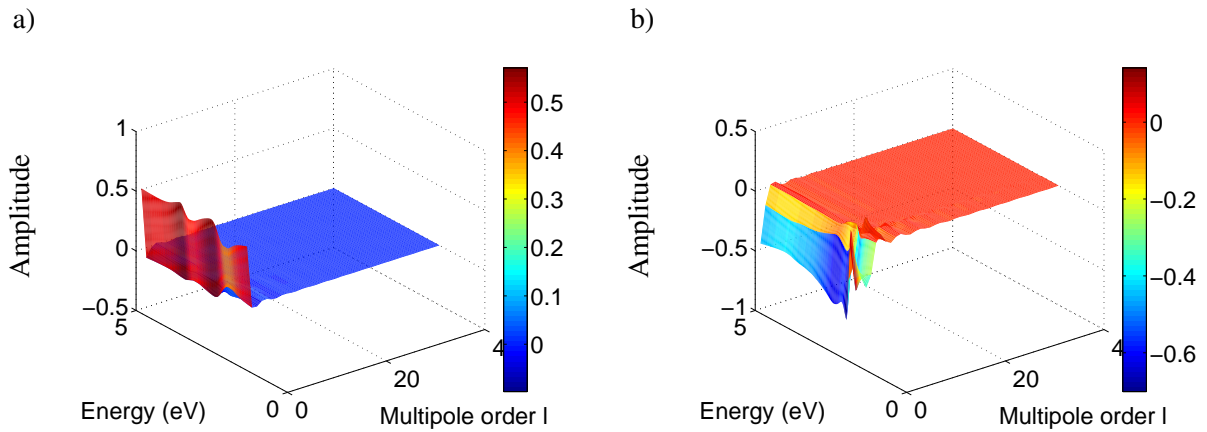


Figure 6.12: $\mathcal{B}_{\ell m}/(E_0 R_c^{\ell-1})$ for the case of a MgO substrate covered with 8 nm radius Ag hemispheres with a 3 nm thick SiO coating, for multipole orders ℓ up to $M = 40$, and for a) $m = 0$ and b) $m = 1$.

conditions, as discussed earlier in this chapter. But still, the reason for this failure to converge is as of now not known. It might stem from an implementation error. Another possibility is that the system of equations is especially hard to solve numerically. The condition numbers of the linear system to be solved for $M = 40$ reach as high as 10^6 . It is, however, not obvious whether these high condition numbers are a natural property of the correct equations or if it results from some sort of error.

For comparison, the expansion coefficients calculated using the old code has also been studied. Figure 6.14 shows the normalized expansion coefficients $A_{\ell 0}/(E_0 R_c^{\ell-2})$ and $B_{\ell 0}/(E_0 R_c^{\ell-1})$ for the default test case without a coating, i.e. 8 nm Ag islands on a MgO substrate, with zero truncation. Especially in figure 6.14 a) it may be seen that neither these coefficients have converged properly at $M = 40$ for certain energies. Thus it seems as bad convergence of the multipole expansion is a problem also for the uncoated system in the unmodified GranFilm code. However, comparing the magnitudes of the coefficients at the bad energy spots at $M = 40$, it is clear that the problem is much more severe for the coated system in the modified code.

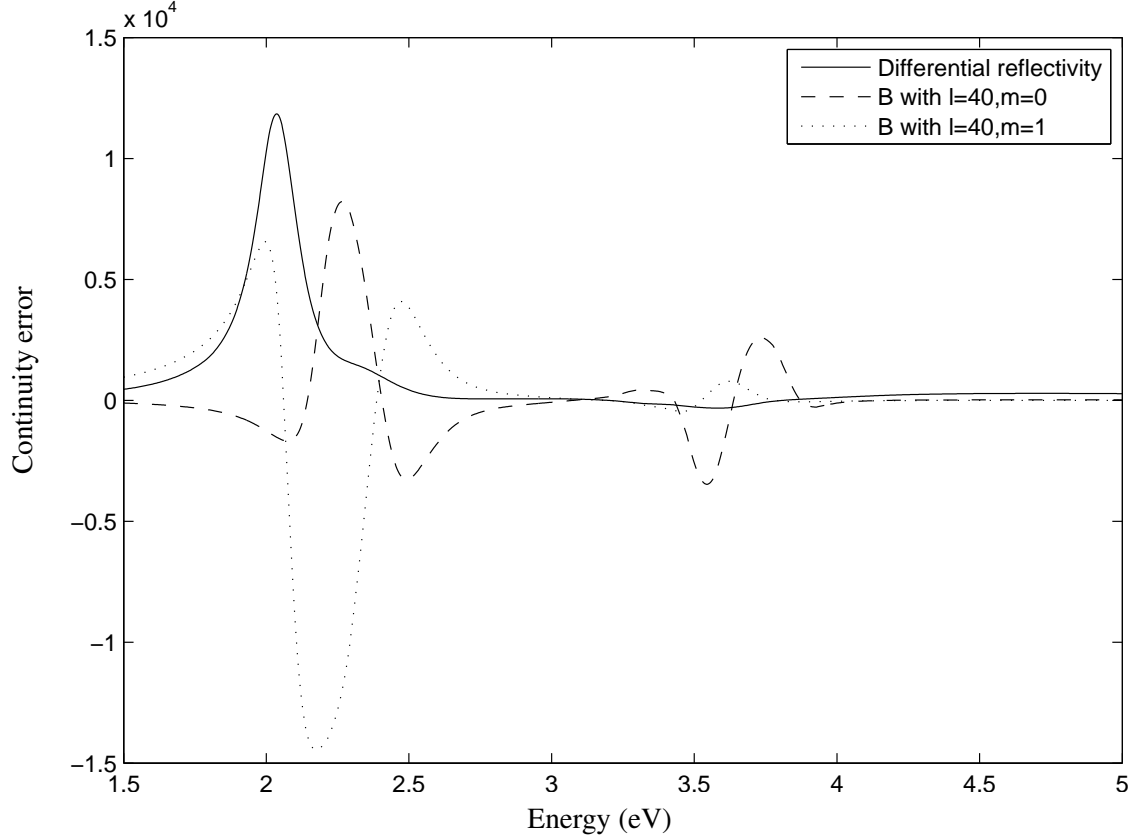


Figure 6.13: B_{400} and B_{401} from figure 6.10, plotted together with the differential reflectivity, where the latter has been scaled up so that it is visible in the graph.

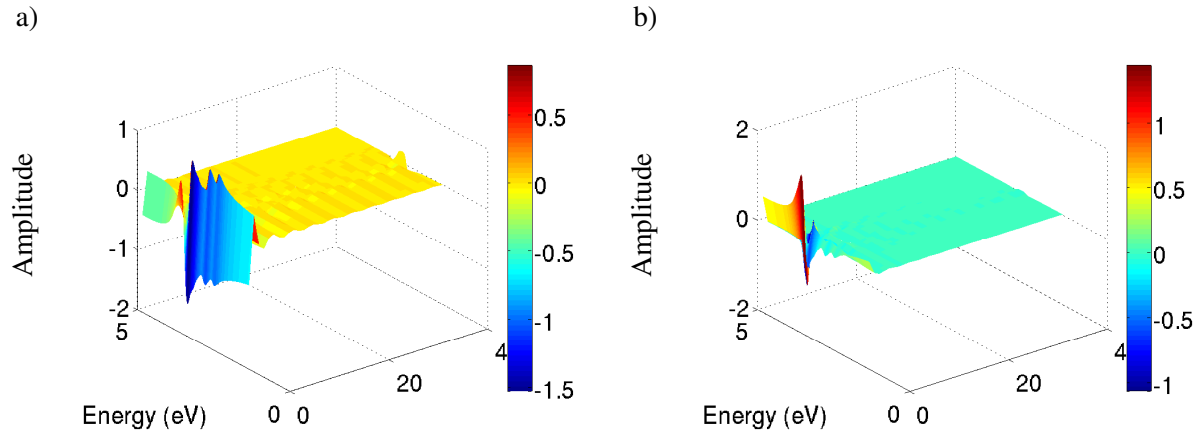


Figure 6.14: a) $A_{\ell 0}/(E_0 R^{\ell-2})$ and b) $B_{\ell 0}/(E_0 R^{\ell-1})$ for a MgO substrate covered with 8 nm radius Ag hemispheres, calculated using the unmodified GranFilm code, for multipole orders ℓ up to $M = 40$.

6.3.2 Convergence of the dipole term

As just seen in section 6.3.1, the multipole expansions does not always converge to zero for ℓ within the limit M . However, in calculating the Fresnel coefficients, only the terms A_{10} and A_{11} are used, and therefore

it might be interesting to see if those values converge towards a fixed value for increasing M . Of course, it is not necessarily so that the values these terms approaches are correct when the expansion has not converged towards zero, but it could still be illuminating to study the behaviour of these two terms isolated. Figure 6.15 gives the change of the terms A_{10} and A_{11} as a function of M . The change is calculated as $A_{1m}(M = i + 2) - A_{1m}(M = i)$, where the coefficients has been calculated for M 's from 10 to 40 with a step size of 2. In the figure, the convergence is plotted for a few selected energies. The first two, $E = 2.29$ eV and $E = 3.49$ eV, are two interesting energies because they have give a rather large rate of change, and because they lie in the interesting area where the differential reflectivity curves peak, as discussed in chapter 5. The third energy, $E = 4.58$ eV is a randomly chosen energy where the change in A_{1m} stays close to 0 for all M , which is the case for most energies away for the dip and the peak. Again, this shows that convergence is good for most energies, unfortunately except for the most interesting ones.

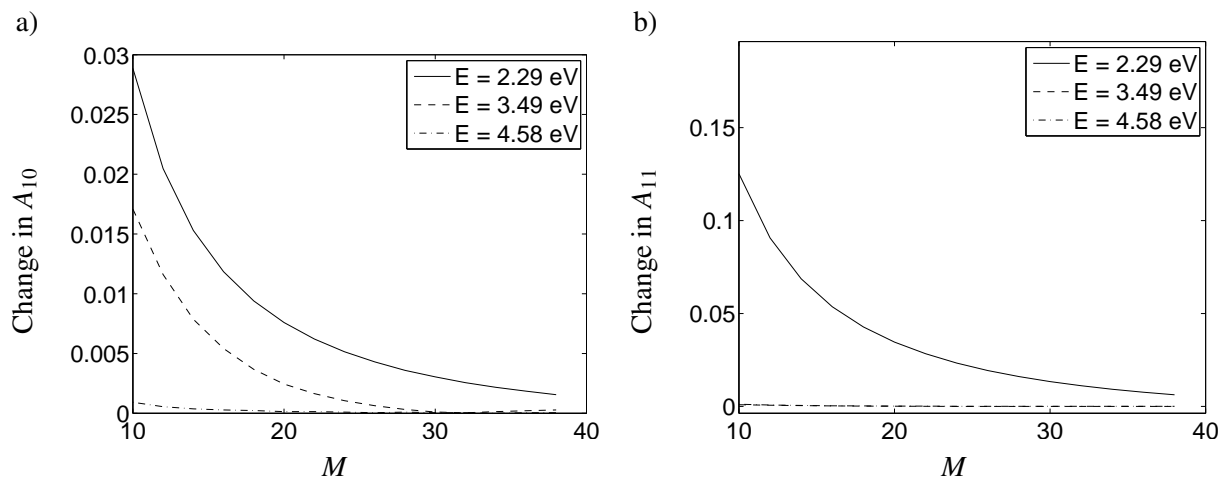


Figure 6.15: Rate of change with increasing M for a) A_{10} and b) A_{11} , measured as the difference between the coefficients for two consecutive M 's. The surface consists of a MgO substrate covered with 8 nm radius Ag hemispheres with a 3 nm thick SiO coating.

6.3.3 Convergence of differential reflectivity

The convergence of the differential reflectivity with respect to M closely follows the convergence of the dipole terms from section 6.3.2. This is natural, since the Fresnel coefficients only depends on these dipole terms, as seen in (2.22). First, in order to get an overview of the range of variation in the differential reflectivity, a selection of curves with M between 2 and 40 has been plotted in figure 6.16. In general, the dip near $E = 3.5$ eV moves somewhat up and to the right, while the peak near $E = 2$ eV moves to the left, the latter seen in the zoom in figure 6.16 b). A possible measure for the convergence of the differential reflectivity may be the area between two curves with adjacent M , measured as the L_2 -norm between the curves, divided by the number of energy points. This leads to the convergence plot given in figure 6.17.

Figure 6.17 shows a relatively good convergence for the differential reflectivity. However, as discussed in relation to the results in chapter 5, what is of most interest is often at what energies the differential reflectivity peaks and dips. Therefore, what might be more interesting than the convergence of the curve as a whole, is the convergence of these peak and dip energies. The peak energy is displayed in figure 6.18 a), and the dip energy in figure 6.19 a). Also, the amount of change between peak energies for two adjacent M 's is given in figure 6.18 b), and the same for the change in dip energy in figure 6.19 b). Note that the

6 Analytical and numerical evaluation

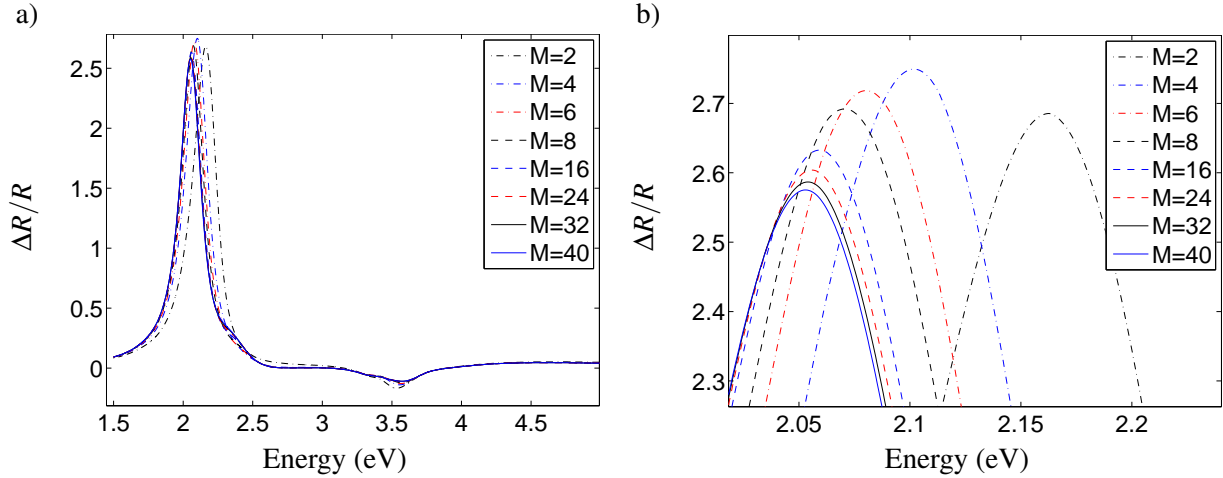


Figure 6.16: Differential reflectivity for a substrate of MgO covered with 8 nm radius Ag hemispheres with a 3 nm thick SiO coating, for different M , for a) the full energy range, and b) zoomed on the peak movement.

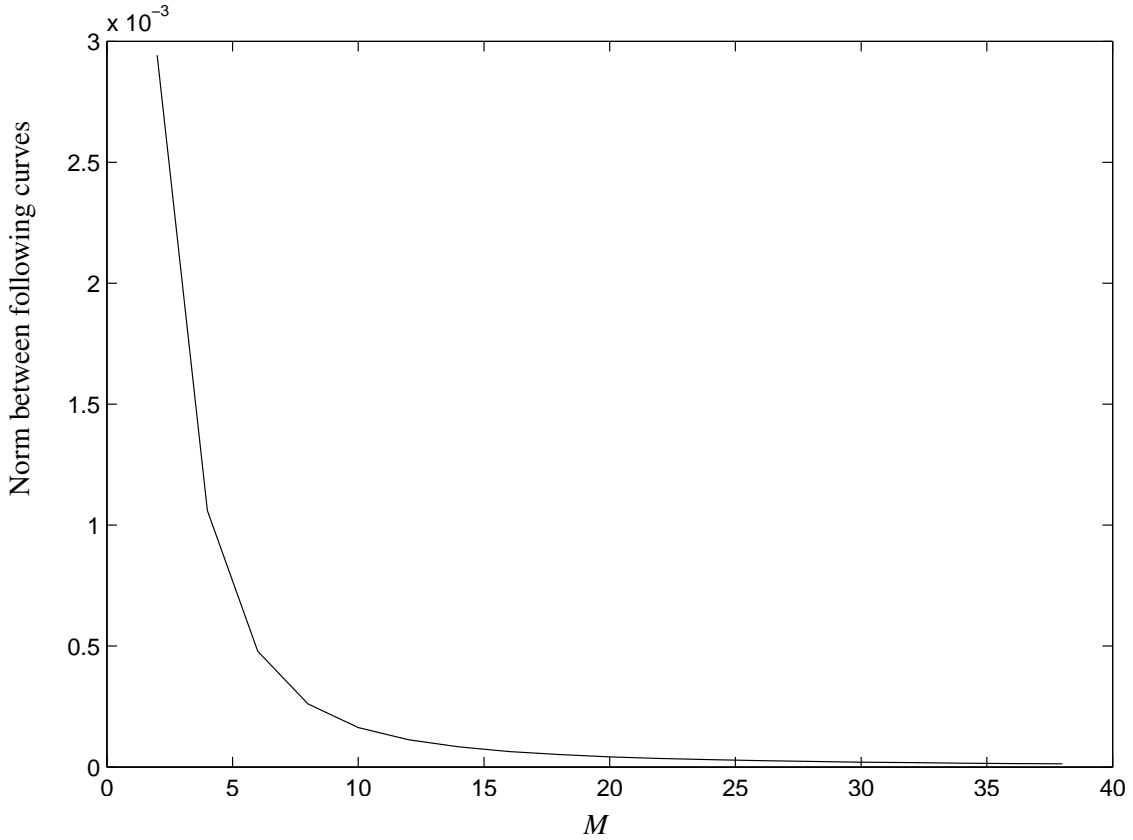


Figure 6.17: Change in differential reflectivity for the thin film from figure 6.16, when M is varied as $M = 2, 4, 6, \dots, 40$, measured as the L_2 -norm between two consecutive curves, normalized by the number of energy points.

curves have an energy resolution of 6144 points over the range from 1.5 eV to 5 eV, so that each energy step equals approximately $5.7 \cdot 10^{-4}$ eV. This explains the zigg-zagging of the b-plots for large M , where the change in peak and dip position varies between zero and one energy points.

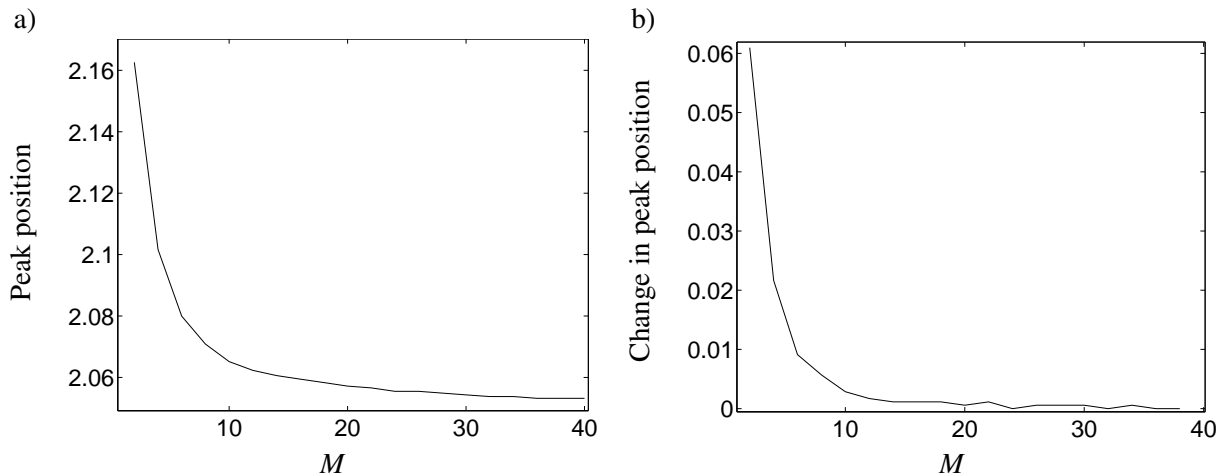


Figure 6.18: a) The energy of the peak in the differential reflectivity of the surface from figure 6.16, and b) the change in this peak position measured as the difference between peak energy for two consecutive curves, for $M = 2, 4, 6, \dots, 40$.

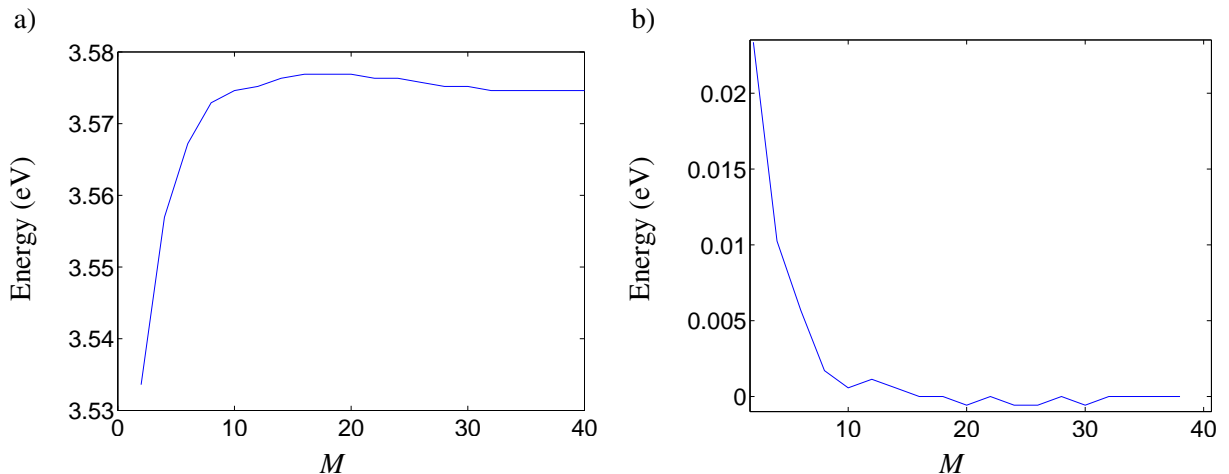


Figure 6.19: a) The energy of the dip in the differential reflectivity of the surface from figure 6.16, and b) the change in this dip position measured as the difference between dip energy for two consecutive curves, for $M = 2, 4, 6, \dots, 40$.

Figures 6.18 and 6.19 show a relatively good convergence of both peak and dip position. Also, the standard choice of multipole expansion cut-off used in this thesis, at $M = 16$, seems like a reasonable choice in that the amount of change in figures 6.18 b) and 6.19 b) reaches a fairly low and almost constant level after this point.

6.3.4 Convergence of the field continuity

The boundary condition fulfilment studied in section 6.2.2 is a very important issue, and it's error convergence should be ensured. A simple measure for this error is to calculate the mean value of the error in the boundary conditions over the spherical interfaces. Figure 6.20 shows this mean error as a function of M , for the energy $E = 3.53$ eV lying within the peak. The potentials have been normalized as discussed in

section 6.2.2.

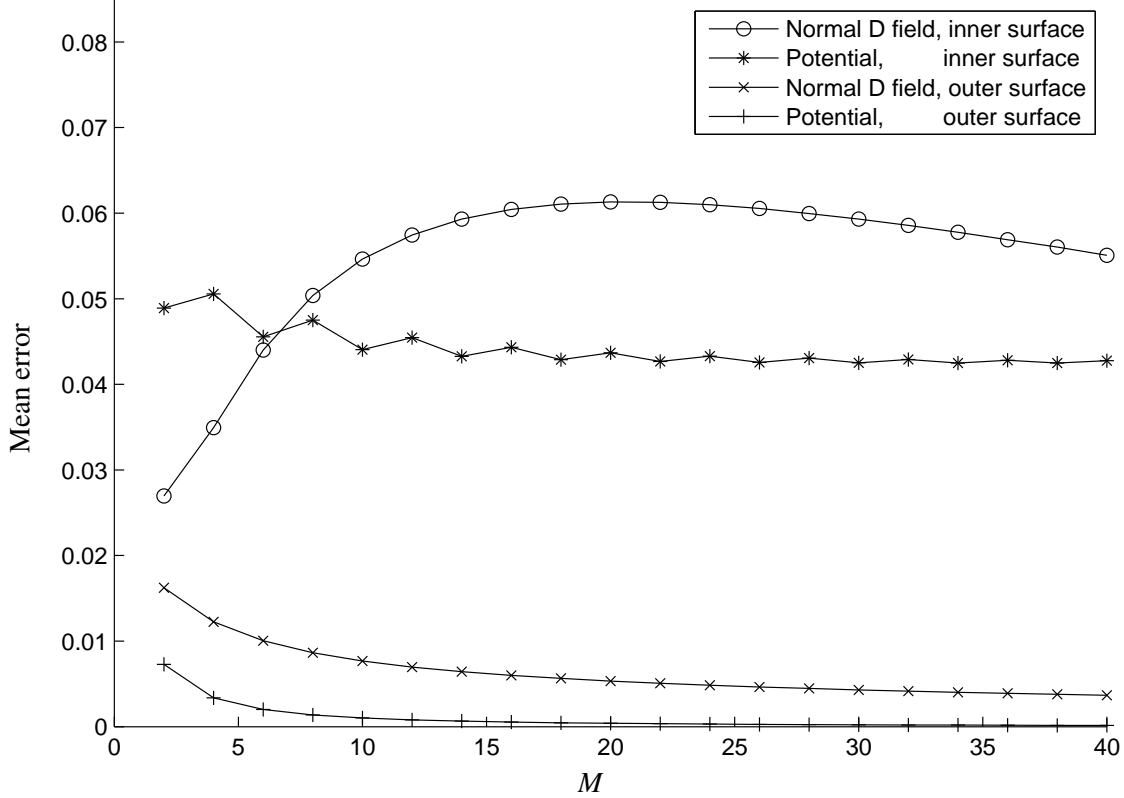


Figure 6.20: Mean value across the two spherical interfaces of the absolute value of the error in the boundary conditions, as a function of the multipole expansion cut-off M . The surface consist of the standard case of a MgO substrate covered with 8 nm radius Ag hemispheres with 3 nm thick SiO.

The plot shows that the normal derivate times permittivity has an error systematically higher than the potential, except for at extremely low M . But more importantly it confirms the results previously summarized in table 6.1, showing that the inner spherical boundary in general has higher continuity errors. In fact, it seems that the errors at the inner interface do not converge towards zero at all. This is most unfortunate, but it would be expected, considering the $B_{\ell m}$ terms' lack of convergence.

7 Conclusion

The main task of this thesis has been to describe the optical response of a surface covered with coated islands. And to a certain limit, this has been achieved. Bedeaux and Vlieger's formalism for treating granular surfaces [2] using excess field has been applied, and in brief the steps in the derivation have been presented in a way that justifies that the results may be used also when describing coated spheres. The derivation of the system of equations for the multipole expansion coefficients has been given briefly in section 3.1.2 and more thoroughly in appendix B. This may be seen as the most significant result of the herein described work.

Further, this system of equations has been tested somewhat for consistency with the uncoated equivalent treated by Bedeaux and Vlieger. These tests have been successful in that they have shown the system of equations (B.33) to behave properly in the limits where the coating has zero thickness, and when it has the same dielectric properties as the island.

Also, a preliminary implementation has been done in Lazzari and Simonsens GranFilm software. This implementation and the numerical results it gives has been evaluated, but with varying results. Numerical consistency with the old GranFilm software for un-coated spheres is not achieved. Also, a study of the convergence of the multipole expansion shows that the potential inside the islands does not converge properly. This further leads to bad boundary condition fulfilment at the inner spherical boundary.

The reason for the issues mentioned above may be a calculation error in the derivation of the system of equations. This derivation has, however, been thoroughly checked, and the analytical validation also implies that this probably is not where the error lies. Another possibility is that it is a result of bad numerical conditioning of the system of equations. This seem possible, e.g. in light of the high condition numbers found in section 6.2.1.1. Also, since the implementation has had a rather preliminary character, programming errors may play a role. Especially in the numerical consistency tests in section 6.2.1 the discrepancies may look as to be caused by some sort of normalisation error. Lastly, of course, the reason for the errors may stem from a combination of the above.

For further work, it would be recommended to reimplement the numerics in the GranFilm software in a more robust way. A more thorough knowledge of the relatively vast framework would prevent programming errors and unforeseen consequences. Alternatively, the equations for the coated system may be implemented in a simplified version of the code, thus ensuring total control of the program flow.

Also, it may be advisable to generalise the formalism so that it in a natural way supports the addition of several layers of coating. This seems relatively straight forward, and would allow for a convenient implementation in the GranFilm software.

Lastly, the important principle should be stressed that the real test of the software's results is whether they are reproduced in experiments. Such experiments with coated island surfaces are as of yet scarce, so that this vital test has to wait.

A Validation of the potential form

The relation between original, reflected and transmitted multipole expansion amplitudes given in (3.8) may be derived directly by imposing the proper boundary condition across the substrate surface [3, p. 333]. However, this may involve some tedious calculations, so in the following there will instead be given only a brief demonstration of that the stated amplitude relations indeed do satisfy one of the continuity requirements, namely that of the potential at the coating-substrate interface. All the other continuity requirements for the substrate surface may be shown to hold in a similar manner. Also, in the same calculation it will be justified that the constant terms in the potentials in region 5 and 6, (3.6e) and (3.6f), are set to be equal.

The first step is to find relations between the coordinates on the substrate surface given in the different coordinate systems. Since this surface lies midway between the centres of the μ and the $\bar{\mu}$ systems, the first result is that the radii are equal, $r_{\bar{\mu}} = r_{\mu} = r_{\text{int}}$. The zenith angle is the same in both coordinate systems, and the relation between the azimuth angles is $\theta_{\bar{\mu}} = \pi - \theta_{\mu}$, leading to $\cos(\theta_{\bar{\mu}}) = \cos(\pi - \theta_{\mu}) = -\cos(\theta_{\mu})$. Then, by studying the potentials' θ -dependence, lying solely in the associated Legendre functions (2.12), it is evident that the relation between the spherical harmonics is

$$Y_{\ell}^m(\theta_{\bar{\mu}}, \phi_{\bar{\mu}}) = (-1)^{\ell+m} Y_{\ell}^m(\theta_{\mu}, \phi_{\mu}). \quad (\text{A.1})$$

Next the continuity of the potential over the coating-substrate interface is imposed,

$$\psi_5(\mathbf{r}_{\text{int}}) = \psi_6(\mathbf{r}_{\text{int}}), \quad (\text{A.2})$$

where \mathbf{r}_{int} is a point on the interface between region 5 and 6. With potentials inserted, this reads

$$\begin{aligned} \psi_c + \sum'_{\ell m} \mathcal{A}_{\ell m} r_{\text{int}}^{-\ell-1} Y_{\ell}^m(\theta_{\mu}, \phi_{\mu}) + \sum'_{\ell m} \mathcal{B}_{\ell m} r_{\text{int}}^{\ell} Y_{\ell}^m(\theta_{\mu}, \phi_{\mu}) \\ + \sum'_{\ell m} (-1)^{(\ell+m)} \frac{\epsilon_5 - \epsilon_6}{\epsilon_5 + \epsilon_6} \mathcal{A}_{\ell m} r_{\text{int}}^{-\ell-1} (-1)^{\ell+m} Y_{\ell}^m(\theta_{\mu}, \phi_{\mu}) \\ + \sum'_{\ell m} (-1)^{\ell+m} \frac{\epsilon_5 - \epsilon_6}{\epsilon_5 + \epsilon_6} \mathcal{B}_{\ell m} r_{\text{int}}^{\ell} (-1)^{\ell+m} Y_{\ell}^m(\theta_{\mu}, \phi_{\mu}) \\ = \psi'_c + \sum'_{\ell m} \frac{2\epsilon_5}{\epsilon_5 + \epsilon_6} \mathcal{A}_{\ell m} r_{\text{int}}^{-\ell-1} Y_{\ell}^m(\theta_{\mu}, \phi_{\mu}) + \sum'_{\ell m} \frac{2\epsilon_5}{\epsilon_5 + \epsilon_6} \mathcal{B}_{\ell m} r_{\text{int}}^{\ell} Y_{\ell}^m(\theta_{\mu}, \phi_{\mu}). \end{aligned} \quad (\text{A.3})$$

The sums have the usual multipole expansion range. Note that the constant potential term of ψ_6 are also given an apostrophe so that it for the sake of argument may be distinguished from the constant term in ψ_5 . Next the \mathcal{A} - and \mathcal{B} -terms are then collected,

$$\begin{aligned} \psi_c - \psi'_c &= \sum'_{\ell m} \mathcal{A}_{\ell m} r_{\text{int}}^{-\ell-1} Y_{\ell}^m(\theta_{\mu}, \phi_{\mu}) \left(\frac{2\epsilon_5}{\epsilon_5 + \epsilon_6} - 1 - (-1)^{2(\ell+m)} \frac{\epsilon_5 - \epsilon_6}{\epsilon_5 + \epsilon_6} \right) \\ &\quad + \sum'_{\ell m} \mathcal{B}_{\ell m} r_{\text{int}}^{\ell} Y_{\ell}^m(\theta_{\mu}, \phi_{\mu}) \left(\frac{2\epsilon_5}{\epsilon_5 + \epsilon_6} - 1 - (-1)^{2(\ell+m)} \frac{\epsilon_5 - \epsilon_6}{\epsilon_5 + \epsilon_6} \right). \end{aligned} \quad (\text{A.4})$$

A Validation of the potential form

Now two conclusions may be drawn. The first is that the left hand side must be equal to zero, so that the two potential terms must be equal. This is because the right hand side needs to be equal to zero because it consists of a sum of linearly independent terms with the constant term extracted. More precisely, the potential has in being expanded in multipoles been projected onto an orthogonal basis, so that the right hand side may never sum up to a r -independent constant term when the constant term has been extracted from the sums.

The second conclusion is that the amplitude relations given in (3.8c) and (3.8d) are the appropriate ones. Once again, the argument follows from the orthogonality of the terms in the sum. Since the sums on the right hand side have to be zero for all points on the coating-substrate interface, the terms must individually be equal to zero. This is ensured by the given amplitude relation, since the parentheses on the right hand side can be seen to equal zero. Of course, other amplitude relations satisfying the potential continuity requirement may be found, so that in order to prove that the ones given are the uniquely correct ones, it must also be checked that they satisfy the other continuity requirement, i.e. the continuity of the normal derivative of the potential, multiplied with the permittivity. This may be done in a completely analogous way, but will not be done here.

B Detailed derivation of the system of equations

In the following, the system of equations given in (B.33) will be derived in full detail. Most of the steps closely follows the treatment by Bedeaux and Vlieger [2]. The extension of an added coating layer is often very natural, so that the interested reader would be advised to seek to Bedeaux and Vlieger's book [2].

B.1 Properties of the spherical harmonics

In order to simplify the derivation of the system of equations, integrals over spherical harmonics will be derived beforehand. The relations between the spherical harmonics (2.11) and the integrals defined in (3.15) will be used. First the angle integral over two Legendre Polynomials centered in the centre of the sphere is considered, with the definition $x = \cos \theta$:

$$\begin{aligned}
& \int_{-1}^{t_r} dx \int_0^{2\pi} d\phi Y_\ell^m(\theta, \phi) [Y_{\ell'}^{m'}(\theta, \phi)]^* \\
&= \int_{-1}^{t_r} dx \int_0^{2\pi} d\phi \left[\frac{(2\ell+1)}{4\pi} \frac{(\ell-m)!}{(\ell+m)!} \right]^{\frac{1}{2}} \left[\frac{(2\ell'+1)}{4\pi} \frac{(\ell'-m')!}{(\ell'+m')!} \right]^{\frac{1}{2}} P_\ell^m(r) P_{\ell'}^{m'}(x) (-1)^{m+m'} e^{i(m-m')\phi} \\
&= \left[\frac{(2\ell+1)}{4\pi} \frac{(\ell-m)!}{(\ell+m)!} \right]^{\frac{1}{2}} \left[\frac{(2\ell'+1)}{4\pi} \frac{(\ell'-m')!}{(\ell'+m')!} \right]^{\frac{1}{2}} \int_{-1}^{t_r} dx P_\ell^m(x) P_{\ell'}^{m'}(x) (-1)^{2m} 2\pi \delta_{mm'} \\
&= \zeta_{\ell\ell'}^m Q_{\ell\ell'}^m(t_r) \delta_{mm'},
\end{aligned} \tag{B.1}$$

B Detailed derivation of the system of equations

where (3.13) and (3.15a) have been used. Equivalently, when one of the Legendre Polynomials is centered at the multipole positions:

$$\begin{aligned} & \int_{-1}^{t_r} dx \int_0^{2\pi} d\phi \left(\frac{r_\eta|_{r=R}}{R} \right)^{-\ell-1} Y_\ell^m(\theta_{\bar{\mu}}, \phi_{\bar{\mu}}) [Y_{\ell'}^{m'}(\theta, \phi)]^* \\ &= \zeta_{\ell\ell'}^m \int_{-1}^{t_r} dx (\chi[\eta](x, R))^{-(\ell+1)/2} P_\ell^m(\cos\theta_\eta) P_{\ell'}^m(x) \delta_{mm'} \\ &= \zeta_{\ell\ell'}^m K_{\ell\ell'}^m[\eta](t_r) \delta_{mm'}, \end{aligned} \quad (\text{B.2})$$

$$\begin{aligned} & \int_{-1}^{t_r} dx \int_0^{2\pi} d\phi \frac{\partial}{\partial(\frac{r}{R})} \left\{ \left(\frac{r_\eta|_{r=R}}{R} \right)^{-\ell-1} Y_\ell^m(\theta_{\bar{\mu}}, \phi_{\bar{\mu}}) \right\}_{r=R} [Y_{\ell'}^{m'}(\theta, \phi)]^* \\ &= \zeta_{\ell\ell'}^m \int_{-1}^{t_r} dx \frac{\partial}{\partial(\frac{r}{R})} \left\{ (\chi[\eta](x, R))^{-(\ell+1)/2} P_\ell^m(\cos\theta_\eta) \right\}_{r=R} P_{\ell'}^m(x) \delta_{mm'} \\ &= \zeta_{\ell\ell'}^m L_{\ell\ell'}^m[\eta](t_r) \delta_{mm'}, \end{aligned} \quad (\text{B.3})$$

$$\begin{aligned} & \int_{-1}^{t_r} dx \int_0^{2\pi} d\phi \left(\frac{r_\eta|_{r=R}}{R} \right)^\ell Y_\ell^m(\theta_{\bar{\mu}}, \phi_{\bar{\mu}}) [Y_{\ell'}^{m'}(\theta, \phi)]^* \\ &= \zeta_{\ell\ell'}^m M_{\ell\ell'}^m[\eta](t_r) \delta_{mm'}, \end{aligned} \quad (\text{B.4})$$

$$\begin{aligned} & \int_{-1}^{t_r} dx \int_0^{2\pi} d\phi \frac{\partial}{\partial(\frac{r}{R})} \left\{ \left(\frac{r_\eta|_{r=R}}{R} \right)^\ell Y_\ell^m(\theta_{\bar{\mu}}, \phi_{\bar{\mu}}) \right\}_{r=R} [Y_{\ell'}^{m'}(\theta, \phi)]^* \\ &= \zeta_{\ell\ell'}^m N_{\ell\ell'}^m[\eta](t_r) \delta_{mm'}, \end{aligned} \quad (\text{B.5})$$

where $\chi[\eta](x, R)$ is introduced by (3.3) and the integral definitions (3.15) have been used. For an integral over all angles, the orthogonality of the spherical harmonics gives

$$\int_{-1}^1 d(\cos\theta) \int_0^{2\pi} d\phi Y_\ell^m(\theta, \phi) [Y_{\ell'}^{m'}(\theta, \phi)]^* = \delta_{\ell\ell'} \delta_{mm'}. \quad (\text{B.6})$$

Finally it will be used that the spherical harmonic with both ℓ and m equal to zero is a constant, according to

$$1 = \sqrt{4\pi} Y_0^0. \quad (\text{B.7})$$

B.2 Potentials with reflected and transmitted amplitudes eliminated

Before starting the task of deriving the system of equations in (B.33), the potentials are restated here for reference. Also, the reflected and transmitted amplitudes have been eliminated using the relations in (3.8),

thus giving

$$\psi_1(\mathbf{r}) = \psi_{\text{inc}}(\mathbf{r}) + \sum'_{\ell m} A_{\ell m} r_\mu^{-\ell-1} Y_\ell^m(\theta_\mu, \phi_\mu) + \sum'_{\ell m} (-1)^{\ell+m} \frac{\varepsilon_1 - \varepsilon_2}{\varepsilon_1 + \varepsilon_2} A_{\ell m} r_{\bar{\mu}}^{-\ell-1} Y_\ell^m(\theta_{\bar{\mu}}, \phi_{\bar{\mu}}), \quad (\text{B.8a})$$

$$\psi_2(\mathbf{r}) = \psi_{\text{inc}}^t(\mathbf{r}) + \sum'_{\ell m} \frac{2\varepsilon_1}{\varepsilon_1 + \varepsilon_2} A_{\ell m} r_\mu^{-\ell-1} Y_\ell^m(\theta_\mu, \phi_\mu), \quad (\text{B.8b})$$

$$\psi_3(\mathbf{r}) = \psi_0 + \sum'_{\ell m} B_{\ell m} r_\mu^\ell Y_\ell^m(\theta_\mu, \phi_\mu) + \sum'_{\ell m} (-1)^{\ell+m} \frac{\varepsilon_3 - \varepsilon_4}{\varepsilon_3 + \varepsilon_4} B_{\ell m} r_{\bar{\mu}}^\ell Y_\ell^m(\theta_{\bar{\mu}}, \phi_{\bar{\mu}}), \quad (\text{B.8c})$$

$$\psi_4(\mathbf{r}) = \psi_0 + \sum'_{\ell m} \frac{2\varepsilon_3}{\varepsilon_3 + \varepsilon_4} B_{\ell m} r_\mu^\ell Y_\ell^m(\theta_\mu, \phi_\mu), \quad (\text{B.8d})$$

$$\begin{aligned} \psi_5(\mathbf{r}) = & \psi_c + \sum'_{\ell m} \mathcal{A}_{\ell m} r_\mu^{-\ell-1} Y_\ell^m(\theta_\mu, \phi_\mu) + \sum'_{\ell m} \mathcal{B}_{\ell m} r_\mu^\ell Y_\ell^m(\theta_\mu, \phi_\mu) \\ & + \sum'_{\ell m} (-1)^{\ell+m} \frac{\varepsilon_5 - \varepsilon_6}{\varepsilon_5 + \varepsilon_6} \mathcal{A}_{\ell m} r_{\bar{\mu}}^{-\ell-1} Y_\ell^m(\theta_{\bar{\mu}}, \phi_{\bar{\mu}}) + \sum'_{\ell m} (-1)^{\ell+m} \frac{\varepsilon_5 - \varepsilon_6}{\varepsilon_5 + \varepsilon_6} \mathcal{B}_{\ell m} r_{\bar{\mu}}^\ell Y_\ell^m(\theta_{\bar{\mu}}, \phi_{\bar{\mu}}), \end{aligned} \quad (\text{B.8e})$$

$$\psi_6(\mathbf{r}) = \psi_c + \sum'_{\ell m} \frac{2\varepsilon_5}{\varepsilon_5 + \varepsilon_6} \mathcal{A}_{\ell m} r_\mu^{-\ell-1} Y_\ell^m(\theta_\mu, \phi_\mu) + \sum'_{\ell m} \frac{2\varepsilon_5}{\varepsilon_5 + \varepsilon_6} \mathcal{B}_{\ell m} r_\mu^\ell Y_\ell^m(\theta_\mu, \phi_\mu), \quad (\text{B.8f})$$

with $\psi_{\text{inc}}(\mathbf{r})$ and $\psi_{\text{inc}}^t(\mathbf{r})$ defined as before,

$$\psi_{\text{inc}}(\mathbf{r}) = -rE_0 \sqrt{\frac{2\pi}{3}} \left[\cos \theta_0 Y_1^0(\theta, \phi) \sqrt{2} + \sin \theta_0 \{ e^{i\phi_0} Y_1^{-1}(\theta, \phi) - e^{-i\phi_0} Y_1^1(\theta, \phi) \} \right], \quad (\text{B.9a})$$

$$\begin{aligned} \psi_{\text{inc}}^t(\mathbf{r}) = & E_0 \left[d\{(\varepsilon_1/\varepsilon_2) - 1\} \cos \theta_0 \right. \\ & \left. - r \sqrt{\frac{2\pi}{3}} [(\varepsilon_1/\varepsilon_2) \cos \theta_0 Y_1^0(\theta, \phi) \sqrt{2} + \sin \theta_0 \{ e^{i\phi_0} Y_1^{-1}(\theta, \phi) - e^{-i\phi_0} Y_1^1(\theta, \phi) \}] \right]. \end{aligned} \quad (\text{B.9b})$$

B.3 Continuity on the outer coating surface

The boundary conditions on the outer spherical surface will be treated first. The first section, concerning the continuity of the potential, will be a bit more thorough than the next three treatments. This is because the derivation in all four cases follow very similar lines, so that the omission of a few steps should not be a problem.

B.3.1 Continuity of the potential at the outer shell

First, the continuity of the potential at the interface between the ambient and the coating will be studied. The potentials (B.8a), (B.8b), (B.8e), (B.8f) are then inserted into the weakly formulated continuity equation

B Detailed derivation of the system of equations

(3.9a), which gives

$$\begin{aligned}
& \int_{-1}^{t_{rc}} dx \int_0^{2\pi} d\phi \left\{ -R_c E_0 \sqrt{\frac{2\pi}{3}} \left[\cos \theta_0 Y_1^0(\theta, \phi) \sqrt{2} + \sin \theta_0 \{ e^{i\phi_0} Y_1^{-1}(\theta, \phi) - e^{-i\phi_0} Y_1^1(\theta, \phi) \} \right] \right. \\
& + \sum'_{\ell m} A_{\ell m}(r_\mu |_{r=R_c})^{-\ell-1} Y_\ell^m(\theta_\mu, \phi_\mu) + \sum'_{\ell m} (-1)^{\ell+m} \frac{\epsilon_1 - \epsilon_2}{\epsilon_1 + \epsilon_2} A_{\ell m}(r_{\bar{\mu}} |_{r=R_c})^{-\ell-1} Y_\ell^m(\theta_{\bar{\mu}}, \phi_{\bar{\mu}}) \\
& - \psi_c - \sum'_{\ell m} \mathcal{A}_{\ell m}(r_\mu |_{r=R_c})^{-\ell-1} Y_\ell^m(\theta_\mu, \phi_\mu) - \sum'_{\ell m} \mathcal{B}_{\ell m}(r_\mu |_{r=R_c})^\ell Y_\ell^m(\theta_\mu, \phi_\mu) \\
& - \sum'_{\ell m} (-1)^{\ell+m} \frac{\epsilon_5 - \epsilon_6}{\epsilon_5 + \epsilon_6} \mathcal{A}_{\ell m}(r_{\bar{\mu}} |_{r=R_c})^{-\ell-1} Y_\ell^m(\theta_{\bar{\mu}}, \phi_{\bar{\mu}}) \\
& \left. - \sum'_{\ell m} (-1)^{\ell+m} \frac{\epsilon_5 - \epsilon_6}{\epsilon_5 + \epsilon_6} \mathcal{B}_{\ell m}(r_{\bar{\mu}} |_{r=R_c})^\ell Y_\ell^m(\theta_{\bar{\mu}}, \phi_{\bar{\mu}}) \right\} [Y_{\ell'}^{m'}(\theta, \phi)]^* \\
& + \int_{t_{rc}}^1 dx \int_0^{2\pi} d\phi \left\{ E_0 d\{(\epsilon_1/\epsilon_2) - 1\} \cos \theta_0 \right. \\
& - E_0 R_c \sqrt{\frac{2\pi}{3}} \left[(\epsilon_1/\epsilon_2) \cos \theta_0 Y_1^0(\theta, \phi) \sqrt{2} + \sin \theta_0 \{ e^{i\phi_0} Y_1^{-1}(\theta, \phi) - e^{-i\phi_0} Y_1^1(\theta, \phi) \} \right] \\
& + \sum'_{\ell m} \frac{2\epsilon_1}{\epsilon_1 + \epsilon_2} A_{\ell m}(r_\mu |_{r=R_c})^{-\ell-1} Y_\ell^m(\theta_\mu, \phi_\mu) \\
& - \psi_c - \sum'_{\ell m} \frac{2\epsilon_5}{\epsilon_5 + \epsilon_6} \mathcal{A}_{\ell m}(r_\mu |_{r=R_c})^{-\ell-1} Y_\ell^m(\theta_\mu, \phi_\mu) - \sum'_{\ell m} \frac{2\epsilon_5}{\epsilon_5 + \epsilon_6} \mathcal{B}_{\ell m}(r_\mu |_{r=R_c})^\ell Y_\ell^m(\theta_\mu, \phi_\mu) \left. \right\} [Y_{\ell'}^{m'}(\theta, \phi)]^* \\
& = 0. \tag{B.10}
\end{aligned}$$

Next, by introducing $\chi[\eta](x, R)$ via (3.3) and by collecting terms by their multipole expansion coefficient, it follows that

$$\begin{aligned}
 & \int_0^{2\pi} d\phi \left\{ \int_{-1}^{t_{rc}} -R_c E_0 \sqrt{\frac{2\pi}{3}} \left[\cos \theta_0 Y_1^0(\theta, \phi) \sqrt{2} + \sin \theta_0 \{ e^{i\phi_0} Y_1^{-1}(\theta, \phi) - e^{-i\phi_0} Y_1^1(\theta, \phi) \} \right] \right. \\
 & \quad - \int_{-1}^{t_{rc}} \psi_c + \int_{t_{rc}}^1 E_0 d\{ (\varepsilon_1/\varepsilon_2) - 1 \} \cos \theta_0 \\
 & \quad - \int_{t_{rc}}^1 E_0 R_c \sqrt{\frac{2\pi}{3}} \left[(\varepsilon_1/\varepsilon_2) \cos \theta_0 Y_1^0(\theta, \phi) \sqrt{2} + \sin \theta_0 \{ e^{i\phi_0} Y_1^{-1}(\theta, \phi) - e^{-i\phi_0} Y_1^1(\theta, \phi) \} \right] \\
 & \quad \left. - \int_{t_{rc}}^1 \psi_c \right\} d(\cos \theta) [Y_{\ell'}^{m'}(\theta, \phi)]^* \\
 & + \sum'_{\ell m} A_{\ell m} \int_0^{2\pi} d\phi \left\{ \int_{-1}^{t_{rc}} (R_c \sqrt{\chi[\mu](x, r)})^{-\ell-1} Y_{\ell}^m(\theta_{\mu}, \phi_{\mu}) + \int_{-1}^{t_{rc}} (-1)^{\ell+m} \frac{\varepsilon_1 - \varepsilon_2}{\varepsilon_1 + \varepsilon_2} (R_c \sqrt{\chi[\bar{\mu}](x, r)})^{-\ell-1} Y_{\ell}^m(\theta_{\bar{\mu}}, \phi_{\bar{\mu}}) \right. \\
 & \quad \left. + \int_{t_{rc}}^1 \frac{2\varepsilon_1}{\varepsilon_1 + \varepsilon_2} (R_c \sqrt{\chi[\mu](x, r)})^{-\ell-1} Y_{\ell}^m(\theta_{\mu}, \phi_{\mu}) \right\} d(\cos \theta) [Y_{\ell'}^{m'}(\theta, \phi)]^* \\
 & - \sum'_{\ell m} \mathcal{A}_{\ell m} \int_0^{2\pi} d\phi \left\{ \int_{-1}^{t_{rc}} (R_c \sqrt{\chi[\mu](x, r)})^{-\ell-1} Y_{\ell}^m(\theta_{\mu}, \phi_{\mu}) + \int_{-1}^{t_{rc}} (-1)^{\ell+m} \frac{\varepsilon_5 - \varepsilon_6}{\varepsilon_5 + \varepsilon_6} (R_c \sqrt{\chi[\bar{\mu}](x, r)})^{-\ell-1} Y_{\ell}^m(\theta_{\bar{\mu}}, \phi_{\bar{\mu}}) \right. \\
 & \quad \left. + \int_{t_{rc}}^1 \frac{2\varepsilon_5}{\varepsilon_5 + \varepsilon_6} (R_c \sqrt{\chi[\mu](x, r)})^{-\ell-1} Y_{\ell}^m(\theta_{\mu}, \phi_{\mu}) \right\} d(\cos \theta) [Y_{\ell'}^{m'}(\theta, \phi)]^* \\
 & - \sum'_{\ell m} \mathcal{B}_{\ell m} \int_0^{2\pi} d\phi \left\{ \int_{-1}^{t_{rc}} (R_c \sqrt{\chi[\mu](x, r)})^{\ell} Y_{\ell}^m(\theta_{\mu}, \phi_{\mu}) + \int_{-1}^{t_{rc}} (-1)^{\ell+m} \frac{\varepsilon_5 - \varepsilon_6}{\varepsilon_5 + \varepsilon_6} (R_c \sqrt{\chi[\bar{\mu}](x, r)})^{\ell} Y_{\ell}^m(\theta_{\bar{\mu}}, \phi_{\bar{\mu}}) \right. \\
 & \quad \left. + \int_{t_{rc}}^1 \frac{2\varepsilon_5}{\varepsilon_5 + \varepsilon_6} (R_c \sqrt{\chi[\mu](x, r)})^{\ell} Y_{\ell}^m(\theta_{\mu}, \phi_{\mu}) \right\} d(\cos \theta) [Y_{\ell'}^{m'}(\theta, \phi)]^* \\
 & = 0.
 \end{aligned} \tag{B.11}$$

B Detailed derivation of the system of equations

The equations are then rearranged so that the previously defined integrals may be substituted, and the radius is pulled out from the integrals, leaving dimensionless integrands:

$$\begin{aligned}
& \int_0^{2\pi} d\phi \left\{ \int_{-1}^{t_{rc}} ((\varepsilon_1/\varepsilon_2) - 1) R_c E_0 \sqrt{\frac{2\pi}{3}} \cos \theta_0 Y_1^0(\theta, \phi) \sqrt{2} \right. \\
& + \int_{-1}^1 E_0 d\{(\varepsilon_1/\varepsilon_2) - 1\} \cos \theta_0 \sqrt{4\pi} Y_0^0(\theta, \phi) - \int_{-1}^{t_{rc}} E_0 R_c \frac{d}{R_c} \{(\varepsilon_1/\varepsilon_2) - 1\} \cos \theta_0 \sqrt{4\pi} Y_0^0(\theta, \phi) \\
& - \int_{-1}^1 E_0 R_c \sqrt{\frac{2\pi}{3}} (\varepsilon_1/\varepsilon_2) \cos \theta_0 Y_1^0(\theta, \phi) \sqrt{2} - \int_{-1}^1 E_0 R_c \sin \theta_0 \{e^{i\phi_0} Y_1^{-1}(\theta, \phi) - e^{-i\phi_0} Y_1^1(\theta, \phi)\} \\
& \left. - \int_{-1}^1 \psi_c \sqrt{4\pi} Y_0^0(\theta, \phi) \right\} d(\cos \theta) [Y_{\ell'}^{m'}(\theta, \phi)]^* \\
& + \sum'_{\ell m} R_c^{-\ell-1} A_{\ell m} \int_0^{2\pi} d\phi \left\{ \int_{-1}^{t_{rc}} (\chi[\mu](x, r))^{-(\ell+1)/2} Y_\ell^m(\theta_\mu, \phi_\mu) + \int_{-1}^{t_{rc}} (-1)^{\ell+m} \frac{\varepsilon_1 - \varepsilon_2}{\varepsilon_1 + \varepsilon_2} (\chi[\bar{\mu}](x, r))^{-(\ell+1)/2} Y_\ell^m(\theta_{\bar{\mu}}, \phi_{\bar{\mu}}) \right. \\
& + \left[\int_{-1}^1 - \int_{-1}^{t_r} \right] \frac{2\varepsilon_1}{\varepsilon_1 + \varepsilon_2} (\chi[\mu](x, r))^{-(\ell+1)/2} Y_\ell^m(\theta_\mu, \phi_\mu) \left. \right\} d(\cos \theta) [Y_{\ell'}^{m'}(\theta, \phi)]^* \\
& - \sum'_{\ell m} R_c^{-\ell-1} \mathcal{A}_{\ell m} \int_0^{2\pi} d\phi \left\{ \int_{-1}^{t_{rc}} (\chi[\mu](x, r))^{-(\ell+1)/2} Y_\ell^m(\theta_\mu, \phi_\mu) + \int_{-1}^{t_{rc}} (-1)^{\ell+m} \frac{\varepsilon_5 - \varepsilon_6}{\varepsilon_5 + \varepsilon_6} (\chi[\bar{\mu}](x, r))^{-(\ell+1)/2} Y_\ell^m(\theta_{\bar{\mu}}, \phi_{\bar{\mu}}) \right. \\
& + \left[\int_{-1}^1 - \int_{-1}^{t_r} \right] \frac{2\varepsilon_5}{\varepsilon_5 + \varepsilon_6} (\chi[\mu](x, r))^{-(\ell+1)/2} Y_\ell^m(\theta_\mu, \phi_\mu) \left. \right\} d(\cos \theta) [Y_{\ell'}^{m'}(\theta, \phi)]^* \\
& - \sum'_{\ell m} R_c^\ell \mathcal{B}_{\ell m} \int_0^{2\pi} d\phi \left\{ \int_{-1}^{t_{rc}} (\chi[\mu](x, r))^{\ell/2} Y_\ell^m(\theta_\mu, \phi_\mu) + \int_{-1}^{t_{rc}} (-1)^{\ell+m} \frac{\varepsilon_5 - \varepsilon_6}{\varepsilon_5 + \varepsilon_6} (\chi[\mu](x, r))^{\ell/2} Y_\ell^m(\theta_{\bar{\mu}}, \phi_{\bar{\mu}}) \right. \\
& + \left[\int_{-1}^1 - \int_{-1}^{t_r} \right] \frac{2\varepsilon_5}{\varepsilon_5 + \varepsilon_6} (\chi[\mu](x, r))^{\ell/2} Y_\ell^m(\theta_\mu, \phi_\mu) \left. \right\} d(\cos \theta) [Y_{\ell'}^{m'}(\theta, \phi)]^* \\
& = 0. \tag{B.12}
\end{aligned}$$

The relations (B.1), (B.2), (B.4), (B.6) and (B.7) are then used, simplifying the system of equations to

$$\begin{aligned}
& (\varepsilon_1/\varepsilon_2 - 1) R_c E_0 \sqrt{\frac{2\pi}{3}} \cos \theta_0 \zeta_{\ell'1}^0 Q_{\ell'1}^0(t_{rc}) \delta_{m'0} \sqrt{2} \\
& + E_0 d\{(\varepsilon_1/\varepsilon_2) - 1\} \cos \theta_0 \sqrt{4\pi} \delta_{m'0} \delta_{\ell'0} - E_0 R_c t_{rc} \{(\varepsilon_1/\varepsilon_2) - 1\} \cos \theta_0 \sqrt{4\pi} \zeta_{\ell'0}^0 Q_{\ell'0}^0(t_{rc}) \delta_{m'0} \\
& - E_0 R_c \sqrt{\frac{4\pi}{3}} (\varepsilon_1/\varepsilon_2) \cos \theta_0 \delta_{m'0} \delta_{\ell'1} - E_0 R_c \sqrt{\frac{2\pi}{3}} \sin \theta_0 \delta_{\ell'1} \{e^{i\phi_0} \delta_{m'-1} - e^{-i\phi_0} \delta_{m'1}\} \\
& - \psi_c \sqrt{4\pi} \delta_{m'0} \delta_{\ell'0} \\
& + \sum'_{\ell m} R_c^{-\ell-1} A_{\ell m} \left\{ \zeta_{\ell\ell_1}^m \left[K_{\ell\ell_1}^m[\mu](t_r) + \left(\frac{\varepsilon_1 - \varepsilon_2}{\varepsilon_1 + \varepsilon_2} \right) (-1)^{\ell_1+m} K_{\ell\ell_1}^m[\bar{\mu}](t_r) + \left(\frac{2\varepsilon_1}{\varepsilon_1 + \varepsilon_2} \right) \{K_{\ell\ell_1}^m[\mu](t_r=1) - K_{\ell\ell_1}^m[\mu](t_r)\} \right] \right\} \\
& - \sum'_{\ell m} R_c^{-\ell-1} \mathcal{A}_{\ell m} \left\{ \zeta_{\ell\ell_1}^m \left[K_{\ell\ell_1}^m[\mu](t_r) + \left(\frac{\varepsilon_5 - \varepsilon_6}{\varepsilon_5 + \varepsilon_6} \right) (-1)^{\ell_1+m} K_{\ell\ell_1}^m[\bar{\mu}](t_r) + \left(\frac{2\varepsilon_5}{\varepsilon_5 + \varepsilon_6} \right) \{K_{\ell\ell_1}^m[\mu](t_r=1) - K_{\ell\ell_1}^m[\mu](t_r)\} \right] \right\} \\
& + \sum'_{\ell m} R_c^\ell \mathcal{B}_{\ell m} \left\{ -\zeta_{\ell\ell_1}^m \left[M_{\ell\ell_1}^m[\mu](t_r) + \left(\frac{\varepsilon_5 - \varepsilon_6}{\varepsilon_5 + \varepsilon_6} \right) (-1)^{\ell_1+m} M_{\ell\ell_1}^m[\bar{\mu}](t_r) + \left(\frac{2\varepsilon_5}{\varepsilon_5 + \varepsilon_6} \right) \{M_{\ell\ell_1}^m[\mu](t_r=1) - M_{\ell\ell_1}^m[\mu](t_r)\} \right] \right\} \\
& = 0. \tag{B.13}
\end{aligned}$$

This is further simplified by using the definitions (3.14a), (3.14b) and (3.12a)

$$\begin{aligned} & \sum'_{\ell m} R_c^{-\ell-1} A_{\ell m} C_{\ell' \ell}^m(\varepsilon_1, \varepsilon_2, t_{rc}) \delta_{m'm} - \sum'_{\ell m} R_c^{-\ell-1} \mathcal{A}_{\ell m} C_{\ell' \ell}^m(\varepsilon_5, \varepsilon_6, t_{rc}) \delta_{m'm} + \sum'_{\ell m} R_c^\ell \mathcal{B}_{\ell m} D_{\ell' \ell}^m(\varepsilon_5, \varepsilon_6, t_{rc}) \delta_{m'm} \\ &= R_c H_{\ell'}^{m'}(t_{rc}) - E_0 d\{(\varepsilon_1/\varepsilon_2) - 1\} \cos \theta_0 \sqrt{4\pi} \delta_{m'0} \delta_{\ell'0} + \psi_c \sqrt{4\pi} \delta_{m'0} \delta_{\ell'0}. \end{aligned} \quad (\text{B.14})$$

The Kronecker delta will kill all terms in the sums with m unequal to m' , so the sums simplify to

$$\begin{aligned} & \sum'_{\ell=|m'|}^{\infty} R_c^{-\ell-1} A_{\ell m'} C_{\ell' \ell}^{m'}(\varepsilon_1, \varepsilon_2, t_{rc}) - \sum'_{\ell=|m'|}^{\infty} R_c^{-\ell-1} \mathcal{A}_{\ell m'} C_{\ell' \ell}^{m'}(\varepsilon_5, \varepsilon_6, t_{rc}) + \sum'_{\ell=|m'|}^{\infty} R_c^\ell \mathcal{B}_{\ell m'} D_{\ell' \ell}^{m'}(\varepsilon_5, \varepsilon_6, t_{rc}) \\ &= R_c H_{\ell'}^{m'}(t_{rc}) - E_0 d\{(\varepsilon_1/\varepsilon_2) - 1\} \cos \theta_0 \sqrt{4\pi} \delta_{m'0} \delta_{\ell'0} + \psi_c \sqrt{4\pi} \delta_{m'0} \delta_{\ell'0}. \end{aligned} \quad (\text{B.15})$$

where $\ell' = 0, 1, 2, 3, \dots$ and $m' = 0, \pm 1, \pm 2, \pm 3, \dots, \pm \ell'$. The $\ell' = 0$ term may be used to find the constant ψ_c [2, p. 232], but is not necessary in order to find the multipole expansion coefficients and may therefore be discarded. It is also evident that the $H_{\ell'}^{m'}$ term equals zero for m unequal to 0, 1 or -1, and since terms with different m 's do not couple in this equation, the system of equations may be reduced to

$$\sum_{\ell=1}^{\infty} R_c^{-\ell-1} A_{\ell m'} C_{\ell' \ell}^{m'}(t_{rc}) - \sum_{\ell=1}^{\infty} R_c^{-\ell-1} \mathcal{A}_{\ell m'} C_{\ell' \ell}^{m'}(t_{rc}) + \sum_{\ell=1}^{\infty} R_c^\ell \mathcal{B}_{\ell m'} D_{\ell' \ell}^{m'}(t_{rc}) = R_c H_{\ell'}^{m'}(t_{rc}), \quad (\text{B.16})$$

where $\ell' = 1, 2, 3, \dots$ and $m' = 0, \pm 1$. Note that the shorthand notation (3.16a) and (3.16b) has been used. As previously argued, the $m = -1$ equation gives the same information as the $m = 1$ equation, and is therefore discarded. The sums are also truncated at $\ell = M$, so that the system of equations for the multipole coefficients may be solved numerically. Dividing through by R_c , renaming ℓ to ℓ_1 and dropping the primes on the running variables, (3.11a) is retrieved,

$$\sum_{\ell_1=1}^M R_c^{-\ell_1-2} A_{\ell_1 m} C_{\ell \ell_1}^m(t_{rc}) - \sum_{\ell_1=1}^M R_c^{-\ell_1-2} \mathcal{A}_{\ell_1 m} C_{\ell \ell_1}^m(t_{rc}) + \sum_{\ell_1=1}^M R_c^{\ell_1-1} \mathcal{B}_{\ell_1 m} D_{\ell \ell_1}^m(t_{rc}) = H_{\ell'}^m(t_{rc}), \quad (\text{B.17})$$

where $\ell = 1, 2, 3, \dots, M$ and $m = 0, 1$.

B Detailed derivation of the system of equations

B.3.2 Continuity of the normal derivative of the potential times the permittivity at the outer shell

The derivation of the normal displacement field continuity equations for the interface between the ambient and the coating follow the same line as the previous derivations. First, the potentials (B.8a), (B.8b), (B.8e), (B.8f) are inserted into the weakly formulated continuity equation (3.9c). This gives

$$\begin{aligned}
& \int_{-1}^{t_{rc}} d(\cos \theta) \int_0^{2\pi} d\phi \left\{ -\varepsilon_1 E_0 \sqrt{\frac{2\pi}{3}} \left[\cos \theta_0 Y_1^0(\theta, \phi) \sqrt{2} + \sin \theta_0 \{ e^{i\phi_0} Y_1^{-1}(\theta, \phi) - e^{-i\phi_0} Y_1^1(\theta, \phi) \} \right] \right. \\
& + \sum'_{\ell m} \varepsilon_1 A_{\ell m} \frac{\partial}{\partial r} [r_\mu^{-\ell-1} Y_\ell^m(\theta_\mu, \phi_\mu)]_{r=R_c} + \sum'_{\ell m} (-1)^{\ell+m} \varepsilon_1 \frac{\varepsilon_1 - \varepsilon_2}{\varepsilon_1 + \varepsilon_2} A_{\ell m} \frac{\partial}{\partial r} [r_{\bar{\mu}}^{-\ell-1} Y_\ell^m(\theta_{\bar{\mu}}, \phi_{\bar{\mu}})]_{r=R_c} \\
& - \sum'_{\ell m} \varepsilon_5 \mathcal{A}_{\ell m} \frac{\partial}{\partial r} [r_\mu^{-\ell-1} Y_\ell^m(\theta_\mu, \phi_\mu)]_{r=R_c} - \sum'_{\ell m} \varepsilon_5 \mathcal{B}_{\ell m} \frac{\partial}{\partial r} [r_\mu^\ell Y_\ell^m(\theta_\mu, \phi_\mu)]_{r=R_c} \\
& - \sum'_{\ell m} (-1)^{\ell+m} \varepsilon_5 \frac{\varepsilon_5 - \varepsilon_6}{\varepsilon_5 + \varepsilon_6} \mathcal{A}_{\ell m} \frac{\partial}{\partial r} [r_{\bar{\mu}}^{-\ell-1} Y_\ell^m(\theta_{\bar{\mu}}, \phi_{\bar{\mu}})]_{r=R_c} \\
& \left. - \sum'_{\ell m} (-1)^{\ell+m} \varepsilon_5 \frac{\varepsilon_5 - \varepsilon_6}{\varepsilon_5 + \varepsilon_6} \mathcal{B}_{\ell m} \frac{\partial}{\partial r} [r_{\bar{\mu}}^\ell Y_\ell^m(\theta_{\bar{\mu}}, \phi_{\bar{\mu}})]_{r=R_c} \right\} [Y_{\ell'}^{m'}(\theta, \phi)]^* \\
& + \int_{t_{rc}}^1 d(\cos \theta) \int_0^{2\pi} d\phi \left\{ -\varepsilon_2 E_0 \sqrt{\frac{2\pi}{3}} \left[(\varepsilon_1 / \varepsilon_2) \cos \theta_0 Y_1^0(\theta, \phi) \sqrt{2} + \sin \theta_0 \{ e^{i\phi_0} Y_1^{-1}(\theta, \phi) - e^{-i\phi_0} Y_1^1(\theta, \phi) \} \right] \right. \\
& + \sum'_{\ell m} \varepsilon_2 \frac{2\varepsilon_1}{\varepsilon_1 + \varepsilon_2} A_{\ell m} \frac{\partial}{\partial r} [r_\mu^{-\ell-1} Y_\ell^m(\theta_\mu, \phi_\mu)]_{r=R_c} \\
& - \sum'_{\ell m} \varepsilon_6 \frac{2\varepsilon_5}{\varepsilon_5 + \varepsilon_6} \mathcal{A}_{\ell m} \frac{\partial}{\partial r} [r_\mu^{-\ell-1} Y_\ell^m(\theta_\mu, \phi_\mu)]_{r=R_c} \\
& \left. - \sum'_{\ell m} \varepsilon_6 \frac{2\varepsilon_5}{\varepsilon_5 + \varepsilon_6} \mathcal{B}_{\ell m} \frac{\partial}{\partial r} [r_\mu^\ell Y_\ell^m(\theta_\mu, \phi_\mu)]_{r=R_c} \right\} [Y_{\ell'}^{m'}(\theta, \phi)]^* \\
& = 0. \tag{B.18}
\end{aligned}$$

Next, as before by introducing $\chi[\eta](x, R)$ via (3.3), and by collecting terms by their multipole expansion coefficients, extracting the radii and rearranging the integrals:

$$\begin{aligned}
 & \int_0^{2\pi} d\phi \left\{ - \int_{-1}^{t_{rc}} (\epsilon_1 - \epsilon_2) E_0 \sqrt{\frac{2\pi}{3}} \sin \theta_0 \{ e^{i\phi_0} Y_1^{-1}(\theta, \phi) - e^{-i\phi_0} Y_1^1(\theta, \phi) \} \right. \\
 & \quad - \int_{-1}^1 \epsilon_1 E_0 \sqrt{\frac{4\pi}{3}} \cos \theta_0 Y_1^0(\theta, \phi) \\
 & \quad \left. - \int_{-1}^1 \epsilon_2 E_0 \sqrt{\frac{2\pi}{3}} \sin \theta_0 \{ e^{i\phi_0} Y_1^{-1}(\theta, \phi) - e^{-i\phi_0} Y_1^1(\theta, \phi) \} \right\} d(\cos \theta) [Y_{\ell'}^{m'}(\theta, \phi)]^* \\
 & + \sum'_{\ell m} R_c^{-\ell-2} A_{\ell m} \int_0^{2\pi} d\phi \left\{ \int_{-1}^{t_{rc}} \epsilon_1 \frac{\partial}{\partial(\frac{r}{R_c})} \left[(\chi[\mu](x, r))^{-\ell-1} Y_\ell^m(\theta_\mu, \phi_\mu) \right]_{r=R_c} \right. \\
 & \quad + \int_{-1}^{t_{rc}} (-1)^{\ell+m} \epsilon_1 \frac{\epsilon_1 - \epsilon_2}{\epsilon_1 + \epsilon_2} \frac{\partial}{\partial(\frac{r}{R_c})} \left[(\chi[\bar{\mu}](x, r))^{-\ell-1} Y_\ell^m(\theta_{\bar{\mu}}, \phi_{\bar{\mu}}) \right]_{r=R_c} \\
 & \quad \left. + \left[\int_{-1}^1 - \int_{-1}^{t_{rc}} \right] \epsilon_2 \frac{2\epsilon_1}{\epsilon_1 + \epsilon_2} \frac{\partial}{\partial(\frac{r}{R_c})} \left[(\chi[\mu](x, r))^{-\ell-1} Y_\ell^m(\theta_\mu, \phi_\mu) \right]_{r=R_c} \right\} d(\cos \theta) [Y_{\ell'}^{m'}(\theta, \phi)]^* \\
 & - \sum'_{\ell m} R_c^{-\ell-2} \mathcal{A}_{\ell m} \int_0^{2\pi} d\phi \left\{ \int_{-1}^{t_{rc}} \epsilon_5 \frac{\partial}{\partial(\frac{r}{R_c})} \left[(\chi[\mu](x, r))^{-\ell-1} Y_\ell^m(\theta_\mu, \phi_\mu) \right]_{r=R_c} \right. \\
 & \quad + \int_{-1}^{t_{rc}} (-1)^{\ell+m} \epsilon_5 \frac{\epsilon_5 - \epsilon_6}{\epsilon_5 + \epsilon_6} \frac{\partial}{\partial(\frac{r}{R_c})} \left[(\chi[\bar{\mu}](x, r))^{-\ell-1} Y_\ell^m(\theta_{\bar{\mu}}, \phi_{\bar{\mu}}) \right]_{r=R_c} \\
 & \quad \left. + \left[\int_{-1}^1 - \int_{-1}^{t_{rc}} \right] \epsilon_6 \frac{2\epsilon_5}{\epsilon_5 + \epsilon_6} \frac{\partial}{\partial(\frac{r}{R_c})} \left[(\chi[\mu](x, r))^{-\ell-1} Y_\ell^m(\theta_\mu, \phi_\mu) \right]_{r=R_c} \right\} d(\cos \theta) [Y_{\ell'}^{m'}(\theta, \phi)]^* \\
 & - \sum'_{\ell m} R_c^{\ell-1} \mathcal{B}_{\ell m} \int_0^{2\pi} d\phi \left\{ \int_{-1}^{t_{rc}} \epsilon_5 \frac{\partial}{\partial(\frac{r}{R_c})} \left[(\chi[\mu](x, r))^{\ell} Y_\ell^m(\theta_\mu, \phi_\mu) \right]_{r=R_c} \right. \\
 & \quad + \int_{-1}^{t_{rc}} (-1)^{\ell+m} \epsilon_5 \frac{\epsilon_5 - \epsilon_6}{\epsilon_5 + \epsilon_6} \frac{\partial}{\partial(\frac{r}{R_c})} \left[(\chi[\bar{\mu}](x, r))^{\ell} Y_\ell^m(\theta_{\bar{\mu}}, \phi_{\bar{\mu}}) \right]_{r=R_c} \\
 & \quad \left. + \left[\int_{-1}^1 - \int_{-1}^{t_{rc}} \right] \epsilon_6 \frac{2\epsilon_5}{\epsilon_5 + \epsilon_6} \frac{\partial}{\partial(\frac{r}{R_c})} \left[(\chi[\mu](x, r))^{\ell} Y_\ell^m(\theta_\mu, \phi_\mu) \right]_{r=R_c} \right\} d(\cos \theta) [Y_{\ell'}^{m'}(\theta, \phi)]^* \\
 & = 0. \tag{B.19}
 \end{aligned}$$

B Detailed derivation of the system of equations

The relations (B.1), (B.3), (B.5), (B.6) and (B.7) are then used, simplifying the system of equations to

$$\begin{aligned}
& -(\varepsilon_1 - \varepsilon_2)E_0\sqrt{\frac{2\pi}{3}}\sin\theta_0\left\{e^{i\phi_0}\zeta_{\ell'1}^{-1}Q_{\ell'1}^{-1}(t_{rc})\delta_{m'-1}-e^{-i\phi_0}\zeta_{\ell'1}^1Q_{\ell'1}^1(t_{rc})\delta_{m'1}\right\} \\
& -\varepsilon_1E_0\sqrt{\frac{4\pi}{3}}\cos\theta_0\delta_{\ell'1}\delta_{m'0} \\
& -\varepsilon_2E_0\sqrt{\frac{2\pi}{3}}\sin\theta_0\delta_{\ell'1}\left\{e^{i\phi_0}\delta_{m'-1}-e^{-i\phi_0}\delta_{m'1}\right\} \\
& +\sum'_{\ell m}R^{-\ell-2}A_{\ell m}\left\{\zeta_{\ell\ell_1}^m\left[\left(\frac{2\varepsilon_1}{\varepsilon_1+\varepsilon_2}\right)L_{\ell\ell_1}^m[\mu](t_r=1)+\varepsilon_1\left(\frac{\varepsilon_1-\varepsilon_2}{\varepsilon_1+\varepsilon_2}\right)\left\{L_{\ell\ell_1}^m[\mu](t_r)+(-1)^{\ell_1+m}M_{\ell\ell_1}^m[\bar{\mu}](t_r)\right\}\right]\right\} \\
& -\sum'_{\ell m}R^{-\ell-2}\mathcal{A}_{\ell m}\left\{\zeta_{\ell\ell_1}^m\left[\left(\frac{2\varepsilon_5}{\varepsilon_5+\varepsilon_6}\right)L_{\ell\ell_1}^m[\mu](t_r=1)+\varepsilon_5\left(\frac{\varepsilon_5-\varepsilon_6}{\varepsilon_5+\varepsilon_6}\right)\left\{L_{\ell\ell_1}^m[\mu](t_r)+(-1)^{\ell_1+m}M_{\ell\ell_1}^m[\bar{\mu}](t_r)\right\}\right]\right\} \\
& +\sum'_{\ell m}R^{\ell-1}\mathcal{B}_{\ell m}\left\{-\zeta_{\ell\ell_1}^m\left[\left(\frac{2\varepsilon_5}{\varepsilon_5+\varepsilon_6}\right)N_{\ell\ell_1}^m[\mu](t_r=1)+\varepsilon_5\left(\frac{\varepsilon_5-\varepsilon_6}{\varepsilon_5+\varepsilon_6}\right)\left\{N_{\ell\ell_1}^m[\mu](t_r)+(-1)^{\ell_1+m}N_{\ell\ell_1}^m[\bar{\mu}](t_r)\right\}\right]\right\} \\
& =0.
\end{aligned} \tag{B.20}$$

This is further simplified using the definitions (3.16c), (3.16d) and (3.12b).

$$\sum'_{\ell m}R_c^{-\ell-2}A_{\ell m}F_{\ell'\ell}^m(t_{rc})\delta_{m'm}-\sum'_{\ell m}R_c^{-\ell-2}\mathcal{A}_{\ell m}\mathcal{F}_{\ell'\ell}^m(t_{rc})\delta_{m'm}+\sum'_{\ell m}R_c^{\ell-1}\mathcal{B}_{\ell m}\mathcal{G}_{\ell'\ell}^m(t_{rc})\delta_{m'm}=J_{\ell'}^{m'}(t_{rc}). \tag{B.21}$$

where $\ell'=0,1,2,3,\dots$ and $m'=0,\pm 1,\pm 2,\pm 3,\dots,\pm \ell'$. Still using the same arguments as in the previous cases, equation (3.11c) is acquired:

$$\sum_{\ell_1=1}^M R^{\ell_1-1}B_{\ell_1 m}D_{\ell\ell_1}^m(t_r)+\sum_{\ell_1=1}^M R^{-\ell_1-2}\mathcal{A}_{\ell_1 m}\mathcal{C}_{\ell\ell_1}^m(t_r)-\sum_{\ell_1=1}^M R^{\ell_1-1}\mathcal{B}_{\ell_1 m}\mathcal{D}_{\ell\ell_1}^m(t_r)=0, \tag{B.22}$$

where $\ell=1,2,3,\dots,M$ and $m=0,1$.

B.4 Continuity on the inner coating surface

In the following, the inner surface boundary conditions will be treated, still following exactly the same lines as in the previous chapter.

B.4.1 Continuity of the potential at the inner shell

The derivation of the potential continuity equation for the interface between the coating and the island start by inserting the potentials (B.8c), (B.8d), (B.8e), (B.8f) into the weakly formulated continuity equation (3.9b). This gives

$$\begin{aligned}
 & \int_{-1}^{t_r} d(\cos \theta) \int_0^{2\pi} d\phi \left\{ \psi_c + \sum'_{\ell m} \mathcal{A}_{\ell m}(r_\mu |_{r=R})^{-\ell-1} Y_\ell^m(\theta_\mu, \phi_\mu) + \sum'_{\ell m} \mathcal{B}_{\ell m}(r_\mu |_{r=R})^\ell Y_\ell^m(\theta_\mu, \phi_\mu) \right. \\
 & + \sum'_{\ell m} (-1)^{\ell+m} \frac{\varepsilon_5 - \varepsilon_6}{\varepsilon_5 + \varepsilon_6} \mathcal{A}_{\ell m}(r_{\bar{\mu}} |_{r=R})^{-\ell-1} Y_\ell^m(\theta_{\bar{\mu}}, \phi_{\bar{\mu}}) + \sum'_{\ell m} (-1)^{\ell+m} \frac{\varepsilon_5 - \varepsilon_6}{\varepsilon_5 + \varepsilon_6} \mathcal{B}_{\ell m}(r_{\bar{\mu}} |_{r=R})^\ell Y_\ell^m(\theta_{\bar{\mu}}, \phi_{\bar{\mu}}) \\
 & \left. - \psi_0 - \sum'_{\ell m} B_{\ell m}(r_\mu |_{r=R})^\ell Y_\ell^m(\theta_\mu, \phi_\mu) - \sum'_{\ell m} (-1)^{\ell+m} \frac{\varepsilon_3 - \varepsilon_4}{\varepsilon_3 + \varepsilon_4} B_{\ell m}(r_{\bar{\mu}} |_{r=R})^\ell Y_\ell^m(\theta_{\bar{\mu}}, \phi_{\bar{\mu}}) \right\} [Y_{\ell'}^{m'}(\theta, \phi)]^* \\
 & + \int_{t_{rc}}^1 d(\cos \theta) \int_0^{2\pi} d\phi \left\{ \psi_c + \sum'_{\ell m} \frac{2\varepsilon_5}{\varepsilon_5 + \varepsilon_6} \mathcal{A}_{\ell m}(r_\mu |_{r=R})^{-\ell-1} Y_\ell^m(\theta_\mu, \phi_\mu) + \sum'_{\ell m} \frac{2\varepsilon_5}{\varepsilon_5 + \varepsilon_6} \mathcal{B}_{\ell m}(r_\mu |_{r=R})^\ell Y_\ell^m(\theta_\mu, \phi_\mu) \right. \\
 & \left. - \psi_0 - \sum'_{\ell m} \frac{2\varepsilon_3}{\varepsilon_3 + \varepsilon_4} B_{\ell m}(r_\mu |_{r=R})^\ell Y_\ell^m(\theta_\mu, \phi_\mu) \right\} [Y_{\ell'}^{m'}(\theta, \phi)]^* \\
 & = 0. \tag{B.23}
 \end{aligned}$$

Next, by introducing $\chi[\eta](x, R)$ with (3.3), and then collecting terms by their multipole expansion coefficient, extracting the radii and rearranging the integrals:

$$\begin{aligned}
 & \int_0^{2\pi} d\phi \int_{-1}^1 d(\cos \theta) (\psi_c - \psi_0) \sqrt{4\pi} Y_0^0(\theta, \phi) [Y_{\ell'}^{m'}(\theta, \phi)]^* \\
 & - \sum'_{\ell m} R^\ell B_{\ell m} \int_0^{2\pi} d\phi \left\{ \int_{-1}^{t_r} (\chi[\mu](x, R))^\ell Y_\ell^m(\theta_\mu, \phi_\mu) + \int_{-1}^{t_r} (-1)^{\ell+m} \frac{\varepsilon_3 - \varepsilon_4}{\varepsilon_3 + \varepsilon_4} (\chi[\bar{\mu}](x, R))^\ell Y_\ell^m(\theta_{\bar{\mu}}, \phi_{\bar{\mu}}) \right. \\
 & \quad \left. + \left[\int_{-1}^1 - \int_{-1}^{t_r} \right] \frac{2\varepsilon_3}{\varepsilon_3 + \varepsilon_4} (\chi[\mu](x, R))^\ell Y_\ell^m(\theta_\mu, \phi_\mu) \right\} d(\cos \theta) [Y_{\ell'}^{m'}(\theta, \phi)]^* \\
 & + \sum'_{\ell m} R^{-\ell-1} \mathcal{A}_{\ell m} \int_0^{2\pi} d\phi \left\{ \int_{-1}^{t_r} (\chi[\mu](x, R))^{-\ell-1} Y_\ell^m(\theta_\mu, \phi_\mu) + \int_{-1}^{t_r} (-1)^{\ell+m} \frac{\varepsilon_5 - \varepsilon_6}{\varepsilon_5 + \varepsilon_6} (\chi[\bar{\mu}](x, R))^{-\ell-1} Y_\ell^m(\theta_{\bar{\mu}}, \phi_{\bar{\mu}}) \right. \\
 & \quad \left. + \left[\int_{-1}^1 - \int_{-1}^{t_r} \right] \frac{2\varepsilon_5}{\varepsilon_5 + \varepsilon_6} (\chi[\mu](x, R))^{-\ell-1} Y_\ell^m(\theta_\mu, \phi_\mu) \right\} d(\cos \theta) [Y_{\ell'}^{m'}(\theta, \phi)]^* \\
 & + \sum'_{\ell m} R^\ell \mathcal{B}_{\ell m} \int_0^{2\pi} d\phi \left\{ \int_{-1}^{t_r} (\chi[\mu](x, R))^\ell Y_\ell^m(\theta_\mu, \phi_\mu) + \int_{-1}^{t_r} (-1)^{\ell+m} \frac{\varepsilon_5 - \varepsilon_6}{\varepsilon_5 + \varepsilon_6} (\chi[\bar{\mu}](x, R))^\ell Y_\ell^m(\theta_{\bar{\mu}}, \phi_{\bar{\mu}}) \right. \\
 & \quad \left. + \left[\int_{-1}^1 - \int_{-1}^{t_r} \right] \frac{2\varepsilon_5}{\varepsilon_5 + \varepsilon_6} (\chi[\mu](x, R))^\ell Y_\ell^m(\theta_\mu, \phi_\mu) \right\} d(\cos \theta) [Y_{\ell'}^{m'}(\theta, \phi)]^* \\
 & = 0. \tag{B.24}
 \end{aligned}$$

B Detailed derivation of the system of equations

The relations (B.1), (B.2), (B.4), (B.6) and (B.7) are then used, simplifying the system of equations to

$$\begin{aligned}
& (\psi_c - \psi_0) \sqrt{4\pi} \delta_{m'0} \delta_{\ell'0} \\
& + \sum'_{\ell m} R^\ell B_{\ell m} \left\{ -\zeta_{\ell\ell_1}^m \left[M_{\ell\ell_1}^m[\mu](t_r) + \left(\frac{\varepsilon_3 - \varepsilon_4}{\varepsilon_3 + \varepsilon_4} \right) (-1)^{\ell_1+m} M_{\ell\ell_1}^m[\bar{\mu}](t_r) + \left(\frac{2\varepsilon_3}{\varepsilon_3 + \varepsilon_4} \right) \{M_{\ell\ell_1}^m[\mu](t_r=1) - M_{\ell\ell_1}^m[\mu](t_r)\} \right] \right\} \\
& + \sum'_{\ell m} R^{-\ell-1} \mathcal{A}_{\ell m} \left\{ \zeta_{\ell\ell_1}^m \left[K_{\ell\ell_1}^m[\mu](t_r) + \left(\frac{\varepsilon_5 - \varepsilon_6}{\varepsilon_5 + \varepsilon_6} \right) (-1)^{\ell_1+m} K_{\ell\ell_1}^m[\bar{\mu}](t_r) + \left(\frac{2\varepsilon_5}{\varepsilon_5 + \varepsilon_6} \right) \{K_{\ell\ell_1}^m[\mu](t_r=1) - K_{\ell\ell_1}^m[\mu](t_r)\} \right] \right\} \\
& - \sum'_{\ell m} R^\ell \mathcal{B}_{\ell m} \left\{ -\zeta_{\ell\ell_1}^m \left[M_{\ell\ell_1}^m[\mu](t_r) + \left(\frac{\varepsilon_5 - \varepsilon_6}{\varepsilon_5 + \varepsilon_6} \right) (-1)^{\ell_1+m} M_{\ell\ell_1}^m[\bar{\mu}](t_r) + \left(\frac{2\varepsilon_5}{\varepsilon_5 + \varepsilon_6} \right) \{M_{\ell\ell_1}^m[\mu](t_r=1) - M_{\ell\ell_1}^m[\mu](t_r)\} \right] \right\} \\
& = 0.
\end{aligned} \tag{B.25}$$

This is further simplified using the definitions (3.16a) and (3.16b).

$$\begin{aligned}
& \sum'_{\ell m} R^\ell B_{\ell m} D_{\ell'\ell}^m(t_r) \delta_{m'm} + \sum'_{\ell m} R^{-\ell-1} \mathcal{A}_{\ell m} \mathcal{C}_{\ell'\ell}^m(t_r) \delta_{m'm} - \sum'_{\ell m} R^\ell \mathcal{B}_{\ell m} \mathcal{D}_{\ell'\ell}^m(t_r) \delta_{m'm} \\
& = (\psi_0 - \psi_c) \sqrt{4\pi} \delta_{m'0} \delta_{\ell'0}.
\end{aligned} \tag{B.26}$$

where $\ell' = 0, 1, 2, 3, \dots$ and $m' = 0, \pm 1, \pm 2, \pm 3, \dots, \pm \ell'$. Using the same arguments as in the previous case of the continuity of the potential at the outer shell, equation (3.11b) is acquired:

$$\sum_{\ell_1=1}^M R_c^{-\ell_1-2} A_{\ell_1 m} F_{\ell\ell_1}^m(t_{rc}) - \sum_{\ell_1=1}^M R_c^{-\ell_1-2} \mathcal{A}_{\ell_1 m} \mathcal{F}_{\ell\ell_1}^m(t_{rc}) + \sum_{\ell_1=1}^M R_c^{\ell_1-1} \mathcal{B}_{\ell_1 m} \mathcal{G}_{\ell\ell_1}^m(t_{rc}) = J_\ell^m(t_{rc}), \tag{B.27}$$

where $\ell = 1, 2, 3, \dots, M$ and $m = 0, 1$.

B.4.2 Continuity of the normal derivative of the potential times the permittivity at the inner shell

In deriving the set of equations for the normal displacement field continuity at the interface between the coating and the island, the potentials (B.8c), (B.8d), (B.8e), (B.8f) are first inserted into the weakly formulated continuity equation (3.9d). This gives

$$\begin{aligned}
 & \int_{-1}^{t_{rc}} d(\cos \theta) \int_0^{2\pi} d\phi \left\{ \right. \\
 & + \sum'_{\ell m} \varepsilon_5 \mathcal{A}_{\ell m} \frac{\partial}{\partial r} [r_\mu^{-\ell-1} Y_\ell^m(\theta_\mu, \phi_\mu)]_{r=R} + \sum'_{\ell m} \varepsilon_5 \mathcal{B}_{\ell m} \frac{\partial}{\partial r} [r_\mu^\ell Y_\ell^m(\theta_\mu, \phi_\mu)]_{r=R} \\
 & + \sum'_{\ell m} (-1)^{\ell+m} \varepsilon_5 \frac{\varepsilon_5 - \varepsilon_6}{\varepsilon_5 + \varepsilon_6} \mathcal{A}_{\ell m} \frac{\partial}{\partial r} [r_{\bar{\mu}}^{-\ell-1} Y_\ell^m(\theta_{\bar{\mu}}, \phi_{\bar{\mu}})]_{r=R} \\
 & + \sum'_{\ell m} (-1)^{\ell+m} \varepsilon_5 \frac{\varepsilon_5 - \varepsilon_6}{\varepsilon_5 + \varepsilon_6} \mathcal{B}_{\ell m} \frac{\partial}{\partial r} [r_{\bar{\mu}}^\ell Y_\ell^m(\theta_{\bar{\mu}}, \phi_{\bar{\mu}})]_{r=R} \\
 & - \sum'_{\ell m} \varepsilon_3 B_{\ell m} \frac{\partial}{\partial r} [r_\mu^\ell Y_\ell^m(\theta_\mu, \phi_\mu)]_{r=R} \\
 & - \sum'_{\ell m} (-1)^{\ell+m} \varepsilon_3 \frac{\varepsilon_3 - \varepsilon_4}{\varepsilon_3 + \varepsilon_4} B_{\ell m} \frac{\partial}{\partial r} [r_{\bar{\mu}}^{-\ell-1} Y_\ell^m(\theta_{\bar{\mu}}, \phi_{\bar{\mu}})]_{r=R} \left. \right\} [Y_{\ell'}^{m'}(\theta, \phi)]^* \\
 & + \int_{t_{rc}}^1 d(\cos \theta) \int_0^{2\pi} d\phi \left\{ \right. \\
 & + \sum'_{\ell m} \varepsilon_6 \frac{2\varepsilon_5}{\varepsilon_5 + \varepsilon_6} \mathcal{A}_{\ell m} \frac{\partial}{\partial r} [r_\mu^{-\ell-1} Y_\ell^m(\theta_\mu, \phi_\mu)]_{r=R} + \sum'_{\ell m} \varepsilon_6 \frac{2\varepsilon_5}{\varepsilon_5 + \varepsilon_6} \mathcal{B}_{\ell m} \frac{\partial}{\partial r} [r_\mu^\ell Y_\ell^m(\theta_\mu, \phi_\mu)]_{r=R} \\
 & - \sum'_{\ell m} \varepsilon_4 \frac{2\varepsilon_3}{\varepsilon_3 + \varepsilon_4} B_{\ell m} \frac{\partial}{\partial r} [r_\mu^\ell Y_\ell^m(\theta_\mu, \phi_\mu)]_{r=R} \left. \right\} [Y_{\ell'}^{m'}(\theta, \phi)]^* \\
 & = 0.
 \end{aligned} \tag{B.28}$$

B Detailed derivation of the system of equations

Next, as before, $\chi[\eta](x, R)$ is introduced with (3.3), the terms are collected by their multipole expansion coefficients, the radii are extracted and the integrals rearranged:

$$\begin{aligned}
& - \sum'_{\ell m} R_c^{\ell-1} B_{\ell m} \int_0^{2\pi} d\phi \left\{ \int_{-1}^{t_{rc}} \varepsilon_3 \frac{\partial}{\partial(\frac{r}{R})} \left[(\chi[\mu](x, r))^{\ell} Y_{\ell}^m(\theta_{\mu}, \phi_{\mu}) \right]_{r=R} \right. \\
& \quad + \int_{-1}^{t_{rc}} (-1)^{\ell+m} \varepsilon_3 \frac{\varepsilon_3 - \varepsilon_4}{\varepsilon_3 + \varepsilon_4} \frac{\partial}{\partial(\frac{r}{R})} \left[(\chi[\bar{\mu}](x, r))^{\ell} Y_{\ell}^m(\theta_{\bar{\mu}}, \phi_{\bar{\mu}}) \right]_{r=R} \\
& \quad \left. + \left[\int_{-1}^1 - \int_{-1}^{t_{rc}} \right] \varepsilon_4 \frac{2\varepsilon_3}{\varepsilon_3 + \varepsilon_4} \frac{\partial}{\partial(\frac{r}{R})} \left[(\chi[\mu](x, r))^{\ell} Y_{\ell}^m(\theta_{\mu}, \phi_{\mu}) \right]_{r=R} \right\} d(\cos \theta) [Y_{\ell'}^{m'}(\theta, \phi)]^* \\
& + \sum'_{\ell m} R_c^{-\ell-2} \mathcal{A}_{\ell m} \int_0^{2\pi} d\phi \left\{ \int_{-1}^{t_{rc}} \varepsilon_5 \frac{\partial}{\partial(\frac{r}{R})} \left[(\chi[\mu](x, r))^{-\ell-1} Y_{\ell}^m(\theta_{\mu}, \phi_{\mu}) \right]_{r=R} \right. \\
& \quad + \int_{-1}^{t_{rc}} (-1)^{\ell+m} \varepsilon_5 \frac{\varepsilon_5 - \varepsilon_6}{\varepsilon_5 + \varepsilon_6} \frac{\partial}{\partial(\frac{r}{R})} \left[(\chi[\bar{\mu}](x, r))^{-\ell-1} Y_{\ell}^m(\theta_{\bar{\mu}}, \phi_{\bar{\mu}}) \right]_{r=R} \\
& \quad \left. + \left[\int_{-1}^1 - \int_{-1}^{t_{rc}} \right] \varepsilon_6 \frac{2\varepsilon_5}{\varepsilon_5 + \varepsilon_6} \frac{\partial}{\partial(\frac{r}{R})} \left[(\chi[\mu](x, r))^{-\ell-1} Y_{\ell}^m(\theta_{\mu}, \phi_{\mu}) \right]_{r=R} \right\} d(\cos \theta) [Y_{\ell'}^{m'}(\theta, \phi)]^* \\
& + \sum'_{\ell m} R_c^{\ell-1} \mathcal{B}_{\ell m} \int_0^{2\pi} d\phi \left\{ \int_{-1}^{t_{rc}} \varepsilon_5 \frac{\partial}{\partial(\frac{r}{R})} \left[(\chi[\mu](x, r))^{\ell} Y_{\ell}^m(\theta_{\mu}, \phi_{\mu}) \right]_{r=R} \right. \\
& \quad + \int_{-1}^{t_{rc}} (-1)^{\ell+m} \varepsilon_5 \frac{\varepsilon_5 - \varepsilon_6}{\varepsilon_5 + \varepsilon_6} \frac{\partial}{\partial(\frac{r}{R})} \left[(\chi[\bar{\mu}](x, r))^{\ell} Y_{\ell}^m(\theta_{\bar{\mu}}, \phi_{\bar{\mu}}) \right]_{r=R} \\
& \quad \left. + \left[\int_{-1}^1 - \int_{-1}^{t_{rc}} \right] \varepsilon_6 \frac{2\varepsilon_5}{\varepsilon_5 + \varepsilon_6} \frac{\partial}{\partial(\frac{r}{R})} \left[(\chi[\mu](x, r))^{\ell} Y_{\ell}^m(\theta_{\mu}, \phi_{\mu}) \right]_{r=R} \right\} d(\cos \theta) [Y_{\ell'}^{m'}(\theta, \phi)]^* \\
& = 0. \tag{B.29}
\end{aligned}$$

The relations (B.1), (B.3), (B.5), (B.6) and (B.7) are then used, simplifying the system of equations to

$$\begin{aligned}
& + \sum'_{\ell m} R^{\ell-1} B_{\ell m} \left\{ -\zeta_{\ell\ell_1}^m \left[\left(\frac{2\varepsilon_3}{\varepsilon_3 + \varepsilon_4} \right) N_{\ell\ell_1}^m[\mu](t_r=1) + \varepsilon_3 \left(\frac{\varepsilon_3 - \varepsilon_4}{\varepsilon_3 + \varepsilon_4} \right) \left\{ N_{\ell\ell_1}^m[\mu](t_r) + (-1)^{\ell_1+m} N_{\ell\ell_1}^m[\bar{\mu}](t_r) \right\} \right] \right\} \\
& + \sum'_{\ell m} R^{-\ell-2} \mathcal{A}_{\ell m} \left\{ \zeta_{\ell\ell_1}^m \left[\left(\frac{2\varepsilon_5}{\varepsilon_5 + \varepsilon_6} \right) L_{\ell\ell_1}^m[\mu](t_r=1) + \varepsilon_5 \left(\frac{\varepsilon_5 - \varepsilon_6}{\varepsilon_5 + \varepsilon_6} \right) \left\{ L_{\ell\ell_1}^m[\mu](t_r) + (-1)^{\ell_1+m} L_{\ell\ell_1}^m[\bar{\mu}](t_r) \right\} \right] \right\} \\
& - \sum'_{\ell m} R^{\ell-1} \mathcal{B}_{\ell m} \left\{ -\zeta_{\ell\ell_1}^m \left[\left(\frac{2\varepsilon_5}{\varepsilon_5 + \varepsilon_6} \right) N_{\ell\ell_1}^m[\mu](t_r=1) + \varepsilon_5 \left(\frac{\varepsilon_5 - \varepsilon_6}{\varepsilon_5 + \varepsilon_6} \right) \left\{ N_{\ell\ell_1}^m[\mu](t_r) + (-1)^{\ell_1+m} N_{\ell\ell_1}^m[\bar{\mu}](t_r) \right\} \right] \right\} \\
& = 0. \tag{B.30}
\end{aligned}$$

This is then further simplified using the definitions (3.16c) and (3.16d).

$$\sum'_{\ell m} R^{\ell-1} B_{\ell m} G_{\ell\ell}^m(t_r) \delta_{m'm} + \sum'_{\ell m} R^{-\ell-2} \mathcal{A}_{\ell m} \mathcal{F}_{\ell\ell}^m(t_r) \delta_{m'm} - \sum'_{\ell m} R^{\ell-1} \mathcal{B}_{\ell m} \mathcal{G}_{\ell\ell}^m(t_r) \delta_{m'm} = 0. \tag{B.31}$$

where $\ell' = 0, 1, 2, 3, \dots$ and $m' = 0, \pm 1, \pm 2, \pm 3, \dots, \pm \ell'$. Still using the same arguments as in the previous cases, equation (3.11c) is retrieved:

$$\sum_{\ell_1=1}^M R^{\ell_1-1} B_{\ell_1 m} G_{\ell \ell_1}^m(t_r) + \sum_{\ell_1=1}^M R^{-\ell_1-2} \mathcal{A}_{\ell_1 m} \mathcal{F}_{\ell \ell_1}^m(t_r) - \sum_{\ell_1=1}^M R^{\ell_1-1} \mathcal{B}_{\ell_1 m} \mathcal{G}_{\ell \ell_1}^m(t_r) = 0, \quad (\text{B.32})$$

where $\ell = 1, 2, 3, \dots, M$ and $m = 0, 1$.

B.5 Summary of the linear system of equations

For reference, the linear system of equations derived in this chapter will be repeated here.

$$\sum_{\ell_1=1}^M R_c^{-\ell_1-2} A_{\ell_1 m} C_{\ell \ell_1}^m(t_{rc}) - \sum_{\ell_1=1}^M R_c^{-\ell_1-2} \mathcal{A}_{\ell_1 m} \mathcal{C}_{\ell \ell_1}^m(t_{rc}) + \sum_{\ell_1=1}^M R_c^{\ell_1-1} \mathcal{B}_{\ell_1 m} \mathcal{D}_{\ell \ell_1}^m(t_{rc}) = H_\ell^m(t_{rc}), \quad (\text{B.33a})$$

$$\sum_{\ell_1=1}^M R^{\ell_1-1} B_{\ell_1 m} D_{\ell \ell_1}^m(t_r) + \sum_{\ell_1=1}^M R^{-\ell_1-2} \mathcal{A}_{\ell_1 m} \mathcal{C}_{\ell \ell_1}^m(t_r) - \sum_{\ell_1=1}^M R^{\ell_1-1} \mathcal{B}_{\ell_1 m} \mathcal{D}_{\ell \ell_1}^m(t_r) = 0, \quad (\text{B.33b})$$

$$\sum_{\ell_1=1}^M R_c^{-\ell_1-2} A_{\ell_1 m} F_{\ell \ell_1}^m(t_{rc}) - \sum_{\ell_1=1}^M R_c^{-\ell_1-2} \mathcal{A}_{\ell_1 m} \mathcal{F}_{\ell \ell_1}^m(t_{rc}) + \sum_{\ell_1=1}^M R_c^{\ell_1-1} \mathcal{B}_{\ell_1 m} \mathcal{G}_{\ell \ell_1}^m(t_{rc}) = J_\ell^m(t_{rc}), \quad (\text{B.33c})$$

$$\sum_{\ell_1=1}^M R^{\ell_1-1} B_{\ell_1 m} G_{\ell \ell_1}^m(t_r) + \sum_{\ell_1=1}^M R^{-\ell_1-2} \mathcal{A}_{\ell_1 m} \mathcal{F}_{\ell \ell_1}^m(t_r) - \sum_{\ell_1=1}^M R^{\ell_1-1} \mathcal{B}_{\ell_1 m} \mathcal{G}_{\ell \ell_1}^m(t_r) = 0, \quad (\text{B.33d})$$

where $\ell = 1, 2, 3, \dots, M$ and $m = 0, 1$.

C Parameters for default test case

Parameter	Default value	Comment
Theta0	45 degrees	
Phi0		Determined according to the chosen polarisation
Polarization	p	
Energy_Range	1.5 to 5 eV	
Radius	8.0 nm	
Truncation_Ratio	0.0	In some cases changed to 0.3
Coating_Thickness	3.0 nm	
Size_Distribution	none	All islands have the same size
Lattice_Constant	13.2	
Lattice_Type	square	Choice: square, hexagonal, MFT (mean field theory), RPT
Coverage	0.30	Island coverage (ignoring the coating)
Ambient_Material	vacuum	
Island_Material	ag	
Substrate_Material	mgo	
Coating_Material	ag	
Finite_Size_Effects	none	
Multipole_Order	16	
Multipole_Position	0	The multipole expansion is placed in the sphere centre
No_Energy_Points	1024	
Island_Island_Interaction	dipole	Choices: none, dipole, quadropole, size

Table C.1: The most relevant parameters for the default setting introduced in section 6.2

Bibliography

- [1] D. Bedeaux and J. Vlieger. *Thin Solid Films*, 102:265, 1983.
- [2] D. Bedeaux and J. Vlieger. *Optical properties of surfaces*. Imperial College Press, second edition, 2004.
- [3] D. J. Griffiths. *Introduction to electrodynamics*. Prentice Hall, third edition, 2004.
- [4] E. Hecht. *Optics*. Addison Wesley, fourth edition, 2002.
- [5] R. Lazzari, J. Jupille, and Y. Borensztein. *Appl. Surf. Sci.*, 142:451, 1999.
- [6] R. Lazzari and I. Simonsen. GranFilm: a software for calculating thin-layer dielectric properties and Fresnel coefficients. *Thin Solid Films*, 419:124–136, 2002.
- [7] R. Lazzari, I. Simonsen, D. Bedeaux, J. Vlieger, and J. Jupille. *Eur. Phys. J. B*, 24:267, 2001.
- [8] J. C. Maxwell Garnett. *Philos. Trans. R. Soc. London, Ser. A*, 203:385, 1904.
- [9] I. Simonsen, R. Lazzari, J. Jupille, and S. Roux. *Phys. Rev. B*, 61:7722, 2000.
- [10] I. Simonsen, R. Lazzari, J. Jupille, and S. Roux. Numerical modeling of the optical response of supported metallic particles. *Physical Review B*, 61(11):7722–7733, 2000.
- [11] M. M. Wind, P. A. Bobbert, and J. Vlieger. *Thin Solid Films*, 164:57, 1988.
- [12] M. M. Wind, P. A. Bobbert, J. Vlieger, and D. Bedeaux. *Physica A*, 143:164, 1987.
- [13] M. M. Wind, J. Vlieger, and D. Bedeaux. *Physica A*, 141:33, 1987.
- [14] T. Yamaguchi, S. Yoshida, and A. Kinbara. *Thin Solid Films*, 18:63, 1973.
- [15] T. Yamaguchi, S. Yoshida, and A. Kinbara. *Thin Solid Films*, 21:173, 1974.